NUCLEAR DATA AND MEASUREMENT SERIES
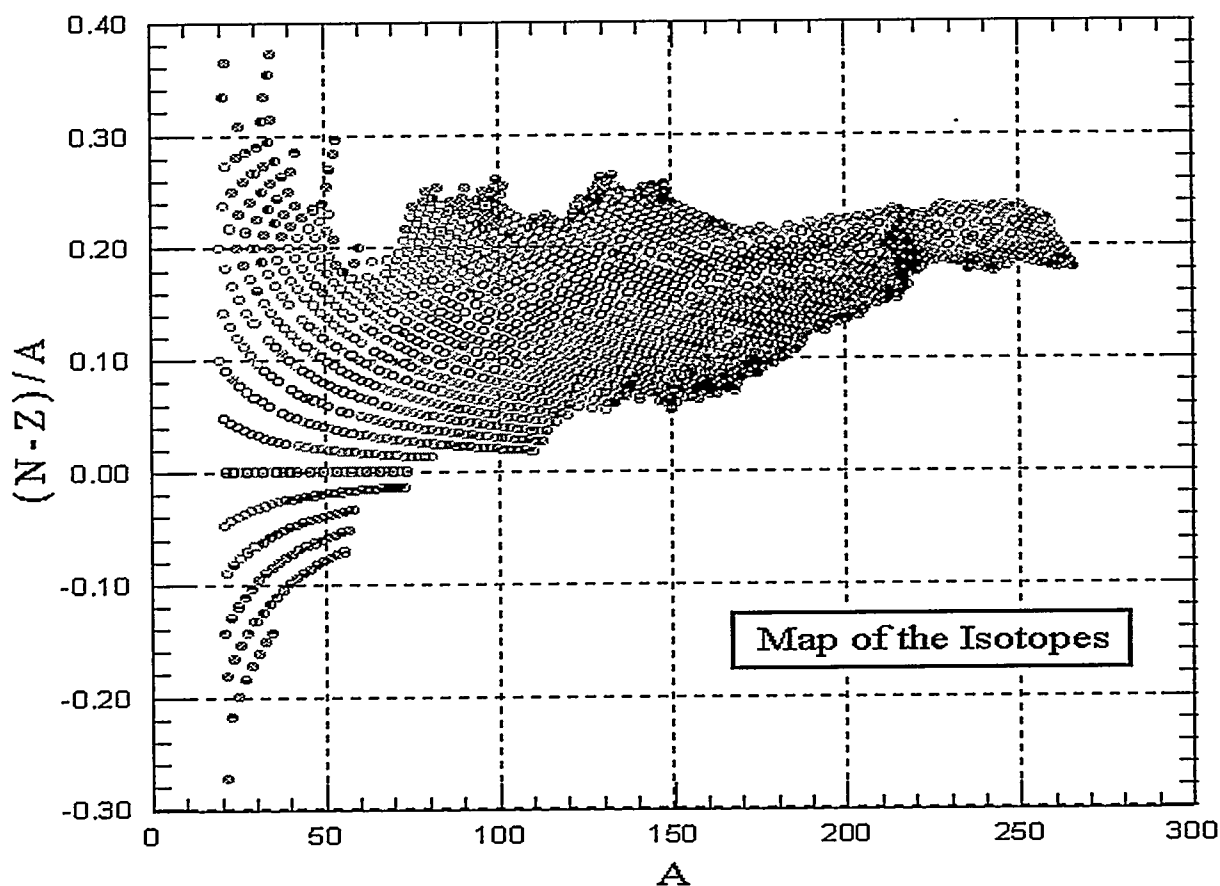
ANL/NDM-146

Non-Destructive Assay of EBR-II Blanket Elements
Using Resonance Transmission Analysis

Raymond T. Klann
Wolfgang P. Poenitz

August 1998

Map of the Isotopes

Argonne National Laboratory, with facilities in the states of Illinois and Idaho, is owned by the UNITED STATES GOVERNMENT and operated by THE UNIVERSITY OF CHICAGO under provisions of Contract W-31-109-Eng-38 with the U.S. DEPARTMENT OF ENERGY (DOE).

DISCLAIMER

Portions of this document may be illegible in electronic image products. Images are produced from the best available original document.

ANL/NDM-146

Non-Destructive Assay of EBR-II Blanket Elements Using Resonance Transmission Analysis [a]

by

Raymond T. Klann and Wolfgang P. Poenitz
Argonne National Laboratory
9700 South Cass Avenue
Argonne, IL 60439
U.S.A.

August 1998

NUCLEAR APPLICATIONS. Resonance Transmission Analysis, Plutonium-239, Uranium-235, Uranium-238, Depleted Uranium, Eperimental Breeder Reactor - II, Fast Reactor Blanket, Nuclear Resonances, Resonance Cross-Sections, Non-destructive Analysis, Nuclear Assay, Non-destructive Examination.

Nuclear Data and Measurement Series

The Nuclear Data and Measurement Series presents results of studies in the field of microscopic nuclear data. The primary objective is the dissemination of information in the comprehensive form required for nuclear technology applications. This Series is devoted to: a) measured microscopic nuclear parameters, b) experimental techniques and facilities employed in measurements, c) the analysis, correlation and interpretation of nuclear data, and d) the compilation and evaluation of nuclear data. Contributions to this Series are reviewed to assure technical competence and, unless otherwise stated, the contents can be formally referenced. This Series does not supplant formal journal publication, but it does provide the more extensive information required for technological applications (*e.g.*, tabulated numerical data) in a timely manner.

Information About Other Issues of the ANL/NDM Series

A list of titles and authors for previous issues appears in each report of the Series. The list for reports ANL/NDM-1 through ANL/NDM-75 appears in ANL/NDM-76. Report ANL/NDM-91 contains the list for reports ANL/NDM-76 through ANL/NDM-90. Report ANL/NDM-128 contains the list for reports ANL/NDM-91 through ANL/NDM-127. Below is the list for ANL/NDM-125 through ANL/NDM-145. Requests for a complete list of titles or for copies of previous reports in this Series should be directed to:

Donald L. Smith
Nuclear Data Program
Technology Development Division
TD-207-DB116
Argonne National Laboratory
9700 South Cass Avenue
Argonne, Illinois 60439
U.S.A.

Tel.:   +1(630)252-6021
Fax: +1(630)252-1774
E-mail: Donald.L.Smith@anl.gov

ANL/NDM-125

A.B. Smith and P.T. Guenther, *Fast-neutron Scattering Near Shell Closures: Scandium*, August 1992.

ANL/NDM-126

A.B. Smith, J.W. Meadows and R.J. Howerton, *A Basic Evaluated Neutronic Data File for Elemental Scandium*, November 1992.

ANL/NDM-127

A.B. Smith and P.T. Guenther, *Fast-neutron Interaction with Collective Cadmium Nuclei*, November 1992.

ANL/NDM-128

Donald L. Smith, *A Least-squares Computational "Tool Kit"*, April 1993.

iii

ANL/NDM-129

Joseph McCabe, A.B. Smith and J.W. Meadows, *Evaluated Nuclear Data Files for the Naturally Occurring Isotopes of Cadmium*, June 1993.

ANL/NDM-130

A.B. Smith and P.T. Guenther, *Fast-neutron Interaction with the Fission Product ^{103}Rh*, September 1993.

ANL/NDM-131

A.B. Smith and P.T. Guenther, *Fast-neutron Scattering from Vibrational Palladium Nuclei*, October 1993.

ANL/NDM-132

A.B. Smith, *Neutron Interaction with Doubly-magic ^{40}Ca*, December 1993.

ANL/NDM-133

A.B. Smith, *Neutron Scattering at Z=50:- Tin*, September 1994.

ANL/NDM-134

A.B. Smith, S. Chiba and J.W. Meadows, *An Evaluated Neutronic File for Elemental Zirconium*, September 1994.

ANL/NDM-135

A.B. Smith, *Neutron Scattering from Elemental Uranium and Thorium*, February 1995.

ANL/NDM-136

A.B. Smith, *Neutron Scattering and Models:- Iron*, August 1995.

ANL/NDM-137

A.B. Smith, *Neutron Scattering and Models:- Silver*, July 1996.

ANL/NDM-138

A.B. Smith, *Neutron Scattering and Models:- Chromium*, June 1996.

ANL/NDM-139

W.P. Poenitz and S.E. Aumeier, *The Simultaneous Evaluation of the Standards and Other Cross Sections of Importance for Technology*, September 1997.

ANL/NDM-140

Jason T. Daly and Donald L. Smith, *A Compilation of Information on the $^{31}P(p, \gamma)^{32}S$ Reaction and Properties of Excited Levels in ^{32}S*, March 1998.

ANL/NDM-141

A.B. Smith, *Neutron Scattering and Models:- Titanium*, July 1997.

ANL/NDM-142

A.B. Smith, *Neutron Scattering and Models:- Molybdenum*, November 1997.

ANL/NDM-143

Roy E. Miller and Donald L. Smith, *A Compilation of Information on the $^{32}S(p, \gamma)^{33}Cl$ Reaction and Properties of Excited Levels in ^{33}Cl*, July 1997.

ANL/NDM-144

Roy E. Miller and Donald L. Smith, *A Compilation of Information on the $^{31}P(p, \alpha)^{28}Si$ Reaction and Propergies of Excited Levels in the Compound Nucleus 32S*, November 1997.

ANL/NDM-145

R.D. Lawson (edited and updated by A.B. Smith), *Abarex - A Neutron Spherical Optical-Statistical Model Code: A User's Manual*, June 1998.

vi

NON-DESTRUCTIVE ASSAY OF EBR-II BLANKET ELEMENTS

USING RESONANCE TRANSMISSION ANALYSIS

Raymond T. Klann

Wolfgang P. Poenitz

Abstract

Resonance transmission analysis utilizing a filtered reactor beam was examined as a means of determining the ^{239}Pu content in Experimental Breeder Reactor - II depleted uranium blanket elements. The technique uses cadmium and gadolinium filters along with a ^{239}Pu fission chamber to isolate the 0.3 eV resonance in ^{239}Pu. In the energy range of this resonance (0.1 eV to 0.5 eV), the total microscopic cross-section of ^{239}Pu is significantly greater than the cross-sections of ^{238}U and ^{235}U. This large difference allows small changes in the ^{239}Pu content of a sample to result in large changes in the mass signal response. Tests with small stacks of depleted uranium and ^{239}Pu foils indicate a significant change in response based on the ^{239}Pu content of the foil stack. In addition, the tests indicate good agreement between the measured and predicted values of ^{239}Pu up to approximately two weight percent.

viii

ACKNOWLEDGEMENT

x

TABLE OF CONTENTS

LIST OF TABLES

LIST OF FIGURES

1. Introduction

1.1. Problem Description

The Experimental Breeder Reactor - II (EBR-II) is an unmoderated, heterogeneous, sodium-cooled, fast-breeder reactor operated by the Argonne National Laboratory (ANL) at the Idaho National Engineering and Environmental Laboratory (INEEL). It is a pool type reactor, with the core, primary pumps, and intermediate heat exchanger submerged in a tank of liquid sodium. The core consists of driver assemblies of uranium-zirconium metal or uranium-plutonium-zirconium metal surrounded by reflector assemblies of stainless steel and blanket assemblies of depleted uranium. These depleted uranium assemblies serve as an additional reflector and a breeder of ^{239}Pu. A schematic of the core from the final reactor run is shown in Figure 1. The rated plant power output is 62.5 MW thermal energy (20 MW electric energy) with a fast neutron flux at the core center of about 2.5 x 10^{15} n/cm^2-sec.

In January, 1994, the Department of Energy made a decision in its fiscal year 1995 budget request to terminate the Integral Fast Reactor Program, along with the associated Actinide Recycle Program effective October 1, 1994. EBR-II operation was terminated on September 30, 1994 after 30 years of operation. The shutdown plan for the reactor calls for the industrially and radiologically safe plant closure condition by the end of the 1998 fiscal year so that the reactor can be transferred to the Office of Environmental Management for ultimate decontamination and decommissioning. The shutdown plan includes removal and temporary storage of the reactor fuel, removal and processing of the primary and secondary system sodium, and safe closure of the reactor system following sodium removal. The EBR-II shutdown activity also includes the treatment of the discharged driver and blanket assemblies in the Fuel Conditioning Facility (FCF).

A total of 353 depleted uranium blanket assemblies that were irradiated in EBR-II still exist today. Each blanket assembly consists of 19 elements as shown in Figure 2. Therefore, there are a total of 6707 blanket elements that must be processed in FCF. Currently, the plan is to process 25 blanket assemblies (475 elements) as part of the demonstration phase of the electrorefining treatment process. Because of criticality concerns and material control and accountability requirements in the processing of fissionable material in FCF, the fissionable material content of each assembly must be known with a reasonable degree of certainty prior to being transferred from EBR-II into FCF.

Over time, a small amount of the ^{238}U was bred into ^{239}Pu by neutron capture and subsequent beta decay through the following reaction:

$$^{238}U(n,\gamma)^{239}U \xrightarrow{\beta^-} {}^{239}Np \xrightarrow{\beta^-} {}^{239}Pu \ . \tag{1}$$
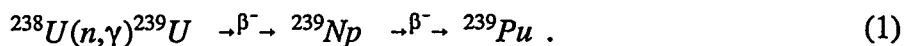
To a much lesser extent, other heavy metals have also been bred into the blanket elements. The neutron capture reaction (n,γ) is highly dependent on neutron energy and exhibits strong resonances in the epithermal energy range as shown in Figure 3. Resonances are isotope-dependent and based

EBR-II Grid Map
9/30/94
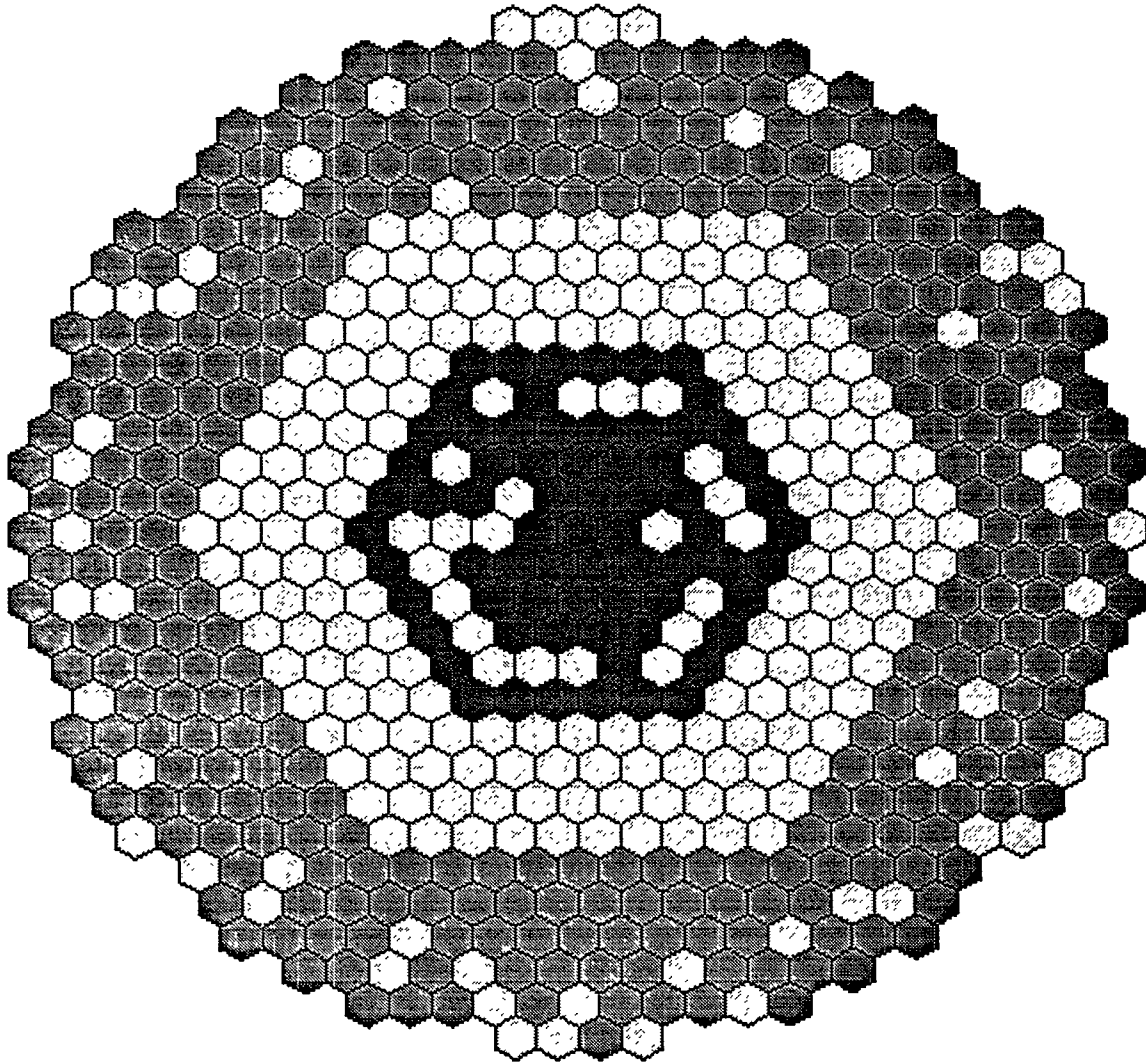
Figure 1: EBR-II Core Configuration from the Final Reactor Run
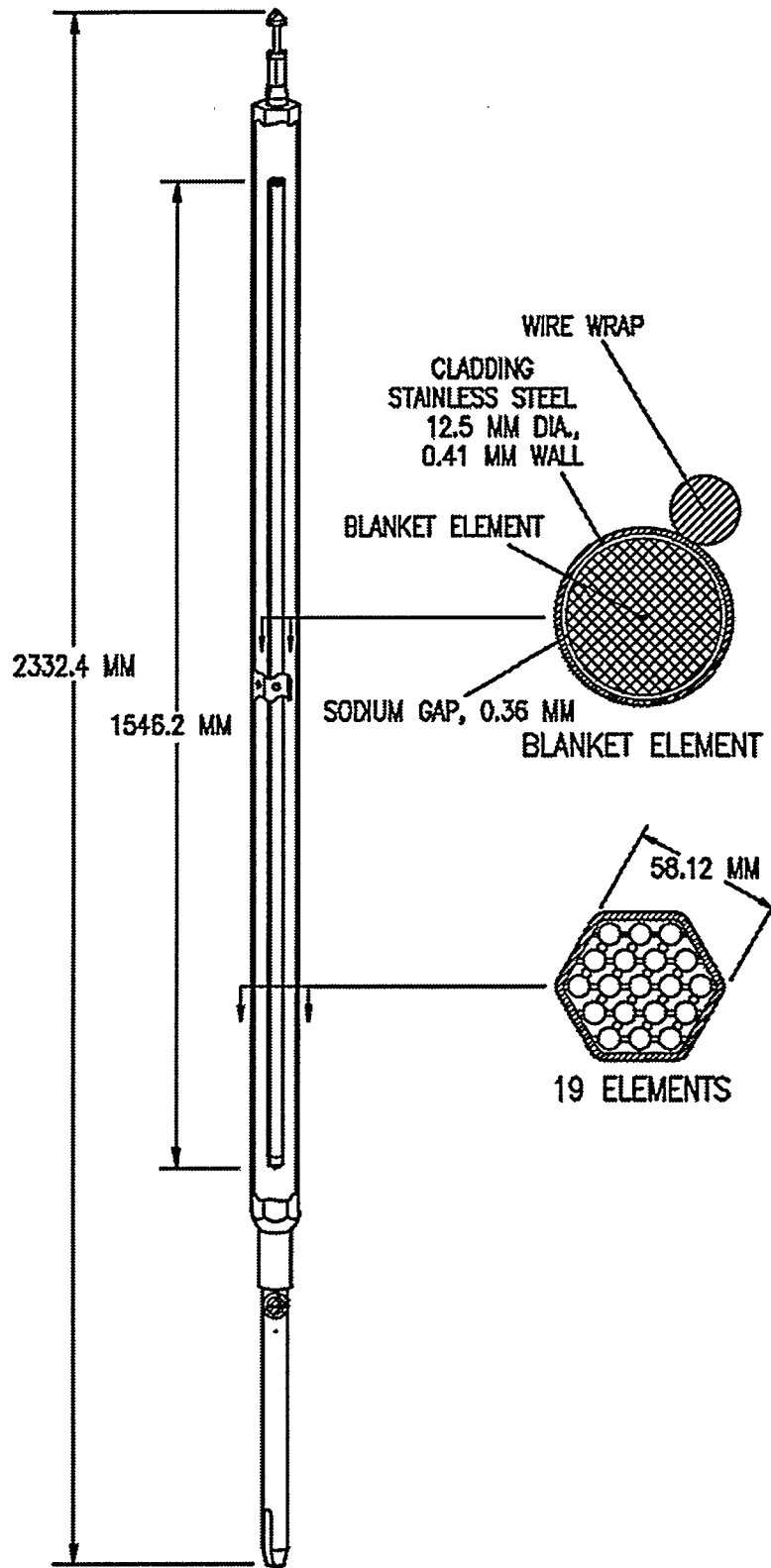
Figure 2: EBR-II Blanket Assembly
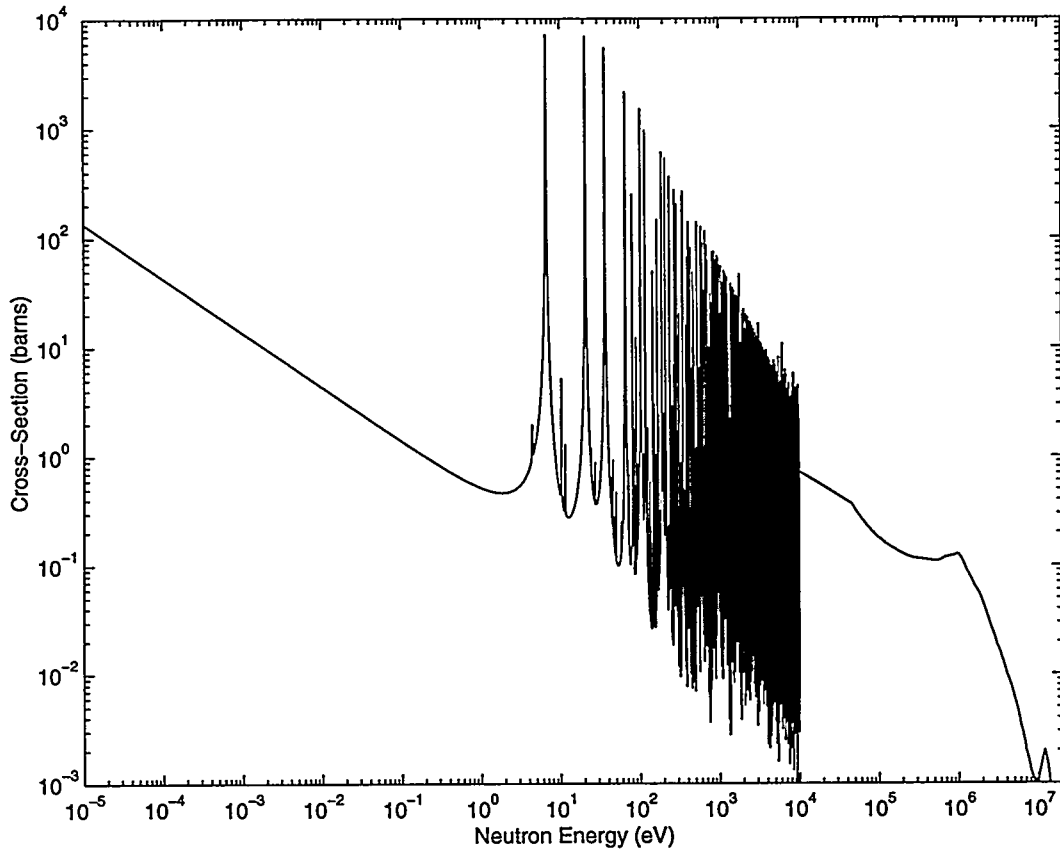
Figure 3: ^{238}U Capture Cross-Section

on the nuclear properties of the specific isotope as described in Chapter 2. Estimates indicate that as much as 1000 grams of ^{239}Pu have been created in some blanket assemblies from an initial ^{238}U weight of about 48 kilograms. However, the estimated quantities of ^{239}Pu are highly uncertain.

The neutron spectra in the core region have been well characterized through calculations, flux measurements, and destructive analysis of numerous driver elements. However, the flux in the blanket region is less well known. Current estimates of the plutonium content in blanket assemblies are based on diffusion theory calculations for the flux in this region.

There are four basic assumptions when generating Fick's law from the neutron transport equation: 1. the media is not highly absorbing, 2. the region of interest is a reasonable distance from localized sources, 3. the flux is linearly anisotropic, and 4. the flux is slowly varying with position. The blanket region was designed as a reflector and absorber to reduce the amount of leakage from the reactor and, as such, is highly absorbing, especially in the resonance energy region as shown in Figure 3. This invalidates the first assumption. The neutron source is highly localized in the core region. Very little fissioning occurs in the blanket region and thus neutrons in the blanket region were primarily generated in the core region and have been transported to the blanket region through

4

leakage and scattering. Therefore, the flux is not uniform, is highly directional, and varies strongly with position due to the large absorption cross-section of ^{238}U in the blanket assemblies. In addition, due to the highly absorbing resonances, the energy spectrum is also highly non-uniform. All of these factors are counter to the assumptions on which diffusion theory is based. Worst of all, diffusion theory is known to under predict the magnitude of the flux in deep penetration problems, therefore, the actual amount of ^{239}Pu bred into the blanket assemblies is also under predicted as the buildup of ^{239}Pu is approximately linear with total fluence.

Knowing that the estimates for plutonium buildup in blanket elements have large uncertainties and are most likely under predicted, a method should be found to measure the amount of ^{239}Pu in a blanket element or assembly. The number of assemblies and elements that are awaiting processing requires the method to be simple, to have a reasonable accuracy, and to be cost effective. This eliminates sampling by chemical analysis as a viable alternative due to the large number of elements and samples that would have to be analyzed. Sampling is a destructive technique and offers the greatest accuracy available. Unfortunately, sampling is labor intensive, time consuming, and not cost effective. Currently, a program is underway at EBR-II to destructively analyze three pins from one blanket assembly. The data from these samples would then be used to validate the computer methodology used to estimate the amount of ^{239}Pu and other heavy metals in blanket assemblies. The computer methodology is based on the REBUS code (ref. 1) developed at ANL. Unfortunately, the REBUS code is based on three-dimensional diffusion theory which was shown above to be questionable for deep penetration problems. A non-destructive analysis approach is proposed here and is the basis of this research.

1.2. Survey of Radiation-Based Non-Destructive Analysis Methods

Methods of radiation-based non-destructive analysis are available, however, most of these have inherent problems or weaknesses for analyzing EBR-II blanket assemblies or elements. A straight-forward approach would be to perform gamma spectroscopy on an element or assembly. Unfortunately, these assemblies have a considerable amount of activity from ^{60}Co activation in the stainless steel cladding and fission product buildup. Readings from one element were well over 200 R/hr at a few inches from the surface (ref. 2). Compton scattering of the energetic gamma rays from ^{60}Co and other isotopes dominate the spectrum and make it difficult to observe the gamma peaks from ^{239}Pu (129 keV, 375 keV, and 414 keV). These peaks are almost impossible to detect for small amounts of ^{239}Pu in a sample. Other techniques using gamma ray transmission measurements also encounter the same problem - the background levels due to Compton scattering are too high to obtain a useful signal. In addition, gamma transmission measurements are limited due to the large attenuation coefficient of the high atomic number materials in a fuel element. Typically, segmented gamma scanning can only be performed on samples with a linear density up to about 120 g/cm^2 (ref. 3). A blanket assembly has a linear density near 180 g/cm^2. With gamma ray techniques not offering much promise, neutron counting techniques were examined as alternatives.

There are several neutron counting techniques that could potentially be used for measuring the amount of ^{239}Pu in the EBR-II blanket assemblies. The techniques are called active or passive

based on whether an external neutron source is used to induce reactions. Passive techniques include direct neutron counting of all neutrons emitted from a sample and coincidence counting of spontaneous fission events. Active techniques include delayed neutron counting, coincidence counting of fission events, multiplicity measurements, and neutron transmission measurements.

Passive direct counting of neutrons emitted from a sample regardless of initiating event is the easiest technique but yields only the most basic information. Because neutrons are counted from a variety of initiating events, such as spontaneous fission and alpha-n events, a significant amount of information (such as burnup, operating history, decay time, and initial composition) must be known a priori in order to obtain useful information from the measurement data. These types of gross measurements have been shown to provide information regarding relative plutonium content assuming the other parameters mentioned above are known (ref. 4). In addition, these methods can require significant counting times to reduce the relative error to acceptable levels and can not be used to determine absolute quantities of individual isotopes.

Coincidence counting is a more sophisticated method of counting spontaneous fission events by looking for correlated events (i.e. multiple concurrent neutron emissions from a single event). By looking at coincidences, alpha-n reactions can be eliminated because only one neutron is emitted from this type of reaction. This allows isotopes that have significant spontaneous fission rates (mainly ^{240}Pu, ^{242}Cm, and ^{244}Cm) to be counted and masses determined (ref. 5). In order to determine quantities of other isotopes, ^{239}Pu in particular, the isotopic composition must be predetermined. For the blanket elements, the isotopic compositions are not known and cannot be reasonably determined from gamma spectroscopy. Therefore, this method could not be used to determine the ^{239}Pu content in EBR-II blanket elements.

There are numerous active techniques available. Most of the widely accepted techniques rely on inducing fissions in the sample and then counting the induced neutron signal. This counting is performed primarily by coincidence counting or by delayed neutron counting. The determination of coincidences and ultimately the number of fission events is accomplished through electronic means or through data manipulation. Coincidences can be determined electronically by counting the number of pulses within a time gate based on an initial signal from a neutron. This is a straightforward approach and commercial units are available. The other method of determining coincidences is through manipulation of data recorded in list mode. List mode data acquisition simply records the time each event occurs. This time sequence of pulses is then analyzed by a variety of techniques.

Active methods have been used for a variety of samples although the current focus of use has been on analyzing waste drums and waste containers (refs. 6 and 7). These methods rely on accurately determining the number of fission events among the noise. To do this, corrections are necessary to account for the geometry and composition of the waste matrix. A system is under development at ANL-West as a means to measure residual material in cladding hulls (ref. 8) and segments of blanket elements are also being examined. However, the current system configuration does not allow the assay of intact blanket elements.

Resonance transmission analysis using the time-of-flight technique has been used by others as an effective and accurate way to determine the isotopic composition of small amounts of uranium and plutonium in a sample. The time-of-flight technique is discussed in chapter 2. In simple terms, it uses a pulsed neutron source and counting over selected time intervals to determine the spectra of the transmitted neutron flux with and without a sample. Once the transmission spectrum is known, the amount of various isotopes can be determined from depressions in the spectrum due to the unique resonances of the isotopes in the sample. Unfortunately, a pulsed neutron source is not available at ANL-West. Instead, it is proposed to utilize a filtered neutron beam from the Neutron Radiography Reactor (NRAD) as a means of obtaining the spectral information necessary to determine the amount of ^{239}Pu in a blanket element sample.

1.3 Proposed Method

On average, the blanket assemblies have a maximum ^{239}Pu content up to about two weight percent. For certain regions of a blanket element, the ^{239}Pu content can be higher than two weight percent due to axial and spatial flux peaking. In order for an analysis method to be successful at determining small amounts of ^{239}Pu in large quantities of depleted uranium, there has to be a significant signal change for a small change in ^{239}Pu content. For the blanket elements, the only way that there can be a large signal change in transmission analysis is if the total neutron cross-section of ^{239}Pu in the sample is a large fraction of the total neutron cross-section of the sample. To accomplish this, a neutron energy or energy region must be chosen such that the microscopic total neutron cross-section of ^{239}Pu is much greater than the microscopic total neutron cross-section of the other isotopes in the sample, mainly ^{238}U and ^{235}U.

^{239}Pu has a resonance at 0.3 eV of greater than 5000 barns as shown in Figure 4. Also shown in Figure 4 are the cross-sections for ^{235}U and ^{238}U. If this resonance can be reasonably isolated, then the amount of ^{239}Pu in a sample can be determined through the value of the transmission in this region. Cadmium and gadolinium filters along with a ^{239}Pu fission chamber are proposed as the means to isolate this resonance. The cadmium filter is used to define the upper bound of the energy region. The gadolinium filter is used to define the lower bound of the energy region. The ^{239}Pu fission chamber is used to enhance the response.

Chapter 2 discusses the background of resonance transmission analysis and describes the many applications where resonance transmission analysis has been used. In all of the applications described in Chapter 2, the time-of-flight technique was used. No references to a filtered beam approach for isolating resonances as described in this research project were found. Chapter 3 discusses the basis for this filtered beam approach. A simple mono-energetic problem is given first. This is then further developed into a two-group energy problem, and ultimately into a continuous energy problem. Also discussed in chapter 3 is the detection of ^{239}Pu using a ^{239}Pu fission chamber and how this improves the response.

Chapter 4 describes the computations used to develop this transmission analysis method and perform scoping studies of the various filters. A simple fortran code was developed (Appendix A)
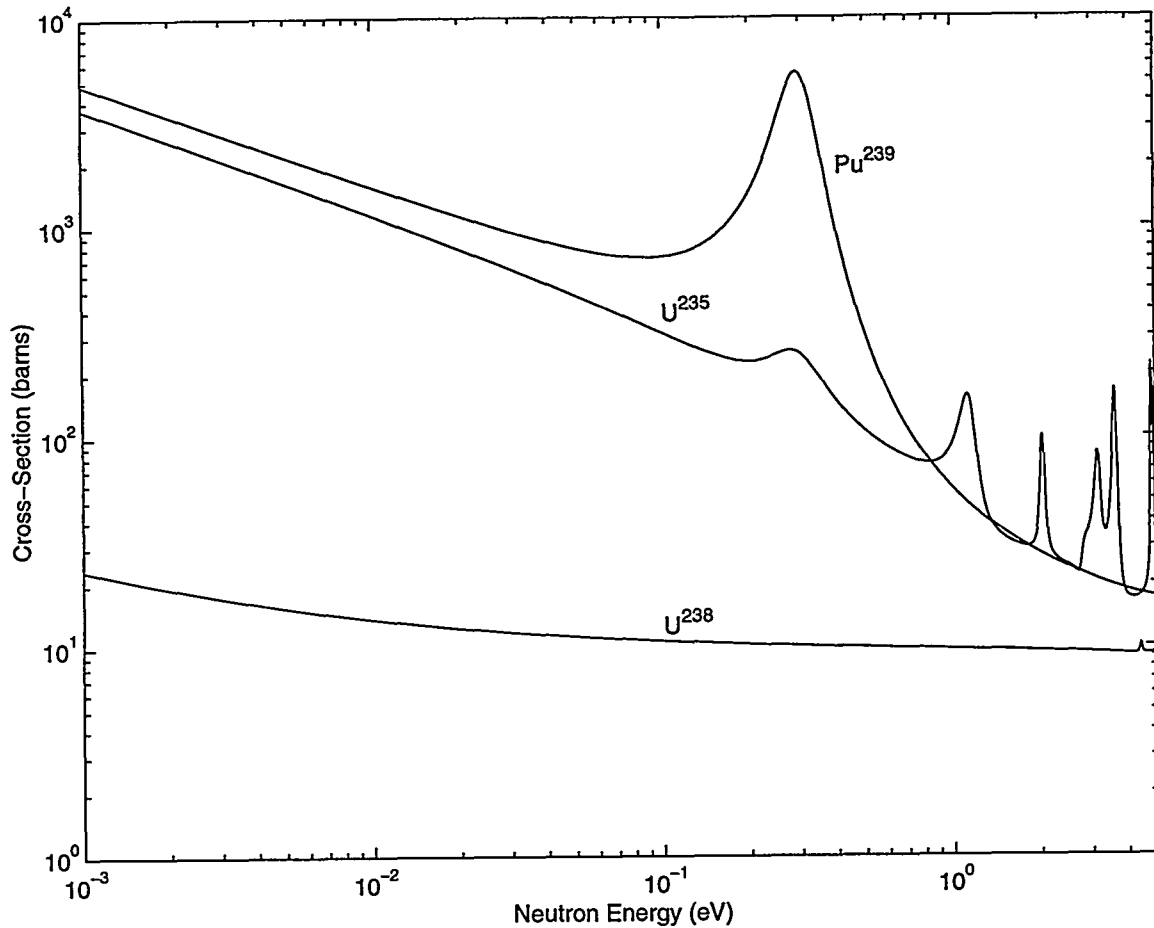
Figure 4: Total Cross-Sections of ^{239}Pu, ^{238}U, and ^{235}U

so that the transmission experiment could be modelled. This code was used to optimize the filter arrangement and study the spectral changes from the various filters and sample within the beam.

Experiments performed at the NRAD facility are discussed in Chapter 5. Included in this chapter are the experimental set up, equipment description, and the experiment plan. Details of the individual components -- such as the detectors, electronics, sample table, sample holders, collimator, and NRAD facility- are given in subsections of Chapter 5. Chapter 6 discusses the results of the experiments listed in Chapter 5 including background and noise reduction measurements, proof-of-principle measurements, and sample composition studies. Conclusions from these tests are included as Chapter 7.

2. Resonance Transmission Analysis

2.1. Resonance Properties

All isotopes, except some of the isotopes of lighter elements, exhibit sharp peaking or resonances in their cross-sections as a function of energy. An example is shown in Figure 5 for Pu^{239} (ref. 9). Figure 5 shows the cross-sections of Pu^{239} for elastic scattering, capture, and fission reactions over the energy range from 10 eV to 20 eV. It should be pointed out that this range is not the only energy range in which resonances occur. Resonances can occur below 10 eV and above 20 eV and do occur in both of these ranges for Pu^{239}. Note that the elastic scattering, capture, and fission reaction cross-sections all exhibit similarities in the energy dependence of the resonances. This is due to the resonance properties of the nuclide.

Neutron-nuclear interactions are typically categorized in two ways - interactions where the neutron interacts with the nuclear potential of the nucleus and interactions where the neutron is absorbed by the nucleus to form a compound nucleus. Potential scattering occurs when the neutron interacts with the nucleus such that the neutron scatters elastically off of the nuclear potential without ever penetrating the nucleus. These interactions are characterized by a relatively flat cross-section profile over the energy range from about 1 eV up to the MeV range (ref. 10).

On the other hand, if a neutron penetrates the nucleus and interacts with the nucleons, a compound nucleus is formed. Once a compound nucleus is formed, a complicated set of interactions occurs (refs. 11 and 12). All nuclei exhibit an energy level structure. There are bound energy levels corresponding to states of energy, E<0, and unbound or virtual energy levels corresponding to states of energy, E>0. These virtual levels are not described by any classical model. Considering the formation of the compound nucleus in collision kinematics, the energy available for an interaction is

$$E_C = \left(\frac{M}{m+M} \right) E \ , \tag{2}$$

where E_C is the energy of the neutron in the center of mass system, M is the mass of nucleus, m is the mass of the neutron, and E is the kinetic energy of the neutron in the laboratory system. The excited level of the compound nucleus also involves the increased binding energy due to the additional neutron, E_B. The probability of interaction is significantly increased if the combined energy, $E_C + E_B$, is very close to one of the virtual energy levels. Therefore, very sharp peaks or resonances are expected for compound nucleus reactions at those neutron energies where this energy matching occurs. The unstable compound nucleus subsequently decays by emitting an energetic particle which can be a neutron, proton, photon, alpha particle, or a combination of such particles. The eventual decay of the compound nucleus occurs essentially independent of the original mode of formation. Therefore, cross-sections for the different reactions exhibit a similar energy dependence. This is not to say that the cross-sections for the different reactions will be identical in

9
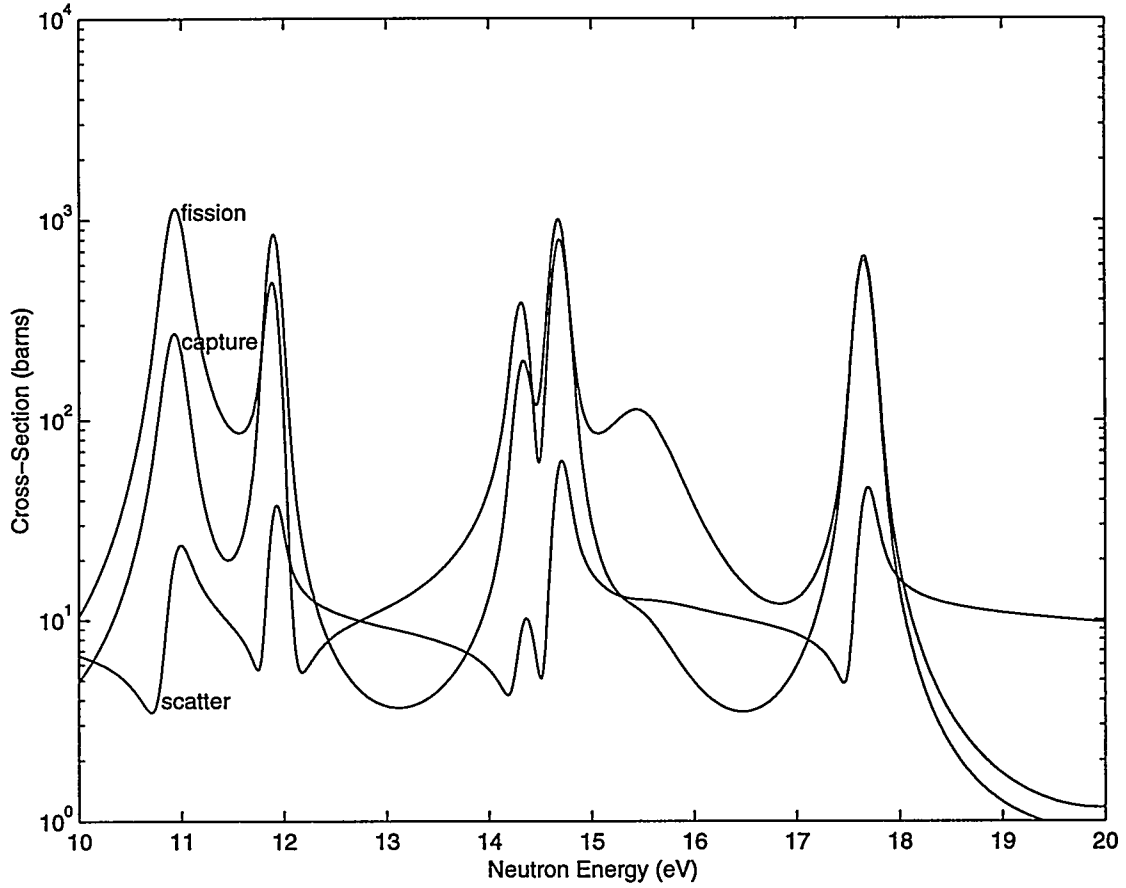
Figure 5: Cross-Sections for ^{239}Pu Exhibiting Resonances

magnitude but that resonances will occur at identical energies for all compound nucleus reactions for a given isotope.

The energy dependence of these resonances can be described by the Breit-Wigner single level resonance formula. The Breit-Wigner formula for absorption (ref. 10) is:

$$\sigma_y(E_C) = \sigma_0 \frac{\Gamma_\gamma}{\Gamma} \left(\frac{E_0}{E_C}\right)^{1/2} \frac{1}{1+y^2} , \tag{3}$$

with

$$y = \frac{2}{\Gamma} (E_C - E_0) , \tag{4}$$

10

$$\sigma_0 = 4\pi\lambda_0^2 \frac{\Gamma_n}{\Gamma} \frac{2J+1}{2(2I+1)} , \tag{5}$$

where Γ is the total width that characterizes the energy level and the full width at half maximum, Γ_γ is the radiative width characterizing the probability that the compound nucleus will decay via gamma emission, σ_0 is the value of the total microscopic cross-section at the resonance energy E_0, λ_0 is the reduced neutron wavelength at E_0, I is the nuclear spin of the target nucleus, and J is the spin of the compound nucleus. The Breit-Wigner formula for other compound nucleus reactions is similar, and is not discussed here.

Without going into detail, it is important to note that resonance cross-sections described by the Breit-Wigner formula are dependent on relative velocity between the neutron and nucleus. This relative velocity is affected by the thermal motion of the nucleus and the neutron which is directly related to the temperature of the system. As the temperature of the system increases, the resonance broadens and its peak magnitude decreases. Such cross-sections are said to be "Doppler-broadened" when they have been averaged over the distribution of nuclear velocities. A formalization of the effect of temperature on resonances is given by Bethe-Placzek (ref. 13). Doppler-broadening is mentioned here as it can have a significant effect on systems detecting resonances or relying on resonances as the analytical basis of the technique. The detectors and samples used in this experiment are maintained at room temperature such that Doppler-broadening does not impact the experimental results. Doppler-broadening would also not impact the measurement of actual blanket elements as long as the elements have a low heat generation rate such that the element temperature is not elevated significantly above room temperature.

2.2. Resonance Transmission Analysis Techniques

As discussed previously, isotopes exhibit resonances over a broad energy range which are unique to each individual isotope. Resonance transmission analysis focuses on these unique resonance properties to extract information about the sample being irradiated through a variety of different techniques. The techniques can be broadly divided into two categories based on whether the resonances that are being utilized are those of the detector or those of the sample. All of the techniques are non-destructive (the sample is maintained intact without damage for future analysis) and require a neutron beam to be transmitted through the sample. In order to obtain information utilizing individual resonances, spectral characteristics must be known or determined in some fashion. This is accomplished through several different techniques including filtering the neutron beam and the time-of-flight (TOF) technique.

The TOF technique is the most widely used method and is described in Section 2.2.2. The TOF technique has been used for temperature profiling, stress analysis, isotopic assay, and producing multiple radiographs (refs. 14-24). Relevant applications of the TOF technique are discussed briefly in Section 2.2.2.1 and Section 2.2.2.2.

Altering the spectrum of the neutron beam through a series of filters is the basis of the present research project. The technical basis for this filtering technique is discussed in Chapter 3. Simpler techniques have been employed for resonance radiography and spectral unfolding (refs. 25-27). These techniques are discussed briefly in Section 2.2.1.1 and Section 2.2.1.2.

2.2.1. Methods utilizing resonances of the detection material

2.2.1.1. Radiography

Neutron radiography is very similar to x radiography. Radiation is transmitted through the sample and the amount of the transmitted flux is recorded two-dimensionally. The neutrons transmitted through the sample interact with a thin activation foil. The foil is placed in contact with a piece of radiographic film, and the gamma emissions from radioactive decay of the foil expose the film. The film is then processed to observe a shadow image of the sample. The image of the sample shows changes in the attenuation properties of the material. For neutrons, changes in the optical density of the film are due to changes in the macroscopic total cross-section of the sample and the thickness of the sample.

Resonance radiography utilizes neutron interactions with materials at neutron energies that correspond to resonances of the converter material used to produce the radiograph or resonances of the sample material being radiographed. Thermal neutron radiography images hydrogen and a number of other materials with high absorption cross-sections without differentiating between them, whereas, resonance radiography has the capability of identifying various isotopes based on their unique resonances. Resonance radiography research to present has developed two methods of resonance radiography - the resonance foil method and the TOF method. The two methods involve different analysis techniques and are used for individualized applications. The resonance foil method is used to generate a single radiograph of a sample while the TOF method is used to produce multiple radiographs of individual isotopes within a sample. The TOF method is discussed in Section 2.2.2.1.

The resonance foil method is currently utilized at the ANL Neutron Radiography Reactor (NRAD) using Indium foils, with a resonance at 1.4 eV, to radiograph irradiated samples such as fuel elements and assemblies (ref. 25). The thermal neutron content of the beam is filtered by cadmium sheets placed in front of and behind the indium foil. Similar techniques have also been employed at other facilities (ref. 26).

2.2.1.2. Spectral analysis

Another technique which utilizes unique resonance properties of the detection material is spectral analysis using activation foils. Foils of different isotopes are activated in a neutron flux. The flux level is determined based on each foil. The flux values determined are different for each isotope due to the unique resonance properties of each foil. By comparing the differences in the flux values, information can be obtained about the spectrum. The description of the NRAD spectrum, used for the computations in Chapter 4, was generated by spectral unfolding (ref. 27).

12

2.2.2. Time-of-flight technique

The time-of-flight (TOF) technique is a unique method that integrates neutron counting in specified time intervals. The TOF technique involves pulsing the neutron source. The sample and detector are located at a considerable distance from the source (generally greater than 10 meters). This distance allows time intervals to be selected that correspond to a small range of neutron velocities. This velocity segmentation process generates a series of energy ranges since

$$E = \frac{1}{2}mv^2 \; , \tag{6}$$

where E is the energy of the neutron, m is the mass of the neutron, and v is the velocity of the neutron. A detector with fast timing is used to perform the neutron counting in each time interval (energy range). With the data segmented by energy, unique applications have been developed utilizing this spectral characterization of the data in conjunction with the unique resonance properties of the isotopes of the sample. Relevant applications where the TOF technique has been applied are briefly discussed in Section 2.2.2.1 and Section 2.2.2.2.

2.2.2.1. Multiple radiographs

The TOF technique has been used in various ways by several groups of researchers. The most straightforward application of the TOF technique has been to produce radiographs of specific isotopes in a sample. This allows a spatial determination of a given isotope that cannot be discerned through other radiographic techniques. One of the earliest demonstrations was performed at Argonne National Laboratory utilizing the Intense Pulsed Neutron Source (ref. 14). This early work radiographed overlapping gold and indium foils. Two images were obtained - one at 1.46 eV which corresponds to a resonance in ^{115}In and one at 4.91 eV which corresponds to a resonance in ^{197}Au.

The National Institute of Standards and Technology (NIST) has been involved in a wide-ranging neutron resonance radiography program (refs. 15 and 16). A sample of rhodium, tungsten, and gold was radiographed. The images of each element were clearly visible using the 1.26 eV resonance of ^{103}Rh, the 4.16 eV resonance of ^{182}W, and the 4.91 eV resonance of ^{197}Au. Remarkably, there was no interference among the images.

2.2.2.2. Isotopic assay

The TOF method has also been used to perform isotopic assays of samples based on the transmission analysis technique. The transmission analysis technique is performed by measuring the total transmission spectrum and then fitting the data to a sum of the transmission spectrum from each isotope of interest. The amount of each isotope is determined by finding the best fit to a prominent resonance of the isotope. Each isotope is fit in succession and the process is iterated until the isotopic abundances do not change between iterations. Transmission analysis has been used by se-

veral researchers (refs. 16, 21, 22, 23, and 24) mainly to determine the isotopic composition of spent fuel pellets.

Researchers at NIST have used transmission analysis for the assay of isotopes in fresh and spent nuclear fuel, nuclear waste, and for organic compounds (refs. 16, 21, 22, and 23). They were able to determine the relative abundance of ^{235}U and ^{238}U in fresh fuel samples to within 0.1%. In spent fuel tests, the effect of greater neutron flux at the axial center of the element was observed by a greater abundance of the heavier plutonium isotopes and the decrease in the relative abundance of ^{235}U. Extensive tests were also performed on waste container assaying. Researchers at NIST were able to detect 10 grams of ^{235}U in a 2 liter bottle containing simulated fly ash with an error of only 2.3%. In a 55 gallon drum, they were able to detect 10 grams of ^{235}U with an error of only 16%. Several tests were also performed on organic compounds to determine the abundance of hydrogen, carbon, nitrogen, and oxygen in a sample.

3. Theoretical Basis

The theoretical basis for resonance transmission analysis is described in the simplest case in Section 3.1 for a mono-energetic mono-directional beam impinging on a sample of uniform thickness. From here it is expanded into a problem with only two energy groups in Section 3.2. By dealing with two energy groups, the effect of the filters and detector start to be addressed. This then leads to the development of the continuous energy problem in Section 3.3. The chapter concludes with a discussion of the detector type and the benefit of using fissioning in ^{239}Pu as the detection reaction for measuring ^{239}Pu in a depleted uranium sample.

3.1. Mono-Energetic Problem

The simplest case to address for transmission analysis is a mono-energetic mono-directional beam impinging on a slab of uniform thickness. To address this case, the derivation of the microscopic cross-section is discussed first. This is then expanded for a slab of finite thickness.

Consider a mono-energetic mono-directional beam impinging on a thin sample. The sample is sufficiently thin such that no nuclei are shielded by other nuclei. In this case, the reaction rate in the sample is simply

$$R = \sigma \phi N_S \qquad (7)$$

where R is the reaction rate in reactions/cm^2-sec, σ is the microscopic cross-section in cm^2, ϕ is the neutron flux in neutrons/cm^2-sec, and N_S is the areal atomic density in atoms/cm^2. The microscopic cross-section is a constant of proportionality that characterizes the probability of an interaction between the neutron and nuclei in the sample.

The reaction rate, R, is for a thin sample and does not consider shielding of the sample nuclei by other sample nuclei. Consider a sample of finite thickness. A differential thickness, dx, is located at a distance x within the sample. Since dx is infinitesimally thin, the reaction rate within the thickness, dx, is

$$R = \sigma \phi(x) N_S = \sigma \phi(x) N dx \qquad (8)$$

where N is the density of atoms in the sample in atoms/cm^3. This reaction rate is identical to the one listed previously, noting that $N_S = N dx$.

Assuming that all reactions in the sample result in a neutron loss, the reaction rate can now be related to the decrease in the beam flux between x and x+dx, as

$$d\phi(x) = [\phi(x+dx) - \phi(x)] = -\sigma \phi(x) N dx \qquad (9)$$

15

where the spatial dependence of the flux has been noted. Rearranging the equation yields

$$\frac{d\phi(x)}{dx} = -\sigma_T N \phi(x) = -\Sigma_T \phi(x) \; , \tag{10}$$

where the macroscopic total cross-section has been introduced as $\Sigma_T = \sigma_T N$. This equation states that the change in the flux as a function of the depth in the sample is directly related to the reaction rate at that position. This equation can be solved by integrating over the thickness of the sample to obtain

$$\phi(x) = \phi(0) \, e^{-\Sigma_T x} \; , \tag{11}$$

where $\phi(0)$ is the flux incident on the slab of thickness t. $\phi(x)$ is considered the transmitted flux, such that the transmission through the sample is defined as

$$T = \frac{\phi(x)}{\phi(0)} = e^{-\Sigma_T x} \; . \tag{12}$$

The transmission is a unitless term which has a value between zero (no transmission) and one (complete transmission), and is an exponential function of the macroscopic cross-section and the sample thickness. A further variable, the mass signal, is defined as

$$M = -\ln(T) = \Sigma_T x \; , \tag{13}$$

which is a direct measure of the macroscopic cross-section since the sample thickness is assumed uniform.

By performing two measurements - one with the sample in place to determine $\phi(x)$ and one without the sample to determine $\phi(0)$ - the mass signal can be determined. With the mass signal and the sample thickness known, the macroscopic total cross-section for the sample can be obtained directly from the above equation. Assuming that the sample contains only ^{238}U and ^{239}Pu, the mass of ^{239}Pu can be determined from the total cross-section as

$$\Sigma_{TOT} = \sigma^{239} N^{239} + \sigma^{238} N^{238} \; , \tag{14}$$

where σ represents the microscopic cross-section for each isotope in barns, and N represents the atom density of each isotope in atoms/cm^3. The atom density, also known as the number density, is defined as

$$N = \frac{\rho N_A}{A} = \frac{m}{V} \frac{N_A}{A} \; , \tag{15}$$

16

where ρ is the density of the isotope in the sample in grams/cm^3, N_A is Avogadro's number of 6.022×10^{23} atoms/mole, A is the atomic mass of the isotope in grams/mole, m is the mass of the sample in grams, and V is the volume of the sample in cm^3. This leads to the following result for the macroscopic total cross-section,

$$\Sigma_{TOT} = \sigma^{239} \frac{m^{239}}{V} \frac{N_A}{239} + \sigma^{238} \frac{m^{238}}{V} \frac{N_A}{238}. \tag{16}$$

Therefore, with only two isotopes in the sample, such that $m = m^{238} + m^{239}$, the result is

$$\Sigma_{TOT} = \sigma^{239} \frac{m^{239}}{V} \frac{N_A}{239} + \sigma^{238} \frac{m - m^{239}}{V} \frac{N_A}{238}. \tag{17}$$

Knowing the total mass of the sample, the only unknown in the above equation is the mass of the ^{239}Pu. The equation can be rearranged to determine the mass of ^{239}Pu in the sample from the mass signal ($M = \Sigma_T x$) as

$$m^{239} = \frac{\dfrac{V}{N_A} \dfrac{M}{x} - \dfrac{\sigma^{238}}{238} m}{\dfrac{\sigma^{239}}{239} - \dfrac{\sigma^{238}}{238}}. \tag{18}$$

This assumes a mono-energetic beam, a mono-directional beam, no fission source from the sample, once a neutron is scattered it is lost, and the sample only contains ^{238}U and ^{239}Pu. Also, in order for this method to be sensitive to small changes in ^{239}Pu content in large amounts of ^{238}U, the microscopic cross-section for ^{239}Pu must be much larger than that for ^{238}U. This is the case for specific neutron energies where resonances occur in ^{239}Pu but not in ^{238}U as discussed previously.

Unfortunately, all of the assumptions are invalid to some extent for the blanket element in the NRAD beam. The beam is most certainly not mono-energetic and exhibits a spectrum which includes a thermal Maxwellian region, a 1/E region, and a fission region. The beam is not mono-directional but has a small angle of divergence. However, the beam is well collimated and the mono-directional assumption can be considered to be valid. The sample contains more than ^{238}U and ^{239}Pu, most notably ^{235}U, stainless steel cladding, and a sodium bond. In addition, there are traces of other actinides in the blanket. These other actinides will also be addressed in the analysis.

The effect of scattering losses and fission neutron interferences may or may not be valid depending on the set-up of the experiment. For a transmission experiment, only the total macroscopic cross-section is considered. This is valid if the solid angle of the detector is small

compared to 4π steradians. The solid angle of a detector is defined as

$$\Omega = \int_A \frac{\cos\alpha}{r^2} dA ,$$
(19)

where r is the distance between the source and a surface element dA, and α is the angle between the normal to the surface element and the source direction. For the common case of a point source located along the axis of a right circular cylindrical detector, the solid angle, Ω, is

$$\Omega = 2\pi \left(1 - \frac{d}{\sqrt{d^2 + a^2}} \right) ,$$
(20)

where d is the distance between the detector and the source and a is the radius of the detector. For the case when d $\gg$ a, the solid angle reduces to

$$\Omega \cong \frac{A}{d^2} = \frac{\pi a^2}{d^2} .$$
(21)

The other consideration for a transmission experiment is that the detector only count neutrons that pass through the sample (background excluded). This allows for the full effect of attenuation from the sample to be considered. If a portion of the beam that does not pass through the sample is detected, then the transmission and the mass signal will be skewed due to this direct beam. This means that the transmission will be over predicted and the mass signal (and conversely the mass of ^{239}Pu) will be under predicted.

There is a method to directly account for the energy spectrum of the beam known as flux averaging, which is performed by averaging the energy dependent cross-sections taking into account the flux spectrum. Flux averaging is defined mathematically as

$$\overline{\Sigma}_T = \frac{\int_E \Sigma_{TOT}(E)\phi(E)dE}{\int_E \phi(E)dE} .$$
(22)

Flux averaging is routinely performed when collapsing a continuous energy spectrum into energy groups for nuclear reactor analyses and is discussed further in Sections 3.2 and 3.3. In the grossest sense, the entire spectrum can be collapsed into one group (i.e. one value for each of the cross-sections of interest) which was effectively defined by the above analysis. Cross-sections typically become very similar among different materials when they are averaged over large energy ranges. This is due to the resonance properties of the isotopes. If two isotopes have similar resonances that

18

differ in energy and the cross-sections are averaged over an energy range that encompasses both resonances, the flux averaged cross-sections become similar. Imagine this occurring over an energy range that includes all of the resonances for the isotopes and it becomes apparent that flux averaging tends to make cross-sections for different isotopes similar.

When averaging the total microscopic cross-sections for ^{238}U and ^{239}Pu over the NRAD spectrum, the result is 20.2 and 271.5 barns, respectively. With these flux-averaged cross-sections, the difference in the mass signal is only 12.2 percent between a depleted uranium sample and a depleted uranium sample containing one weight percent ^{239}Pu. With this small of a change in the mass signal, this one-group approach could not be used for determining even smaller changes in ^{239}Pu content on the order of tenths of a weight percent with any reasonable accuracy. Performing the same exercise with cross-sections at 0.3 eV results in a 503 percent change in the mass signal between a depleted uranium sample and a depleted uranium sample containing one weight percent ^{239}Pu. This level of sensitivity is more amenable for the determination of smaller quantities of ^{239}Pu on the order of tenths of a weight percent or less.

3.2. Two-Group Problem

Because a mono-energetic neutron source that corresponds to the 0.3 eV resonance in ^{239}Pu is not available, spectral effects must be considered in the analysis. The next logical step is a spectrum composed of two different energies or energy groups. For this case, the continuous energy spectrum will be divided into two energy groups - group 1 containing neutrons with energies above 0.5 eV and group 2 containing neutrons with energies less than 0.5 eV. This arrangement is typically employed for a two group problem as group 1 represents the fast energy group and group 2 represents the thermal energy group. The boundary of 0.5 eV is chosen as it corresponds to the cadmium cutoff energy. Cadmium can be used as a filter to easily absorb neutrons at energies below this energy allowing neutrons above this energy to preferentially pass through the filter. This does not account for resonances which also preferentially absorb neutrons, however, for the time being these will be ignored. It is assumed for the sake of this two group analysis that the cadmium acts as a perfect filter media. The transmitted flux through an ideal filter can be treated with a Heaviside or unit step function, u(E-E$_c$) such that

$$\phi = \int_E \phi_0(E)\, u(E-E_c)\, dE\ , \tag{23}$$

where E$_c$ is the cutoff energy of the filter. This means that the transmitted flux through the filter is

$$\phi = 0 \qquad\qquad \textit{for } E<E_c\ ,\ \textit{and} \tag{24}$$

$$\phi = \int_E \phi_0(E)\, dE \qquad \textit{for } E>E_c\ . \tag{25}$$

19

With a cutoff energy of 0.5 eV, the cadmium filter absorbs all neutrons below 0.5 eV and allows all neutrons above 0.5 eV to pass through the filter.

A gadolinium filter is also employed to remove neutrons with energies below 0.1 eV. This filter remains in place during all of the measurements. This serves to perturb the spectrum by absorbing neutrons below 0.1 eV. By removing neutrons with energies less than 0.1 eV, the gadolinium filter serves two purposes. First, it defines the lower energy bound of the 0.3 eV resonance of ^{239}Pu. The energy of 0.1 eV corresponds to a valley in the cross-section of ^{239}Pu as was shown in Figure 4. Second, the gadolinium filter minimizes the effect on the mass signal from ^{235}U. ^{235}U has a large total cross-section at energies below 0.1 eV. By removing the neutrons that have energies less than 0.1 eV, the difference between the cross-sections of ^{239}Pu and ^{235}U is increased. This allows the mass signal to be more sensitive to changes in ^{239}Pu content than ^{235}U content. In effect, this means that energy group 2 contains neutrons with energies between 0.1 eV and 0.5 eV, and energy group 1 contains neutrons with energies greater than 0.5 eV. These filters were chosen such that energy group 2 (from 0.1 eV to 0.5 eV) contains the 0.3 eV resonance in ^{239}Pu. Therefore, by only considering the transmission through group 2, the difference in cross-sections between ^{238}U and ^{239}Pu should be larger than when the cross-sections were averaged over all energies, and hopefully, will approach the difference between the cross-sections at 0.3 eV.

To develop the two-group problem, the continuous energy flux is integrated over the energy ranges discussed above as

$$\phi = \int_{0}^{0.1\,eV} \phi(E)\,dE + \int_{0.1\,eV}^{0.5\,eV} \phi(E)\,dE + \int_{0.5\,eV}^{\infty} \phi(E)\,dE , \qquad (26)$$

such that

$$\phi = \phi_1 + \phi_2 . \qquad (27)$$

The total macroscopic cross-sections are flux averaged in each of the two groups as

$$\overline{\Sigma_{TI}} = \frac{\int_{0.5\,eV}^{\infty} \Sigma_T(E)\,\phi(E)\,dE}{\int_{0.5\,eV}^{\infty} \phi(E)\,dE} , \qquad (28)$$

and

$$\overline{\Sigma_{T2}} = \frac{\displaystyle\int_{0.1\,eV}^{0.5\,eV} \Sigma_T(E)\,\phi(E)\,dE}{\displaystyle\int_{0.1\,eV}^{0.5\,eV} \phi(E)\,dE} \quad . \tag{29}$$

As in the mono-energetic case, the transmission, T, will be determined. Only the transmission for energy group 2 is of interest. As before, the transmission is defined as the transmitted flux divided by the incident flux such that

$$T_2 = \frac{\phi_2(x)}{\phi_2(0)} \; ., \tag{30}$$

where, as in the mono-energetic problem, the transmitted flux is simply

$$\phi_2(x) = \phi_2(0)\,e^{-\overline{\Sigma_{T2}}x} \; . \tag{31}$$

The variable x denotes the thickness of the sample. Unfortunately, $\phi_2(x)$ and $\phi_2(0)$ are not directly measurable quantities as the energies of neutrons in the beam are not only contained in the energy region from 0.1 to 0.5 eV. This is where the positioning of the cadmium filter and sample come into effect. With the sample and cadmium filter removed from the beam, the flux at the detector is

$$\phi_{NS-NF} = \phi_1(0) + \phi_2(0) \; . \tag{32}$$

This states that the flux at the detector when there is no sample and no cadmium filter in the beam (NS-NF subscript) is the sum of the initial fluxes in groups 1 and 2. The energy dependence of the detector is not included in the discussion. The effect of the detector response will be discussed later is Section 3.4. ϕ_{NS-NF} is a measurable quantity. Another measurement can be performed by placing the cadmium filter in the beam. Assuming an ideal filter, the flux at the detector is

$$\phi_{NS-F} = \phi_1(0) \; ., \tag{33}$$

since the neutrons in group 2 were removed by the filter. Subtracting the filtered flux from the unfiltered flux yields

$$\phi_{NS-NF} - \phi_{NS-NF} = \phi_2(0) \; . \tag{34}$$

By performing these two measurements, the initial flux in group 2 is obtained. Performing two more measurements with the sample in place yields

21

$$\phi_{S-NF} = \phi_1(0) \, e^{-\overline{\Sigma_{T1}}x} + \phi_2(0) \, e^{-\overline{\Sigma_{T2}}x} \text{ , and} \tag{35}$$

$$\phi_{S-F} = \phi_1(0) \, e^{-\overline{\Sigma_{T1}}x} \text{ .}$$

Subtracting the filtered flux from the unfiltered flux with the sample in place yields

$$\phi_{S-NF} - \phi_{S-F}(x) = \phi_2(0) \, e^{-\overline{\Sigma_{T2}}x} \text{ .} \tag{37}$$

By performing these two measurements, the transmitted flux in group 2 is obtained. Therefore, the transmission for group 2 can be defined as

$$T_2 = \frac{\phi_{S-NF} - \phi_{S-F}}{\phi_{NS-NF} - \phi_{NS-F}} = e^{-\overline{\Sigma_{T2}}x} \text{ . .} \tag{38}$$

The mass signal can be obtained from the transmission as

$$\tag{39}$$

The result is identical to the mono-energetic case except that the cross-section has been flux-averaged over the energy range from 0.1 eV to 0.5 eV. This means that, with adequate knowledge of the flux in this energy range such that the cross-sections can be properly flux-averaged, the mass of ^{239}Pu in the sample can be directly determined from the four measurements described above.

As before, this assumes that the sample only contains ^{238}U and ^{239}Pu. The sample will also have stainless steel, sodium, a small amount of ^{235}U, a small amount of other heavy metal isotopes, a smaller amount of fission products, and some tramp elements. Therefore, the total mass of the sample is

$$m = m^{239} + m^{238} + m^{235} + m^{SS} + m^{Na} + m^{FP} + m^{Tramp} \text{ .} \tag{40}$$

There are several ways to address the various terms. First, the amount of ^{239}Pu and ^{238}U are unknown. The cross-section for ^{235}U in the energy region from 0.1 to 0.5 eV is significant so this term will be left unchanged. It is assumed that the ^{235}U content does not significantly change from irradiation. In chapter 4, it will be demonstrated that the change in ^{235}U content with irradiation is so small that the mass can be treated as constant. The remaining terms can be lumped into one such that the macroscopic cross-section becomes

$$\Sigma = \sigma^{239}N^{239} + \sigma^{238}N^{238} + \sigma^{235}N^{235} + \sigma^{other}N^{other} + \sigma^{Na}N^{Na}$$
$$+ \sigma^{HM}N^{HM} + \sigma^{FP}N^{FP} + \sigma^{Tramp}N^{Tramp} \quad .. \tag{41}$$

The lumped term contains numerous isotopes some of which can have large microscopic cross-sections in the energy range from 0.1 to 0.5 eV. However, this lumped term can be neglected as long as the macroscopic cross-section for the lumped term is small compared to the total macroscopic cross-section. This will be the case for insignificant quantities of isotopes regardless of microscopic cross-section, such as fission product poisons. This will also be true for isotopes with small microscopic cross-sections in this energy range that have significant mass, such as the sodium bond and cladding. Another issue is that some of the heavy metals can have significant spontaneous neutron sources, most notably ^{240}Pu and several Cm isotopes, which could potentially affect the results. However, considering the small solid angle of the detector, the isotropy and high energy of the fission neutrons emitted, and the relatively small amounts of these isotopes, these can also be neglected as insignificant.

If the microscopic total cross-sections are flux averaged over the energy range from 0.1 eV to 0.5 eV the results are 242.7 barns for ^{235}U, 1498.4 barns for ^{239}Pu, and 10.4 barns for ^{238}U. Using these values, there is a 135 percent change in mass signal between a depleted uranium sample and a depleted uranium sample containing one weight percent ^{239}Pu. This is reasonable, but, it is still significantly less than the 503 percent difference in mass signal possible using cross-sections under the peak of the resonance (0.3 eV). The response can be further enhanced by considering the detector response as described in Section 3.4.

In theory, with flux averaging over these two groups, the series of four measurements could be performed on a sample and the amount of ^{239}Pu could be calculated directly from the mass signal. In practice, the filters are not ideal such that the transmission calculation is not as simple as the two-group problem. Because the filter materials have resonances and do not have a distinct cutoff energy, the transmission must consider the continuous energy spectrum.

3.3 Continuous Energy Problem

The continuous energy problem is an expansion of the method described in Section 3.2 for the two energy group problem. The difference is in the treatment of the filters. In the two energy group problem, the filters were treated as ideal. As discussed before, the transmitted flux through a filter is

$$\phi = \int_E \phi_0(E) \, u(E-E_c) \, dE , \tag{42}$$

where E_c is the cutoff energy of the filter. For the continuous energy problem, the transmitted flux through a filter is treated as

$$\phi = \int_E \phi_0(E) e^{-\Sigma_T(E)x} dE , \qquad (43)$$

where Σ_T is the macroscopic total cross-section of the filter, x is the thickness of the filter, and ϕ_0 is the flux incident on the filter.

As in the two-group problem, the flux at the detector will be developed for each combination of filter and sample position. First, without the sample or filters in the beam the flux at the detector is simply

$$\phi = \int_E \phi_0(E) dE . \qquad (44)$$

The gadolinium filter is placed in the beam and the transmitted flux at the detector becomes

$$\phi_{NS-NF} = \phi = \int_E \phi_0(E) e^{-\Sigma_G(E)x_G} dE , \qquad (45)$$

where Σ_G is the macroscopic total cross-section of the gadolinium filter and x_G is the thickness of the gadolinium filter. There is no sample or cadmium filter in the beam, so $\phi_{NS-NF}=\phi$. The cadmium filter is placed in the beam for the second measurement such that the flux at the detector is

$$\phi_{NS-F} = \int_E \phi_0(E) e^{-\Sigma_G(E)x_G-\Sigma_C(E)x_C} dE , \qquad (46)$$

where Σ_C is the macroscopic total cross-section of the cadmium filter and x_C is the thickness of the cadmium filter. The sample is then added for the last two measurements as before, so that

$$\phi_{S-NF} = \int_E \phi_0(E) e^{-\Sigma_G(E)x_G-\Sigma_S(E)x_S} dE , \quad and \qquad (47)$$

$$\phi_{S-F} = \int_E \phi_0(E) e^{-\Sigma_G(E)x_G-\Sigma_C(E)x_C-\Sigma_S(E)x_S} dE , \qquad (48)$$

where Σ_S is the macroscopic total cross-section of the sample and x_S is the thickness of the sample. The equations for the flux at the detector involve numerous terms that are energy dependent so that flux averaging cannot be performed to obtain a simple exponential term for the transmission.

24

However, assume that the transmission can be calculated as before,

$$T = \frac{\phi_{S-NF} - \phi_{S-F}}{\phi_{NS-NF} - \phi_{NS-F}} = e^{-\overline{\Sigma_{T2}}x} .$$

(49)

Substituting the previous expressions for the four measurement cases yields

$$T = \frac{\int_E \phi_0(E)\, e^{-\Sigma_G(E)x_G - \Sigma_C(E)x_C - \Sigma_S(E)x_S}dE \;-\; \int_E \phi_0(E)\, e^{-\Sigma_G(E)x_G - \Sigma_C(E)x_C - \Sigma_S(E)x_S}dE}{\int_E \phi_0(E)\, e^{-\Sigma_G(E)x_G}dE \;-\; \int_E \phi_0(E)\, e^{-\Sigma_G(E)x_G - \Sigma_C(E)x_C}dE} .$$

(50)

This quotient of integrals is complex and cannot be easily examined to explore trends in the transmission based on changes in the various parameters. However, if the limits of integration are diminishingly small such that the problem represents a mono-energetic problem the result is

$$T = \frac{\phi_0\, e^{-\Sigma_G x_G - \Sigma_S x_S} - \phi_0\, e^{-\Sigma_G x_G - \Sigma_C x_C - \Sigma_S x_S}}{\phi_0\, e^{-\Sigma_G x_G} - \phi_0\, e^{-\Sigma_G x_G - \Sigma_C x_C}} ,$$

(51)

which can be simplified to

$$T = e^{-\Sigma_S x_S} ,.$$

(52)

This is simply the mono-energetic transmission through a sample as developed in Section 3.1. The transmission for the two energy group problem cannot be derived from the continuous energy solution without treating the filters as ideal. If the filters are treated ideally, the equation for the transmission will collapse to the solution for the two-group problem.

The only way to calculate the transmission for the continuous energy case is to use computer modelling in continuous energy or in multi-group format. A code was written to perform these calculations in multi-group format (11099 groups) with Monte-Carlo sampling for the transmission through the sample. This code is discussed in Chapter 4 as it was used primarily for the sensitivity studies. The code determined the total flux at the detector for a depleted uranium sample and a depleted uranium sample containing one weight percent of ^{239}Pu. The result was a 55 percent difference in the mass signal between the two samples. This is much less than the result for the two-group problem (135% difference in the mass signal); a decrease in the response was expected, although the magnitude of the decrease was much larger than anticipated. The decrease is due to the effect of the filters. In the two-group case, the filters were treated ideally. In the continuous energy case, the attenuation through the filters was treated as a function of energy. In addition, there is no

25

distinct cutoff energy associated with each filter due to the energy dependence of the cross-sections for the filter materials. These effects resulted in contributions to the signal from neutrons not within the energy range from 0.1 to 0.5 eV. These contributions resulted in the reduced response. However, there is a method to further improve the system response based on the detector response function, which is discussed in Section 3.4.

The continuous energy solution has been included here merely to show the complex nature of the neutron transport and that in reality the composition could not be directly calculated from one series of measurements without a calibration curve to account for the combination of these numerous terms into one equation.

The approach to be used is to compare the value of the transmission to those from a calibration curve of response versus the amount of ^{239}Pu in the element. A response function can be generated from continuous energy computations to express the ^{239}Pu content as a function of the mass signal. By performing a series of measurements on samples with known amounts of ^{239}Pu, a calibration curve can be generated that relates the amount of ^{239}Pu to the mass signal computed from the measurements. These measurements are performed to confirm the results from the calculations and to determine the bias in the measurement system. By measuring the mass signal from an unknown sample, the amount of ^{239}Pu can then be determined from the calibration curve. This approach is more practical than calculating the ^{239}Pu content directly from a given measurement. As discussed above, the method of calculation is not simple due to numerous materials present in the sample, uncertainties in the sample thickness x, uncertainties in the flux levels, and errors associated with the measurements and other parameters in the calculations.

3.4. Detector Response

The mono-energetic, two-group, and continuous energy solutions previously developed did not account for the energy dependent response of the detector. The neutrons reaching the detector will have to interact with the detector to be recorded. For a given energy, the response of the detector can be defined as

$$C = \epsilon_C \phi \Sigma_D V = \epsilon_C \phi \sigma_D N V ,\tag{53}$$

where C is the detector response expressed as a count rate, Σ_D is the macroscopic neutron cross-section of the detector for the interaction being recorded by the detector, ϕ is the flux at the detector, σ_D is the microscopic neutron cross-section of the detector, N is the atom density of the detector material, and ϵ_C is the collection efficiency of the detector. Note that ϵ_C is a collection efficiency based on neutrons interacting with the detector, i.e. an interaction occurs in the detector and this is the probability that it will be recorded. This is generally close to unity for fission chambers with thin deposits. Accounting for the energy dependence of the flux and the detector cross-section, the count rate is

$$C = B \int \sigma_D(E)\phi(E) \ dE ,\tag{54}$$

26

where B is a constant which is equal to

$$B = \epsilon_c N V t .$$

$$(55)$$

The detector response can then be combined with the definitions of the flux at the detector from the four measurements, such that the transmission becomes

$$T = \frac{\int\limits_E \phi_0(E)\, \sigma_D(E)\, e^{-\Sigma_G(E)x_G - \Sigma_S(E)x_S} dE \;-\; \int\limits_E \phi_0(E)\, \sigma_D(E)\, e^{-\Sigma_G(E)x_G - \Sigma_C(E)x_C - \Sigma_S(E)x_S} dE}{\int\limits_E \phi_0(E)\, \sigma_D(E)\, e^{-\Sigma_G(E)x_G} dE \;-\; \int\limits_E \phi_0(E)\, \sigma_D(E)\, e^{-\Sigma_G(E)x_G - \Sigma_C(E)x_C} dE} .$$

$$(56)$$

Notice that although the cross-section of the detector appears in every term of the equation, it cannot be reduced from the equation since it is an energy dependent function. The constant, B, appears in all terms and was cancelled from the equation. Because the transmission equation is too cumbersome to manipulate easily and the detector cross-section appears in each term, consider only one term at a time. The count rate when there is no sample and no cadmium filter in the beam is

$$C_{NS-NF} = B \int\limits_E \sigma_D(E)\,\phi_0(E)\, e^{-\Sigma_G(E)x_G - \Sigma_S(E)x_S} dE .$$

$$(57)$$

Simplifying this equation by grouping several terms together yields

$$C_{NS-NF} = \int\limits_E \sigma_D(E)\, A(E)\, dE ,$$

$$(58)$$

where

$$A(E) = B\,\phi_0(E)\, e^{-\Sigma_G(E)x_G} dE .$$

$$(59)$$

To explore the response due to the detection cross-section, assume that A(E) is constant. It is immediately apparent that the count rate will be heavily weighted to the energies where the detection cross-section is large such as at thermal energies and at energies corresponding to resonances. Since the energy region of most interest for this experiment is 0.1 to 0.5 eV, the detector should have a large cross-section in this region and much smaller cross-section at other energies. ^{239}Pu is ideally suited for this application as it has a resonance at 0.3 eV. This was expected since the experiment is based on isolating this resonance. A similar result is obtained for the measurement without the sample but with the cadmium filter in the beam. The point being made is that for the two measurements without the sample in place, ^{239}Pu is an ideal choice for the detector material.

27

Consider the two measurements when the sample is placed the beam. The count rate for the case without the cadmium filter is

$$C_{S-NF} = B \int_E \sigma_D(E)\,\phi_0(E)\,e^{-\Sigma_G(E)x_G - \Sigma_s(E)x_s}\,dE \; ,.$$

(60)

Simplifying this equation by grouping several terms together yields

$$C_{S-NF} = \int_E \sigma_D(E)\,A(E)\,e^{-\Sigma_s(E)x_s}\,dE \; .,$$

(61)

where A(E) was defined previously. Again it is assumed that the A(E) term is constant. The attenuation from the sample is included in the remaining energy dependent function.

Consider three possibilities for the effect of the detection reaction on the count rate. First, the detector uses the same reaction or a similar reaction for detection as the reaction being detected (i.e. the detector is based on the ^{239}Pu fission cross-section for the detection of ^{239}Pu reactions in the sample). Second, the detection reaction does not depend on energy such that σ_D is constant. Third, the detection reaction is counter to the reaction being detected such that the detector has a high probability of interaction when the ^{239}Pu cross-section is low and vice-versa. This case can be idealized as

$$\sigma_D(E) = \frac{1}{\sigma_T^{239}(E)} \; .$$

(62)

The second and third detector response functions were chosen as extreme cases to explore the effect on the response due to the detection cross-section. In reality, detectors based on these response functions are not possible, although, a response function approaching a flat response can be obtained.

Figure 6 demonstrates the effect of these three cases as a function of the total microscopic cross-section of the sample. The normalized response,

$$R = \sigma_D\,e^{-\sigma N x} \; ,$$

(63)

which is simply the normalized count rate without including the A(E) term, is plotted for the three cases. Realistic values for the blanket elements were used to generate the data shown in Figure 6. The sample thickness was assumed to be 1.1 cm. The density of the ^{239}Pu was assumed to be 0.19 g/cc, which corresponds to approximately one weight percent of ^{239}Pu in a depleted uranium sample (ρ=18.9 g/cc).

28
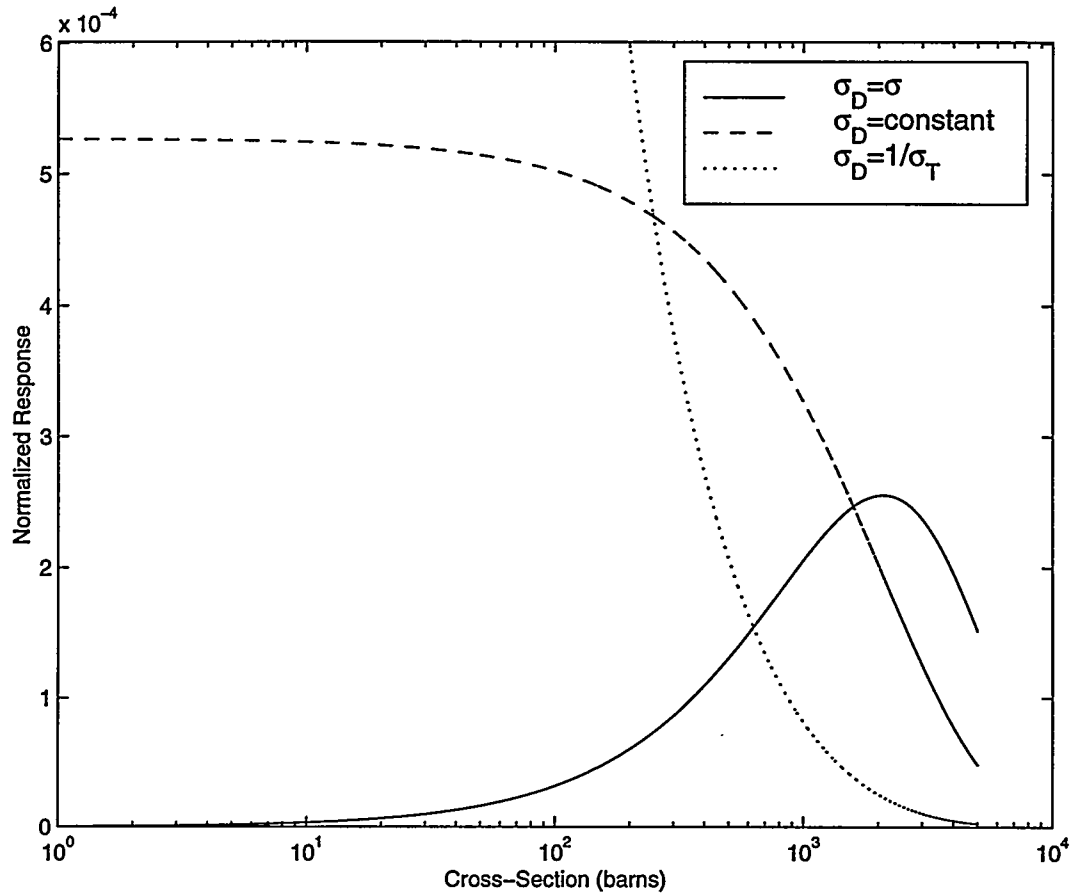
Figure 6: Detector Response Based on Detection Cross-Section

The first case, which represents similar detection and sample cross-sections, is shown as $\sigma_D = \sigma$. The transmission peaks between 2000 to 3000 barns and drops off below 1000 barns. This is close to ideal for emphasizing the effect of the resonances. The response is enhanced when the cross-section is high and is minimized when the cross-section is low.

The second case, which represents a constant detector cross-section, is shown as σ_D=constant. This curve shows a fairly flat response for sample cross-sections less than 100 barns and drops off above 100 barns. The response is much lower above 1000 barns compared to the levels below 100 barns. This is as expected and shows the exponential attenuation of the sample in the equation for the response.

The third case, which represents a detector cross-section profile that is opposite to that of ^{239}Pu, shows an extreme decline in response with increasing cross-section and is directly counter to detecting the neutron transmission through resonances. Responses for this case favor energies where the cross-sections are low.

Reviewing the three cases plotted in Figure 6, it is apparent that the case where the detection cross-section is identical or similar to the cross-section of the isotope being detected is ideal. For a transmission experiment, it is desirable to have a large cross-section for the isotope being detected, such as the case for ^{239}Pu in the energy range from 0.1 to 0.5 eV. This facilitates large changes in response for small changes in the ^{239}Pu content, i.e. it maximizes the sensitivity of the measurement. Because the beam is highly attenuated in this energy region compared to other energy regions where the cross-section is lower, it is desirable to have a detector with a high cross-section for interaction in this energy region and lower cross-section elsewhere. The ^{239}Pu cross-section is best suited for the detection media. This is due to the multiplication of the probabilities. If the detection cross-section is similar to the sample cross-section then the probability of transmission through the sample is multiplied by the probability of interaction in the detector. So the difference in response among groups with low cross-sections and high cross-sections becomes extreme. This can be demonstrated by an example. As defined previously, the normalized response at a given cross-section is

$$R(\sigma) = \sigma_D e^{-\sigma Nx} \quad . \tag{64}$$

Comparing the ratio of the response for cross-sections of 1000 barns and 10 barns with the three different detection response functions yields:

for σ_D = constant

$$\frac{R(1000)}{R(10)} = \frac{e^{-1000Nx}}{e^{-10Nx}} = e^{-990Nx} \quad , \tag{65}$$

for $\sigma_D = \sigma$

$$\frac{R(1000)}{R(10)} = \frac{1000 \, e^{-1000Nx}}{10 \, e^{-10Nx}} = 100 \, e^{-990Nx} \quad , \tag{66}$$

and for $\sigma_D = 1/\sigma$

$$\frac{R(1000)}{R(10)} = \frac{\dfrac{1}{1000} e^{-1000Nx}}{\dfrac{1}{10} e^{-10Nx}} = \frac{1}{100} e^{-990Nx} \quad . \tag{67}$$

The ratio when the detection cross-section is similar to the reaction being detected, is 100 times larger than when the detection cross-section is constant. The difference is due to the ratio of the detection cross-sections (1000/10 = 100). This demonstrates that detection with the same isotope

Table 1: Mass Signal Estimates for Idealized Cases*				
Case	Depleted Uranium Sample	1 wt% ^{239}Pu in Sample	ΔM	ΔM (%)
One Energy Group	1.077	1.208	0.131	12.2%
Two Energy Groups Idealized Filters	0.575	1.353	0.778	135.3%
Continuous Energy σ_D=constant	0.554	0.857	0.303	54.7%
Continuous Energy with ^{239}Pu detector	0.565	1.827	1.262	223.4 %
Mono-Energetic (0.3 eV)	0.565	3.406	2.841	502.8 %

*These cases assume a slab sample of 1.1 cm which is the diameter of the depleted uranium rod in a blanket element. Effects from cladding and bond sodium were neglected.

to be detected will be weighted to neutron energies with larger cross-sections by a factor of σ, and detection by other isotopes will have a lower weighting. Therefore, the response will be more sensitive to changes in those groups with higher cross-sections.

This result was based on assuming a constant value for A(E). Most notably, the flux is not constant and exhibits a strong dependence on energy. Because of this energy dependence, the direct benefit from a ^{239}Pu detector cannot be calculated analytically. To determine the benefit, the continuous energy problem was considered in full detail. Table 1 highlights the change in mass signal between a depleted uranium sample and a depleted uranium sample containing one weight percent of ^{239}Pu for the mono-energetic, one-group, two-group, and continuous energy problems described in Sections 3.1 through Section 3.3. Also shown in Table 1 is the change in mass signal for the continuous energy problem when the detector response is included. The results listed in Table 1 clearly show a marked improvement when a ^{239}Pu detector is used compared to a detector with a constant detector response. The benefit of the ^{239}Pu detector is a 317 percent increase in response over the continuous energy case with a constant detector cross-section. Also, it is 62 percent better than the two-group case with idealized filters. The response for the continuous energy case with the ^{239}Pu detector is large, although, it is not nearly as large as the mono-energetic (0.3 eV) case. However, it is still a large enough change in response to clearly indicate that small variations in the ^{239}Pu content can be detected. Assuming a 2% error in the measurement technique, it appears feasible to be able to determine changes in the ^{239}Pu content on the order of 0.02 weight percent of ^{239}Pu in a blanket element.

4. Computational Results

The theoretical basis was described in Chapter 3. For the cases discussed, gross assumptions were made regarding the filter effects, beam characteristics, and sample characteristics. Computer modelling was performed to determine if this filtered resonance transmission analysis technique is feasible for the determination of the ^{239}Pu content in a blanket element.

A Fortran code was written to model the continuous energy transmission problem using multi-group theory. The computer model and results are presented in Section 4.1. Using the transmission code, sensitivity studies of the cadmium filter thickness, gadolinium filter thickness, sample composition, beam diameter, and sample thickness were performed. The results are detailed in Section 4.2. The chapter concludes with a discussion of the error analysis for the transmission measurements in Section 4.3.

4.1 Transmission Calculations

The transmission model is described in Section 4.1.1 and the code is shown in Appendix A. Results based on the transmission code for the mass signal as a function of ^{239}Pu content in the sample are shown in Section 4.1.2.

4.1.1. Transmission model

In Section 3.3, the transmission was derived from a continuous energy spectrum based on four measurements with different sample and cadmium filter combinations. This derivation could not be solved analytically due to the complexity of the equation. Two different approaches can be used to solve this equation - deterministic methods or Monte Carlo techniques. Monte Carlo techniques do not solve the explicit equation but obtain answers by simulating individual particles and tracking the aspects of these particles. The average behavior of particles is then inferred from the average behavior of simulated particles. Deterministic methods solve the Boltzmann transport equation for the average particle behavior.

The transmission code is a hybrid of the two approaches. A multi-group approach is used with the continuous energy spectrum divided into 11099 groups. The cross-sections and flux are averaged over each group. The transmitted flux through the filters and sample for each energy group is treated as an exponential function as discussed in Chapter 3. The detector response in each group is calculated and the total detector response is computed as the sum of the detector responses for all the energy groups. The total detector response is calculated for each of the four measurements with different sample and cadmium filter combinations. These responses are then used to compute the transmission and mass signal for the sample. The Monte Carlo technique is introduced for the transmission through the sample. For a sample with uniform thickness, the multi-group approach would not require Monte Carlo sampling as each equation for the transmitted flux could be solved deterministically assuming no scattering contribution or fission source contribution to the detector response. However, for a blanket element the transmission length of the sample is not constant and

depends on the distance from the axis of the blanket element. If a neutron passes through the centerline of the element the transmission length will be the diameter of the element, but if the neutron does not pass through the centerline the transmission length can be much less. The total transmitted flux through the sample is the sum of all of the neutrons passing through the sample regardless of transmission length. Rather than solving for the average transmission length based on the sample diameter and beam diameter, Monte Carlo sampling is employed.

The multi-group approach requires a knowledge of the spectral shape of the flux. The flux profile is collapsed from the continuous energy spectrum into energy groups. Cross-sections are flux averaged over each energy group as described in Chapter 3. The multi-group solution, since it is based on a priori knowledge of the flux, is only as good as the flux knowledge and cross-section data provided. The spectrum for the NRAD beam was derived from results of flux mapping experiments by Imel and Urbatsch (ref. 27). The spectrum is characterized in three different energy regions:

for E < 0.175 eV (Maxwellian region)

$$\phi(E) = C_1 E e^{\left(-\frac{E}{kT}\right)}, \tag{68}$$

for 0.175 eV < E < 100 keV (1/E region)

$$\phi(E) = \frac{C_2}{E}, \quad and \tag{69}$$

for E > 100 keV (fission spectrum)

$$\phi(E) = C_3 e^{-1.036 \cdot 10^{-6} E} \sinh\left(\sqrt{2.29 \cdot 10^{-6} E}\right), \tag{70}$$

where E is the neutron energy in eV, kT=0.03 eV, C_1=1.1320x10^{11}, C_2=1.1140x10^7, and C_3=1.8019x10^2. The spectrum is shown graphically in Figure 7. These equations were used to define the 11099 spectral groups. The energy group structure is shown in Table 2. This allowed for a detailed description of the continuous energy spectrum at energies less than 300 eV. For practical purposes this fine group solution can be treated as a continuous energy solution.

The code allows the user to input the thickness and density of the gadolinium filter, the thickness and density of the cadmium filter, the sample type (slab or rod), the half-thickness (or radius) of the sample, the composition and density of the sample (^{235}U, ^{238}U, and ^{239}Pu weight percent), the radius of the beam incident on the sample, the detector thickness, and the number of neutron histories to run. The code uses cross-section data which were collapsed using the NRAD spectrum from the evaluated nuclear data file ENDF/B-VI (Ref. 9). Effects from the cladding, bond sodium, and tramp elements were neglected.
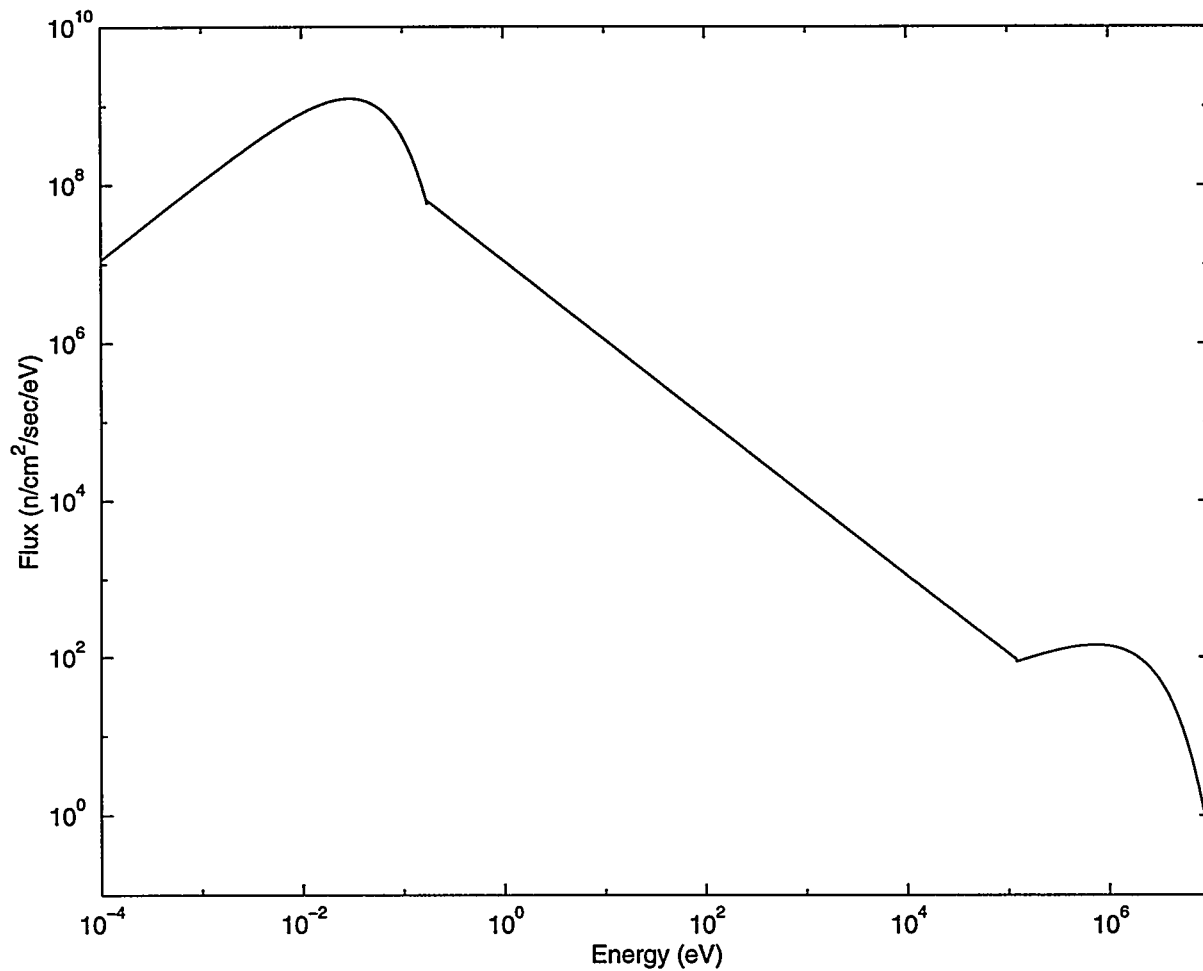
Figure 7: NRAD Spectrum

Table 2: Energy Group Structure		
Energy Range	Group Width	Number of Groups
0.00001 eV - 0.001 eV	0.001 eV	1
0.001 eV - 0.01 eV	0.009 eV	1
0.01 eV - 80.0 eV	0.01 eV	7999
80.0 eV - 300 eV	0.1 eV	2200
300 eV - 1 keV	1.0 eV	700
1 keV - 10 keV	1 keV	9
10 keV - 1 MeV	10 keV	99
1 MeV - 10 MeV	100 keV	90
Total		11099

Table 3: Mass Signal Estimates from Calculations		
^{239}Pu Composition (wt %)	Transmission	Mass Signal
0	0.584	0.538
0.25	0.405	0.905
0.5	0.293	1.229
0.75	0.221	1.508
1	0.173	1.756
1.25	0.139	1.972
1.5	0.116	2.156
1.75	0.098	2.327
2	0.084	2.473

4.1.2. Results

The initial model included a 0.01 cm (0.004 inches) gadolinium filter and a 0.1 cm (0.04 inches) thick cadmium filter. The sample was treated as a rod with a radius of 0.550 cm. The ^{235}U content of the sample was 0.2 weight percent. The diameter of the beam was 0.556 cm (0.21875 inches), which is slightly larger than the radius of the depleted uranium rod in a blanket element.

The results for the transmission calculations are listed in Table 3 for a range of ^{239}Pu up to two weight percent. The results are shown graphically in Figure 8. The results show a significant change in mass signal as expected. The change in mass signal is 1.218 between a depleted uranium sample and a depleted uranium sample containing one weight percent ^{239}Pu. This result agrees well with the value of 1.262 reported in Table 1 in Section 3.4 for a sample with a uniform thickness equal to the diameter of the depleted uranium rod in a blanket element. The decrease is due to the decrease in the average transmission length. The mass signal is a measure of the macroscopic cross-section of the sample times the transmission length. Since the composition is essentially identical for the slab and rod samples (the ^{235}U content is slightly different between the two cases by 0.02 weight percent), the difference in the results must be due to the smaller average transmission length. In actuality, the mass signal is a complex function due to the energy dependence of the flux and cross-sections as discussed in Section 3.3.

Figure 9 is a plot of the calculated detector response for the four configurations of sample and cadmium filter. The notation used in Figure 9 to describe the cases is the same as that used in Chapter 3. As an example, the plot noted as NS-F is for the case with no sample in the beam but the cadmium filter is in the beam. The gadolinium filter is in the beam for all cases. The figure is a log-log plot of the detector response versus the neutron energy. The y axis is shown as response. The response for each group is the number of neutrons in that group from the total number of neutron histories. For the case shown, the number of neutron histories was 10^7 so these values can be normalized by dividing by 10^7.
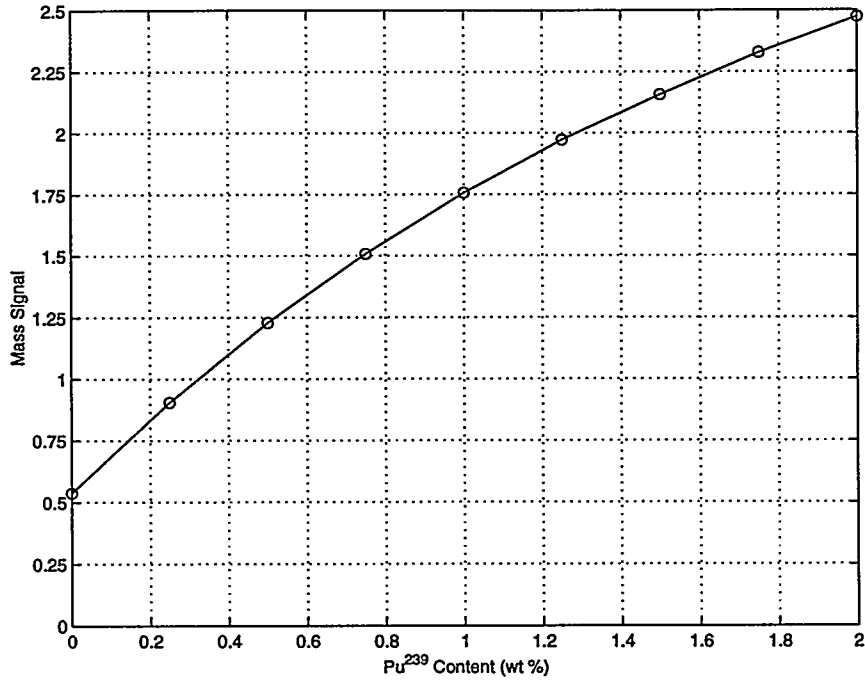
Figure 8: Mass Signal Estimates from Calculations
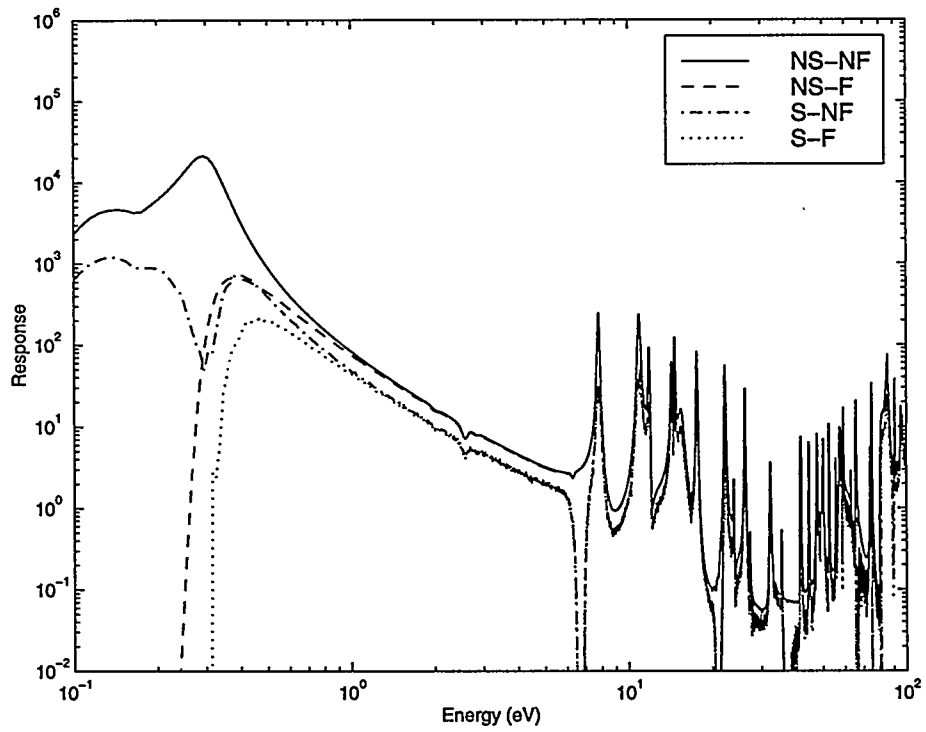
Figure 9: Spectral Detector Response of Different Filter/Sample Combinations
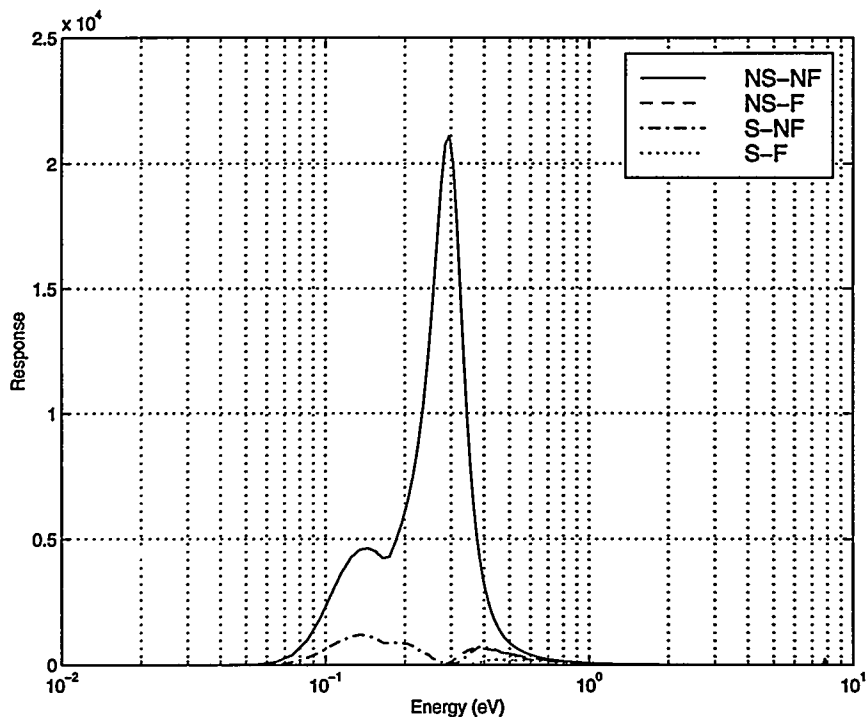
Figure 10: Spectral Detector Response (Semi-log Plot)

Although Figure 9 is only shown up to 100 eV, the resonance behavior of the filter and sample materials is readily apparent. Figure 9 demonstrates that the problem is more complicated than the two-group idealized filter model. It is also apparent that the 0.3 eV resonance in ^{239}Pu clearly dominates the spectrum. The difference between the two curves, S-NF and NS-NF, is due to attenuation from the sample. The S-NF plot shows a deep depression in the spectrum around 0.3 eV of approximately two orders of magnitude. This depression is due to the effect that the ^{239}Pu in the sample has on the attenuation. The S-F and NS-F cases also show a large drop off of greater than five orders of magnitude due to the cadmium filter. This supports the assumption that essentially everything below the cadmium cutoff energy is removed from the beam.

The benefit of the Pu detector is shown in Figure 10. Figure 10 is a plot of the same information as in Figure 9 only plotted on a semi-log scale. This figure shows the dramatic peaking in the energy range of interest (0.1 eV to 0.5 eV) and demonstrates that this filtered beam transmission method effectively isolates the 0.3 eV resonance in ^{239}Pu.

Also shown in Figure 10 is the effect of the gadolinium filter. The gadolinium filter significantly reduces the neutrons below the resonance (less than 0.1 eV) while still allowing the neutrons with higher energies to pass through it with little effect. There is a small bump or second peak in the response spectrum at about 0.15 eV. This peak is due to the gadolinium filter not totally removing the neutrons from an increased neutron flux. As shown in Figure 7, the flux is increasing in this energy range as the neutron energy decreases.

Table 4: Effect of Gadolinium Filter Thickness[*]						
Filter Thickness (cm)	0 wt% ^{239}Pu		2 wt% ^{239}Pu		Change in Mass Signal	Relative Error (%)
	Transmission	Mass Signal	Transmission	Mass Signal		
0.005	0.581	0.543	0.107	2.235	1.692	0.64
0.01	0.583	0.538	0.077	2.558	2.02	0.77
0.02	0.587	0.532	0.063	2.772	2.24	0.97
0.03	0.59	0.527	0.059	2.837	2.31	1.15

[*]The cadmium filter thickness was 0.050 cm. The sample was a rod sample with radius of 0.550 cm. The beam diameter was 0.556 cm.

4.2. Sensitivity Studies

Using the transmission code, numerous scoping calculations were performed to determine the effect of the various parameters on the mass signal result from the experiment. For all cases, the number of neutron histories was maintained constant at 10^7 to be able to determine the effect of the sensitivity on the relative error associated with the changes in parameters. The parameters studied included the gadolinium filter thickness, the cadmium filter thickness, the sample thickness, the beam diameter, and variations in the ^{235}U content in the sample.

4.2.1. Gadolinium filter thickness

The gadolinium filter thickness was varied between 0.005 cm and 0.030 cm. The results are shown in Table 4 for a depleted uranium rod sample and a sample containing two weight percent of ^{239}Pu. As shown in Table 4, the change in mass signal increases as the gadolinium filter thickness is increased. This is as expected since by increasing the thickness of gadolinium, the effective cutoff energy of the filter is increased. This means that more neutrons with slightly higher energies are being removed from the beam. Increasing the thickness of the gadolinium filter acts to increase the lower energy bound of the resonance interval and tighten the range of the resonance. This is readily apparent from the two plots in Figure 11. Figure 11 shows the spectral response of the detector for a 0.005 cm gadolinium filter and a 0.030 cm gadolinium filter. The responses shown in Figure 11 are for the NS-NF case (no sample or cadmium filter in the beam) which only include the effect of the gadolinium filter and detector response in the calculation. The case with a 0.030 cm thick filter shows one distinct peak over the energy range shown, whereas, the case with a 0.005 cm thick filter shows an additional peak at a slightly lower energy. By increasing the thickness of the filter, the second peak is removed, and the shape of the resonance is improved.

There are drawbacks to continually increasing the thickness of the filter. The detector response (i.e. count rate) is reduced and the relative error of the mass signal is increased. For the depleted uranium case the relative error was calculated at 0.64 percent with a 0.005 cm thick filter. The relative error increased to 1.15 percent for the case with a 0.030 cm filter thickness. The
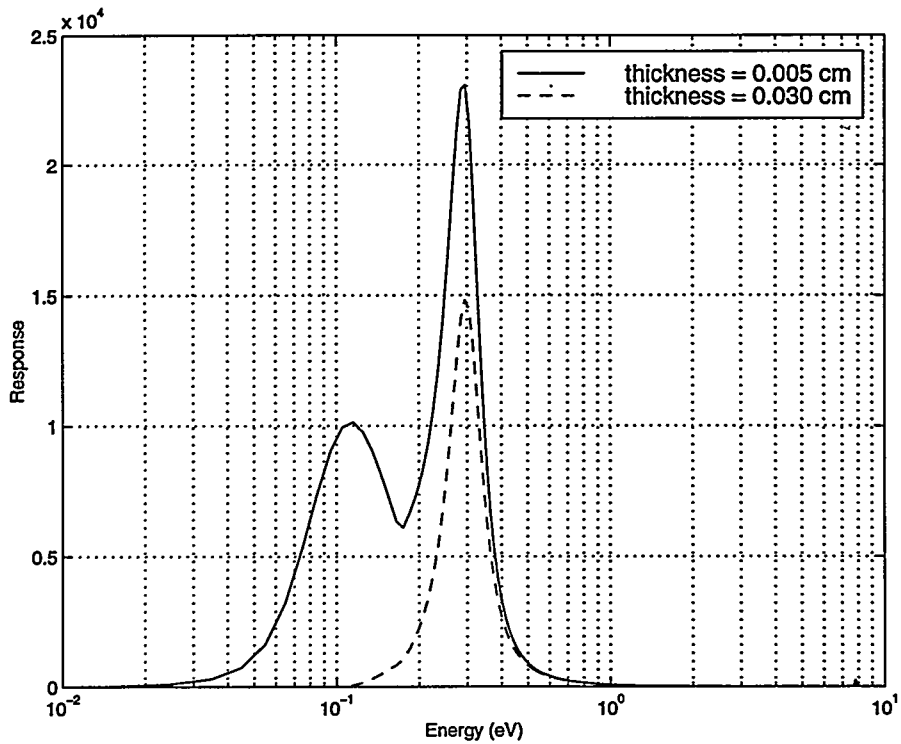
Figure 11: Detector Response for 0.005 cm and 0.030 cm Gadolinium Filters
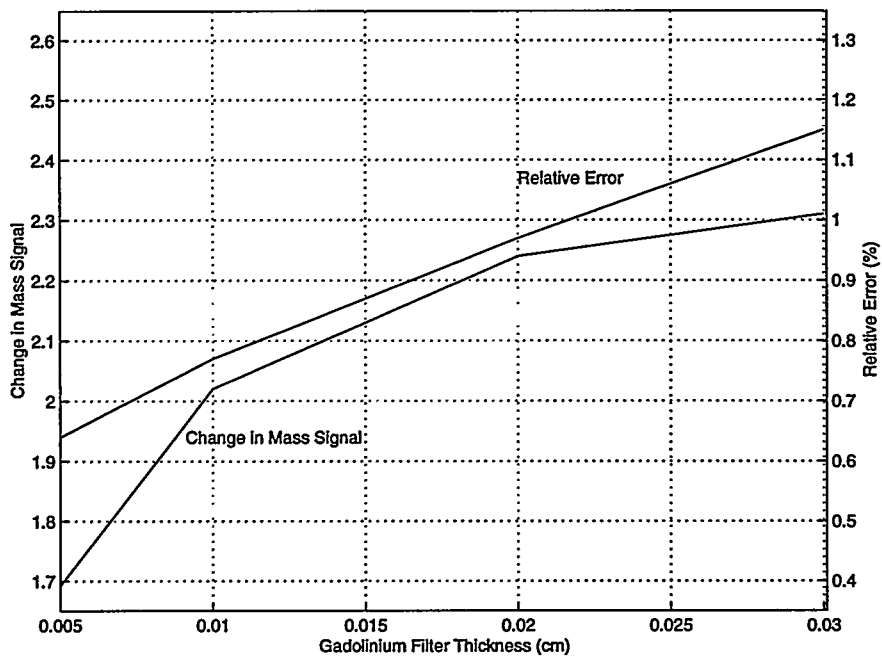
Figure 12: Effect of Gadolinium Filter Thickness

39

increase in relative error is due to the reduction in the total count rate of the detector. As the filter thickness increases, the total count rate of the detector decreases and the relative error increases. As shown in Figure 11, the signal is reduced by approximately 40% at the energy of 0.3 eV (the peak of the resonance) between the two cases.

Figure 12 is a plot of the relative error and change in mass signal as a function of gadolinium filter thickness using the data listed in Table 4. The relative error in the mass signal is approximately linear with the thickness of the gadolinium filter over the range shown. The change in the mass signal is also an increasing function of the gadolinium filter thickness. However, it increases more rapidly than the relative error for thicknesses less than 0.01 cm and increases more slowly for increasing thicknesses. Based on these results, a value of 0.01 cm for the gadolinium filter thickness was chosen for subsequent calculations and measurements. This allows for a modest improvement in the change in mass signal while not significantly increasing the relative error. The response with a 0.01 cm filter was shown in Figure 10. The lower energy peak is reduced but not completely eliminated. In addition, the detector response under the 0.3 eV resonance is not significantly reduced.

4.2.2. Cadmium filter thickness

The cadmium filter thickness was varied between 0.05 cm and 0.3 cm. The results are shown in Table 5 for the depleted uranium rod sample and a sample containing two weight percent of ^{239}Pu. As the cadmium filter thickness is increased, the change in mass signal between the two cases decreases. Figure 13 shows the spectral response for filter thicknesses of 0.05 cm, 0.1 cm, and 0.3 cm. The cases shown in Figure 13 include the gadolinium filter but do not include the sample (NS-F measurement). As the filter thickness is increased it serves to eliminate more neutrons at the lower energies, so that the cutoff energy creeps upward. In addition, more neutrons with slightly higher energies are removed from the beam which results in a lower response for thicker filters at energies up to approximately 8 eV. Above 8 eV, the response is essentially identical for the filter thicknesses studied.

The effect from the cadmium filter on the change in mass signal is opposite to the effect from the gadolinium filter. The cadmium filter is used to limit the upper energy of the resonance, whereas, the gadolinium filter is used to limit the lower energy of the resonance. As the upper cutoff energy is increased, the effect on the mass signal is detrimental as it acts to broaden the area of interest and increase the response at energies with lower cross-sections. By including a larger response at energies that correspond to lower cross-sections for ^{239}Pu, the response-weighted total macroscopic cross-section of the ^{239}Pu in the sample is reduced. This results in a smaller change in mass signal between a depleted uranium sample and a sample containing ^{239}Pu. This is evidenced by the data in Table 4. Notice that the transmission and mass signal for the depleted uranium sample do not change when the cadmium filter thickness is increased, however, there is a noticeable decrease in the mass signal as a function of cadmium filter thickness for the sample with two weight percent ^{239}Pu.

	Table 5: Effect of Cadmium Filter Thickness[*]					
Filter Thickness (cm)	**0 wt% ^{239}Pu**		**2 wt% ^{239}Pu**		**Change in Mass Signal**	**Relative Error (%)**
	Transmission	**Mass Signal**	**Transmission**	**Mass Signal**		
0.05	0.583	0.538	0.077	2.558	2.02	0.77
0.08	0.584	0.538	0.082	2.505	1.967	0.71
0.1	0.584	0.538	0.084	2.479	1.941	0.69
0.2	0.584	0.537	0.093	2.372	1.835	0.65
0.3	0.585	0.537	0.098	2.321	1.784	0.64

[*]The gadolinium filter thickness was held constant at 0.010 cm for all cases shown. The sample was a rod sample with a radius of 0.550 cm. The beam diameter was 0.556 cm.
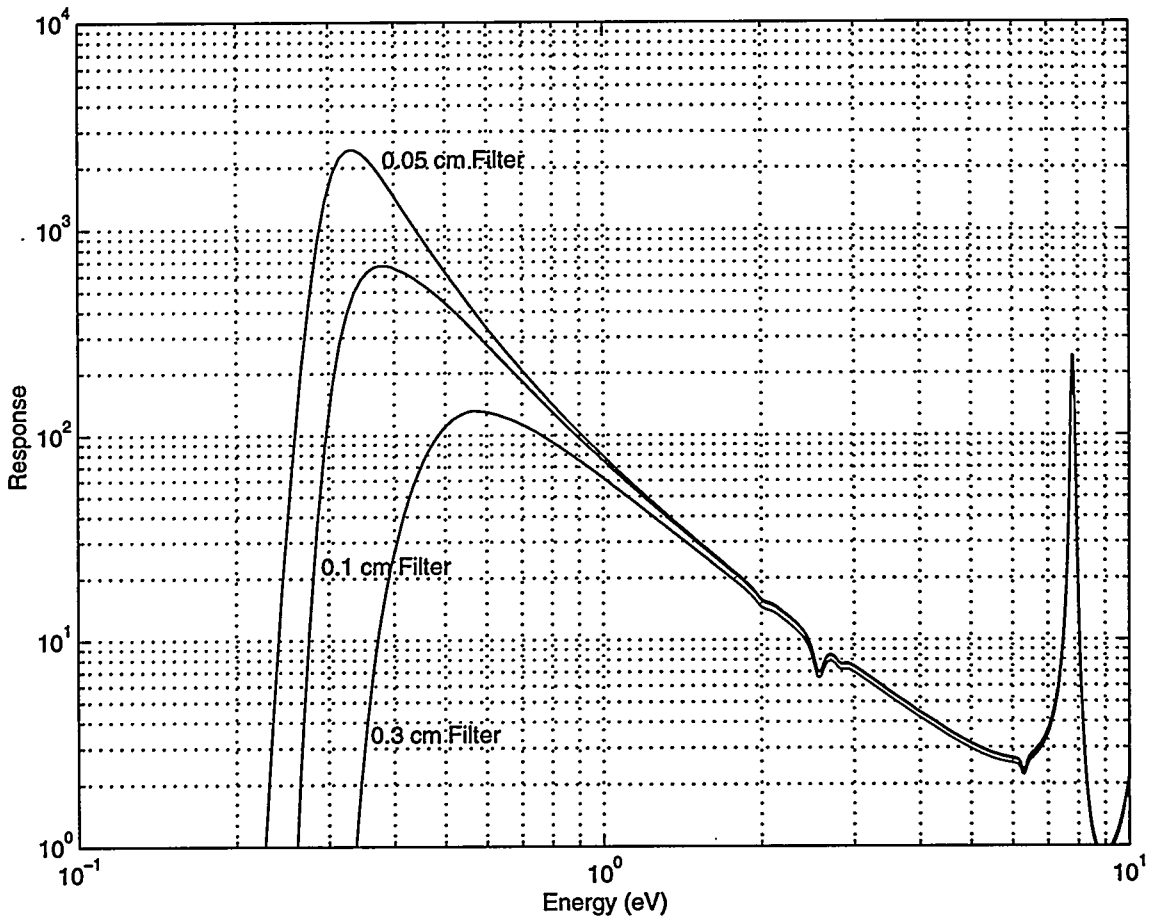
Figure 13: Spectral Detector Response Based on Cadmium Filter Thickness

41
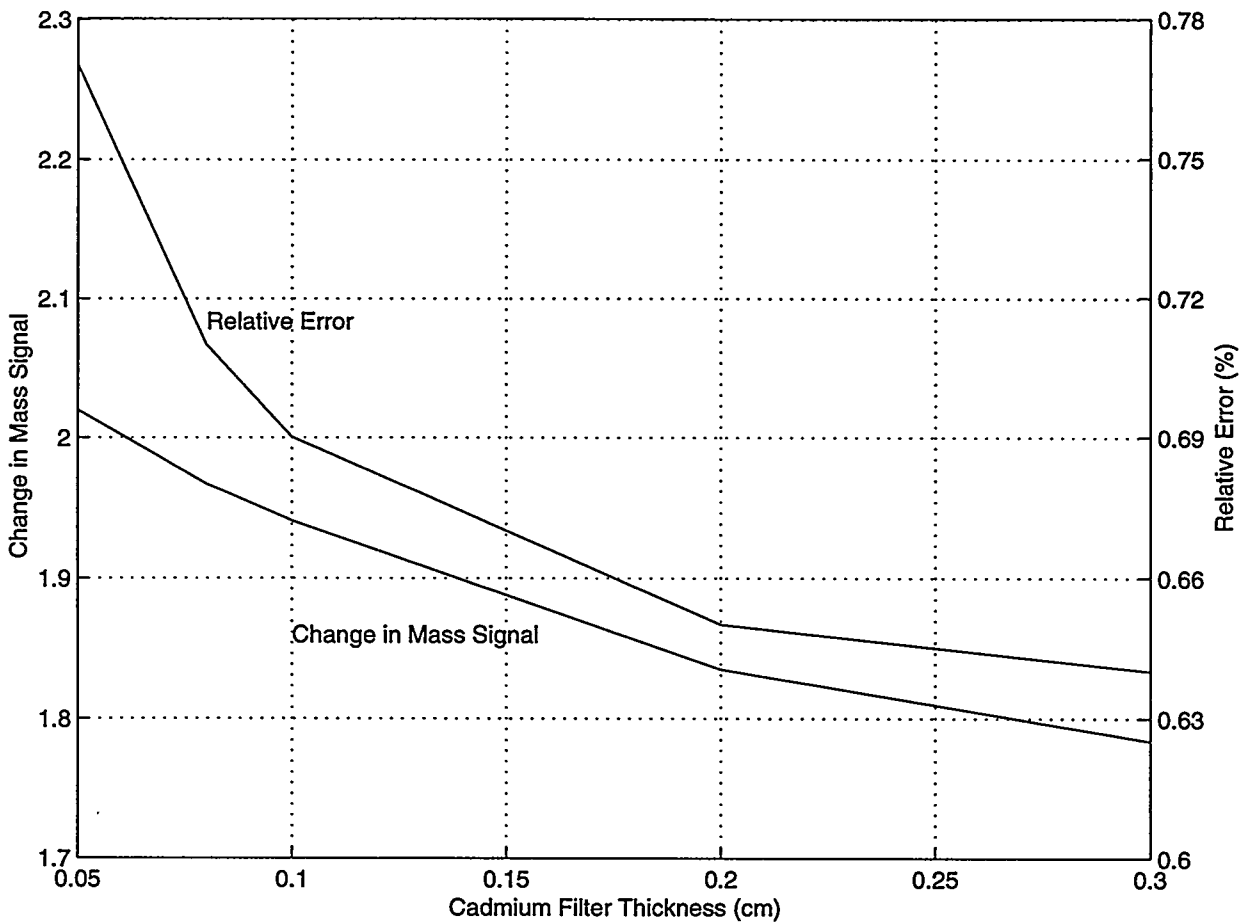
Figure 14: Effect of Cadmium Filter Thickness

Figure 14 shows the change in mass signal and relative error as a function of the cadmium filter thickness. As mentioned, the change in mass signal decreases as the cadmium filter thickness increases. The relative error also decreases as the filter becomes thicker. The values for the change in mass signal and relative error appear to be correlated for filter thicknesses above 0.1 cm. The values deviate at filter thicknesses less than 0.1 cm, such that the relative error increases at a faster rate than the change in mass signal. A thickness of 0.1 cm was chosen to use for the experiment as a compromise between the change in mass signal and the relative error based on the cadmium filter thickness.

4.2.3. ^{235}U content

The nominal ^{235}U content in an unirradiated depleted uranium element is 0.22 weight percent. This value is a nominal value, and as such the ^{235}U content in depleted uranium can be greater or less than 0.22 weight percent. From irradiation, ^{235}U will be depleted such that the value of ^{235}U in the

42

Table 6: Effect of ^{235}U Content on Mass Signal		
^{235}U Content (wt %)	Transmission	Mass Signal
0	0.597	0.516
0.1	0.59	0.527
0.2	0.584	0.538
0.25	0.581	0.544
0.3	0.577	0.549
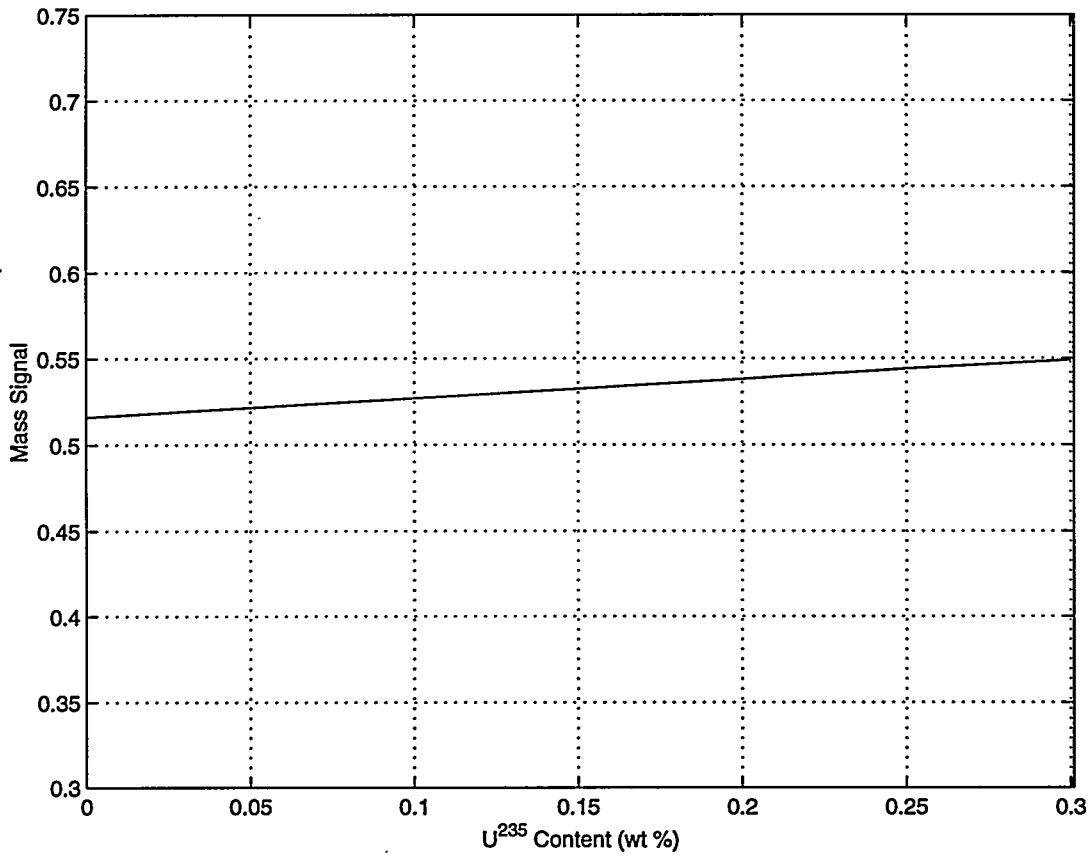
Figure 15: Effect of ^{235}U Content on Mass Signal

sample will be less than 0.22 weight percent. Calculations were performed for depleted uranium rod samples with varying amounts of ^{235}U in the range from 0.02 weight percent of ^{235}U up to 0.28 weight percent of ^{235}U. The results are listed in Table 6 and shown graphically in Figure 15. The mass signal varies by only 0.033 from 0.00 weight percent to 0.30 weight percent. This value is so small compared to the change in mass signal from ^{239}Pu that it can be neglected. As an example, the mass signal varies by 1.935 between a depleted uranium sample and a sample containing two weight percent ^{239}Pu as shown previously in Table 3. The variance in the mass signal from the ^{235}U (0.033) represents only 1.7% of the change in mass signal from the ^{239}Pu (1.935). This translates into an additional error in the determination of the ^{239}Pu content in a sample of 0.03 weight percent. This is so small that it can be neglected.

4.2.4. Sample Thickness

The sample thickness for a slab sample was varied over the range from 0.85 cm up to 1.15 cm. The nominal diameter of a blanket element is 1.100 cm. The calculations were run over much smaller thicknesses to look at the response of the mass signal. The sensitivity to sample thickness is important when considering the actual blanket elements. The blanket elements are cylindrical, and as such vary in transmission thickness based on the distance from the centerline. Therefore, the response will be different than the slab response due to the non-uniform thickness.

The results are listed in Table 7 and shown graphically in Figure 16. The mass signal response is linear over the range shown. This is as expected for samples of uniform thickness. The mass signal is simply the macroscopic cross-section of the sample multiplied by the transmission length. For slab samples, the transmission length for a perpendicular beam is the slab thickness. Therefore, the mass signal is a linear function of the sample thickness as shown in Figure 16.

4.2.5. Beam diameter

The experiment uses ZPPR foils to create a sample of uniform thickness, so as long as the diameter of the beam is less than the foil diameter, the size of the beam does not affect the mass signal result. This is because the transmission length is constant. However, in the case of blanket elements, the transmission length is not constant as the sample is cylindrical. Therefore, the diameter of the beam impinging on the sample will affect the mass signal result.

Results of calculations performed by varying the diameter of the beam impinging on the sample are listed in Table 8. The sample was a rod sample with a diameter of 1.100 cm which contained 0.2 weight percent ^{235}U. The gadolinium filter thickness was 0.01 cm and the cadmium filter thickness was 0.1 cm. The results are shown graphically in Figure 17. Figure 17 shows two plots - 1) the change in mass signal between a depleted uranium sample and a sample containing two weight percent ^{239}Pu and 2) the relative counting time. The counting times shown in Table 8 and Figure 17 are related to the counting time for a beam with a radius of one centimeter. The values for the relative counting time are simply $1/R^2$, where R is the beam radius. The relation assumes a constant flux, and was performed so that the counting statistics are identical regardless of beam dia-

Table 7: Effect of Sample Thickness on Mass Signal		
Sample Thickness (cm)	Transmission	Mass Signal
0.85	0.646	0.437
0.9	0.63	0.463
0.95	0.613	0.489
1	0.598	0.515
1.03	0.589	0.53
1.04	0.586	0.534
1.05	0.583	0.54
1.075	0.576	0.552
1.1	0.568	0.565
1.15	0.554	0.591

*The sample was modeled as a depleted uranium slab with the thicknesses shown. The thickness of the gadolinium filter was 0.01 cm. The thickness of the cadmium filter was 0.1 cm.
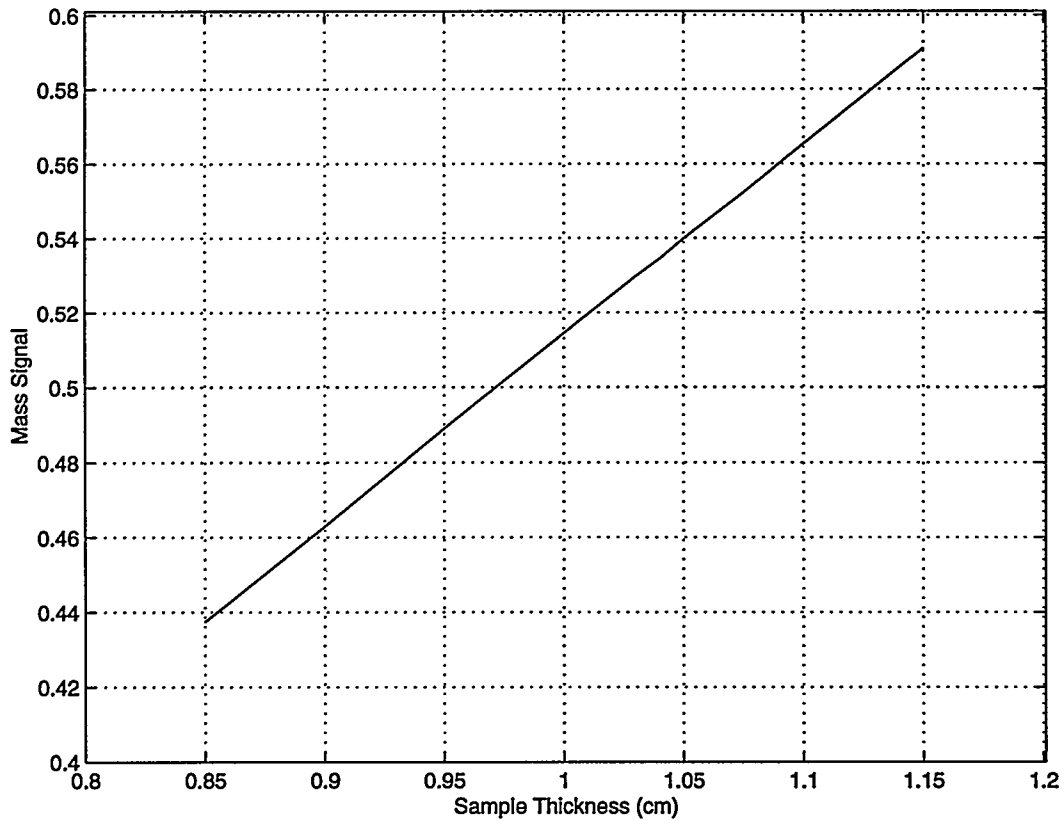
Figure 16: Effect of Sample Thickness on Mass Signal

meter. For example, the count time would be 100 times greater with a beam diameter of 0.2 cm compared to a beam diameter of 2 cm to obtain the same total count rate. This allows a comparison between the change in mass signal and the additional count time necessary to obtain identical statistics.

It is desirable to have the largest change in mass signal possible between a depleted uranium sample and a sample containing two weight percent ^{239}Pu. The larger the change in the mass signal the larger the sensitivity to changes in ^{239}Pu content. The largest change in mass signal under these conditions is with a slab sample having a thickness of 1.100 cm which is equivalent to the diameter of the depleted uranium rod in a blanket fuel element. From Table 8, this difference in mass signal is 1.999. From Table 8, it is observed that there is a 1.4 percent loss in the change in mass signal for a beam diameter of 0.4 cm. The loss in sensitivity is only about 3.4 percent with a beam diameter of 0.6 cm, and is about 10 percent for a diameter of 0.8 cm. The loss in sensitivity becomes extreme for diameters greater than 0.8 cm.

Ideally, a pin-hole collimator would be used to obtain a beam so small that the transmission length would be the diameter of the sample and the maximum change in mass signal could be obtained. This is shown in Table 8 for a beam with a diameter of 0.02 cm where the change in mass signal is identical to the slab sample results. Realistically, the diameter of the beam must be large enough to allow for practical counting times. As shown in Figure 17, the relative counting time increases drastically for decreasing beam diameters less than 0.2 cm, and the relative counting time does not significantly decrease for beam diameters greater than about 0.6 cm.

It appears from Figure 17, that a beam diameter of about 0.5 cm would be ideal for measuring the blanket elements. A beam diameter of 0.5 cm would maximize the sensitivity to the change in mass signal (about 2.3% loss from the slab sample result) while minimizing the count time. At smaller beam diameters, the counting time is increased drastically for minor improvements in the sensitivity. At larger beam diameters, the sensitivity to the change in mass signal is significantly decreased for only minor reductions in the counting time.

4.3. Error Analysis

The relative error has been briefly mentioned in previous sections without a detailed discussion of the statistical error associated with this method or the measurements proposed. The basis of the error analysis and error propagation described here is provided in reference 28.

The transmission, as previously defined, is

$$T = \frac{C_{S-NF} - C_{S-F}}{C_{NS-NF} - C_{S-NF}} = \frac{C_1 - C_2}{C_3 - C_4} \tag{71}$$

where the subscript notation has been shortened for notational simplicity. In terms of the measure-

46

Table 8: Effect of Beam Diameter on Mass Signal*						
Beam Diameter (cm)	0 wt% [239]Pu		2 wt% [239]Pu		Change in Mass Signal	Relative Count Time
	Transmission	Mass Signal	Transmission	Mass Signal		
Slab	0.57	0.562	0.077	2.561	1.999	1
0.02	0.57	0.562	0.077	2.561	1.999	10000
0.1	0.57	0.562	0.077	2.559	1.997	400
0.2	0.572	0.559	0.078	2.551	1.992	100
0.3	0.574	0.555	0.079	2.538	1.983	44.4
0.4	0.577	0.55	0.08	2.521	1.971	25
0.5	0.581	0.543	0.082	2.497	1.954	16
0.6	0.587	0.533	0.085	2.465	1.931	11.1
0.7	0.593	0.522	0.089	2.424	1.902	8.2
0.8	0.602	0.507	0.093	2.372	1.865	6.3
0.9	0.613	0.489	0.1	2.299	1.81	4.9
1	0.627	0.467	0.111	2.194	1.727	4
1.1	0.647	0.435	0.139	1.973	1.538	3.3

*The gadolinium filter thickness was 0.010 cm. The cadmium filter thickness was 0.1 cm. The sample was a rod sample with a radius of 0.550 cm. For the slab case shown, the slab thickness was 1.100 cm.
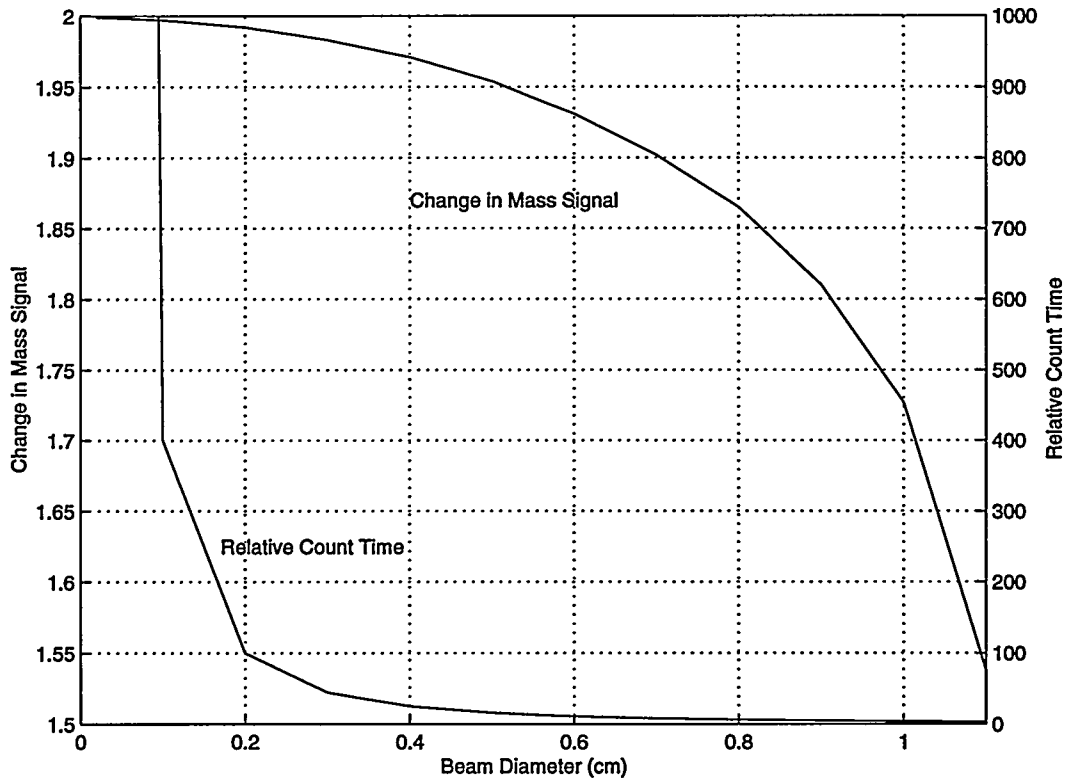
Figure 17: Effect of Beam Diameter on Mass Signal

47

ment of random nuclear processes, the variance associated with each measurement, C, assuming a Poisson or Gaussian distribution can be represented by

$$\sigma_{C_n} = \sqrt{C_n} \, . \tag{72}$$

The variance, or error, associated with each individual measurement, C_1 through C_4, must be propagated through the equation to obtain the standard deviation on the transmission value. To do this, the error propagation formula is used. The error propagation formula states that the standard deviation for any quantity u derived from independent variables for which the variance of each is known, can be calculated from the following:

$$\sigma_u^2 = \left(\frac{\partial u}{\partial x} \right)^2 \sigma_x^2 + \left(\frac{\partial u}{\partial y} \right)^2 \sigma_y^2 + \left(\frac{\partial u}{\partial z} \right)^2 \sigma_z^2 + \ldots \tag{73}$$

where u=u(x,y,z,...) represents the derived quantity. Applying this in stages to the transmission (equation 69), the standard deviation for the numerator is

$$\sigma_{numerator} = \sqrt{\sigma_{C_1}^2 + \sigma_{C_2}^2} = \sqrt{C_1 + C_2} \, , \tag{74}$$

and the standard deviation for the denominator is

$$\sigma_{denominator} = \sqrt{\sigma_{C_3}^2 + \sigma_{C_4}^2} = \sqrt{C_3 + C_4} \, . \tag{75}$$

The error propagation formula can then be written for the transmission in terms of the numerator and denominator as

$$\left(\frac{\sigma_T}{T} \right)^2 = \left(\frac{\sigma_{numerator}}{numerator} \right)^2 + \left(\frac{\sigma_{denominator}}{denominator} \right)^2 . \tag{76}$$

This equation can be rearranged to write the standard deviation of the transmission as

$$\sigma_T = T \sqrt{ \left(\frac{\sigma_{numerator}}{numerator} \right)^2 + \left(\frac{\sigma_{denominator}}{denominator} \right)^2 } \, . \tag{77}$$

The standard deviation can then be written in terms of the four measurement values by substituting the values into the above equation. This substitution results in the following for the deviation:

$$\sigma_T = \left(\frac{C_1 - C_2}{C_3 - C_4}\right) \sqrt{\frac{C_1 + C_2}{(C_1 - C_2)^2} + \frac{C_3 + C_4}{(C_3 - C_4)^2}} . \tag{78}$$

To determine the standard deviation of the mass signal, the standard deviation must be propagated further. The mass signal as previously defined is $M = -\ln(T)$. Therefore, the standard deviation on the mass signal is σ_T/T, which can be written in terms of the four measurement values as

$$\sigma_M = \frac{\sigma_T}{T} = \sqrt{\frac{C_1 + C_2}{(C_1 - C_2)^2} + \frac{C_3 + C_4}{(C_3 - C_4)^2}} . \tag{79}$$

This states that the standard deviation of the mass signal is directly related to all four of the measurement values. Using the ratios from a series of calculations for a rod sample with 0.02 weight percent ^{235}U, the relative error in mass signal as a function of count rate can be determined. The results for the case with a 0.01 cm gadolinium filter and a 0.1 cm cadmium filter are shown in Table 9 for 10^3, 10^4, and 10^5 counts for the measurement with the weakest response. The response will be the weakest when both filters and the sample are in the beam. The results shown in Table 9 indicate that the count time should be such that at least 10000 counts are obtained for all measurements for the relative error to be less than one percent.

The relative error based on the ^{239}Pu content in the sample is shown in Figure 18 for the case of 10000 counts for the S-F measurement. Note that the relative error reaches a minimum at approximately one weight percent and increases with increasing ^{239}Pu content. The standard deviation increases with increasing ^{239}Pu content as shown in Table 9. However, the mass signals are larger above one weight percent ^{239}Pu, and hence, the relative error decreases. This is a fortunate consequence for the measurement of blanket elements. The average ^{239}Pu content in the blanket elements is approximately one weight percent which corresponds with the minimum in the relative error.

An additional error is introduced in using this information to determine the ^{239}Pu content. In practice, the transmission through samples with known quantities of ^{239}Pu will be used to determine the mass signal. These measurements will be used to determine a calibration curve between the mass signal and ^{239}Pu content. The calibration curve is a polynomial function which relates the measured quantity (mass signal) to the unknown quantity (^{239}Pu content). Assume that the calibration curve is a third order polynomial expansion of

$$P = AM^3 + BM^2 + CM + D , \tag{80}$$

where M is the mass signal, P is the ^{239}Pu content (in weight percent) and A, B, C, and D are constants determined from the fitting routine. The standard deviation using the error propagation formula is

49

Table 9: Standard Deviation in Mass Signal								
^{239}Pu content (wt %)	Mass Signal	10^3 counts		10^4 counts		10^5 counts		
		σ_m	Percent Error	σ_m	Percent Error	σ_m	Percent Error	
0	0.468	0.0212	4.53	0.007	1.43	0.002	0.45	
0.25	0.805	0.0245	3.05	0.008	0.96	0.003	0.31	
0.5	1.105	0.0286	2.59	0.009	0.82	0.003	0.26	
0.75	1.363	0.0331	2.43	0.0105	0.77	0.003	0.24	
1	1.595	0.0383	2.4	0.0121	0.76	0.004	0.24	
1.25	1.803	0.0439	2.44	0.0139	0.77	0.004	0.24	
1.5	1.985	0.0498	2.51	0.0157	0.79	0.005	0.25	
1.75	2.152	0.0562	2.61	0.0178	0.83	0.006	0.26	
2	2.291	0.0622	2.71	0.0197	0.86	0.006	0.27	
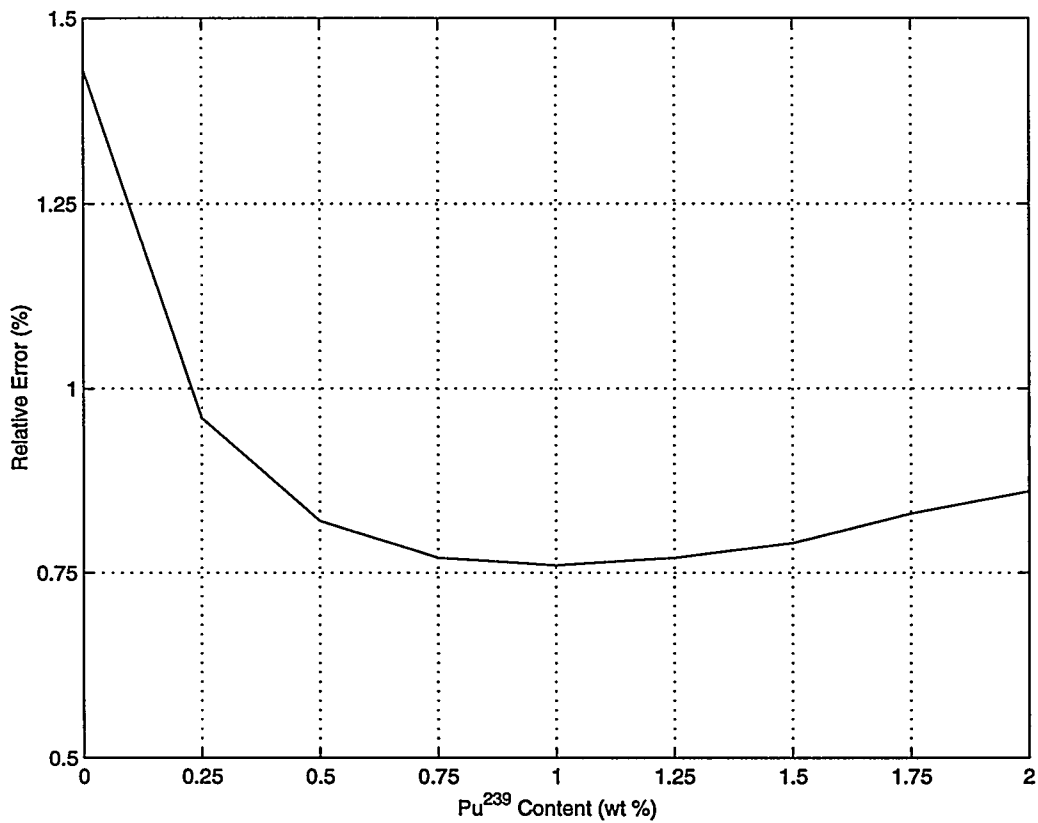
Figure 18: Relative Error Based on ^{239}Pu Content

50

Table 10: Reportable Error in Mass Signal for Hypothetical Case							
Mass Signal	^{239}Pu composition (wt %)	10^3 counts		10^4 counts		10^5 counts	
		σ_{Pr}	Percent Error	σ_{Pr}	Percent Error	σ_{Pr}	Percent Error
0.4676	0	0.0222	4.53	0.007	1.43	0.002	0.45
0.8046	0.25	0.0273	10.92	0.009	3.45	0.003	1.09
1.1045	0.5	0.0357	7.14	0.0113	2.26	0.004	0.71
1.363	0.75	0.0472	6.29	0.0149	1.99	0.005	0.63
1.5953	1	0.0623	6.23	0.0197	1.97	0.006	0.62
1.8031	1.25	0.0811	6.49	0.0256	2.05	0.008	0.65
1.9848	1.5	0.1029	6.86	0.0325	2.17	0.0103	0.69
2.1519	1.75	0.1288	7.36	0.0407	2.33	0.0129	0.74
2.2908	2	0.1551	7.75	0.049	2.45	0.0155	0.78

$$\sigma_P = \sqrt{\left(\frac{\partial P}{\partial M}\right)^2 \sigma_M^2 + \left(\frac{\partial P}{\partial A}\right)^2 \sigma_A^2 + \left(\frac{\partial P}{\partial B}\right)^2 \sigma_B^2 + \left(\frac{\partial P}{\partial C}\right)^2 \sigma_C^2 + \left(\frac{\partial P}{\partial D}\right)^2 \sigma_D^2} , \qquad (81)$$

which can be expanded into

$$\sigma_P = \sqrt{\left(3AM^2 + 2BM + C\right)^2 \sigma_M^2 + M^6 \sigma_A^2 + M^4 \sigma_B^2 + M^2 \sigma_C^2 + \sigma_D^2} . \qquad (82)$$

This represents the error in the ^{239}Pu content as a function of the mass signal and standard deviation in the mass signal and polynomial constants. Using the data from Table 9, the constants - A, B, C, and D - were determined to be 0.0945, -0.1095, 0.7797, and -0.3520, respectively. A measurement is performed on a sample with an unknown ^{239}Pu content and the mass signal and associated standard deviation, M and σ_M, are determined as previously discussed. The measured mass signal and standard deviation are then used with the calibration curve to determine the ^{239}Pu content, P_m.

For a hypothetical case, the standard deviation is increased by a factor of 1.414 as the measured value and calibration value are based on the same calculation, therefore, the standard deviation is identical for both cases. Table 10 shows the results for the hypothetical cases described previously in Table 9. Based on the values shown in Table 10, the counting time for the experiment should be chosen so that the total counts for the case with both filters and the sample in the beam should be at least 10000 counts. This will reduce the reported error on the ^{239}Pu content to less than 0.05 weight percent over the range from 0.00 to 2.00 weight percent. In relative terms, the error will be less than 2.5 percent in this range excluding very low ^{239}Pu contents.

Several issues related to the measurements have not been discussed up to this point. First, the NRAD flux cannot be maintained perfectly constant throughout all of the measurements. There will be some slight variation in flux level even when the reactor is automatically controlled. Therefore, a variable flux level should be taken into account in the measurement values. This is accomplished by providing an additional detector to monitor the flux. The count rate values, C_1 through C_4, are then divided by the monitor values, M_1 through M_4, to obtain a ratio for each of the four measurements.

The second issue that must be addressed is the background. A certain number of the total counts registered for each measurement are due to background radiation interacting with the detector. The background level has been found to be constant for all four measurements. In this case the background level can then be subtracted from each measurement value. This is performed by subtracting the background ratio from each measurement ratio.

The mass signal calculated from the four measurements accounting for flux monitoring and background subtraction is

$$M = -\ln\left(\frac{\left(\frac{C_1}{M_1} - \frac{C_B}{M_B}\right) - \left(\frac{C_2}{M_2} - \frac{C_B}{M_B}\right)}{\left(\frac{C_3}{M_3} - \frac{C_B}{M_B}\right) - \left(\frac{C_4}{M_4} - \frac{C_B}{M_B}\right)}\right) = -\ln\left(\frac{\frac{C_1}{M_1} - \frac{C_2}{M_2}}{\frac{C_3}{M_3} - \frac{C_4}{M_4}}\right). \tag{83}$$

The standard deviation associated with the mass signal above is

$$\sigma_M = M\sqrt{\left(\frac{\sigma_N}{N}\right)^2 + \left(\frac{\sigma_D}{D}\right)^2} \tag{84}$$

where M is the mass signal from the above equation, and N and D denote the numerator and denominator terms from the mass signal equation. The standard deviation on the numerator and denominator are

$$\sigma_N = \sqrt{\left(\frac{C_1}{M_1}\right)^2\left(\frac{1}{C_1} + \frac{1}{M_1}\right) + \left(\frac{C_2}{M_2}\right)^2\left(\frac{1}{C_2} + \frac{1}{M_2}\right)}, \tag{85}$$

$$\sigma_D = \sqrt{\left(\frac{C_3}{M_3}\right)^2\left(\frac{1}{C_3} + \frac{1}{M_3}\right) + \left(\frac{C_4}{M_4}\right)^2\left(\frac{1}{C_4} + \frac{1}{M_4}\right)}, \tag{86}$$

52

respectively. It should be noted that these adjustments to the mass signal equation do not change the results for the mass signal. The addition of the flux monitor does increase the error on the mass signal. If the flux monitor count rate is extremely large compared to the count rates for the measurements, then this additional error associated with the flux monitoring is negligible and can be ignored. The error associated with the background measurement does not factor into the error in the mass signal since the background measurements were reduced from the equation. This is only true if the background measurements are correlated for all four measurements, i.e. the background readings do not depend on the positioning of the filters and sample, which has been experimentally investigated.

5. Experiments

Ample calculations were performed to allow a minimum of experiments to demonstrate the feasibility of the method and to do scoping measurements to verify the effect of the various parameters of interest. The experiment was located in the East Radiography Station (ERS) Cell of the NRAD Reactor Facility. The experimental set-up and equipment are described in Section 5.1. Included are subsections which describe the individual components of the system. Section 5.2 describes the overall measurement plan and also discusses the procedure used for each series of measurements.

5.1. Experiment Set-up

The equipment to perform these measurements consists of three major systems in addition to the reactor facility - the beam collimator, the experiment table and the detection equipment. Figure 19 shows a schematic of the layout of the experimental equipment. The individual components are described in Sections 5.1.1 through 5.1.4 below. The collimator and experiment table are both located in the ERS Cell of the NRAD Reactor Facility. The detectors are also located within the cell, however, the associated electronics are located external to the cell. Cabling between the electronics and the detectors are located in conduit that penetrates the shielding walls of the ERS Cell. While this experiment is installed in the ERS Cell, the radiography capability in the ERS Cell is disabled.

5.1.1. NRAD reactor

The NRAD Reactor was installed in the Hot Fuel Examination Facility (HFEF) at Argonne National Laboratory in 1977. The reactor is a 250 kW steady-state heterogeneous water-moderated TRIGA type reactor. It is located in a water tank below the HFEF hot cell. The core and reactor tank are shown in Figure 20. For more details regarding the NRAD reactor facility refer to References 30, 31, and 32.

The ERS cell and radiography station were designed to provide a beam of neutrons so that reactor fuel elements and structural components located in the main cell of HFEF could be radiographed without leaving the cell. The east beam tube looks directly at the core and offers a harder spectrum than other reactor facilities that have tangential beams. Refer to Chapter 4 for a discussion of the spectrum of the beam. A schematic of the NRAD beam tubes and ERS cell are shown in Figure 21.

The east beam tube is divided into several sections. Within the reactor tank there is the removable beam tube, aperture mechanism, and fixed in-tank beam tube. A schematic of the in-tank portion is shown in Figure 22.

The east beam then penetrates the ERS Cell shield wall with a through-the-wall collimator. A schematic of the through-the-wall collimator is shown in Figure 23. The through the wall

54
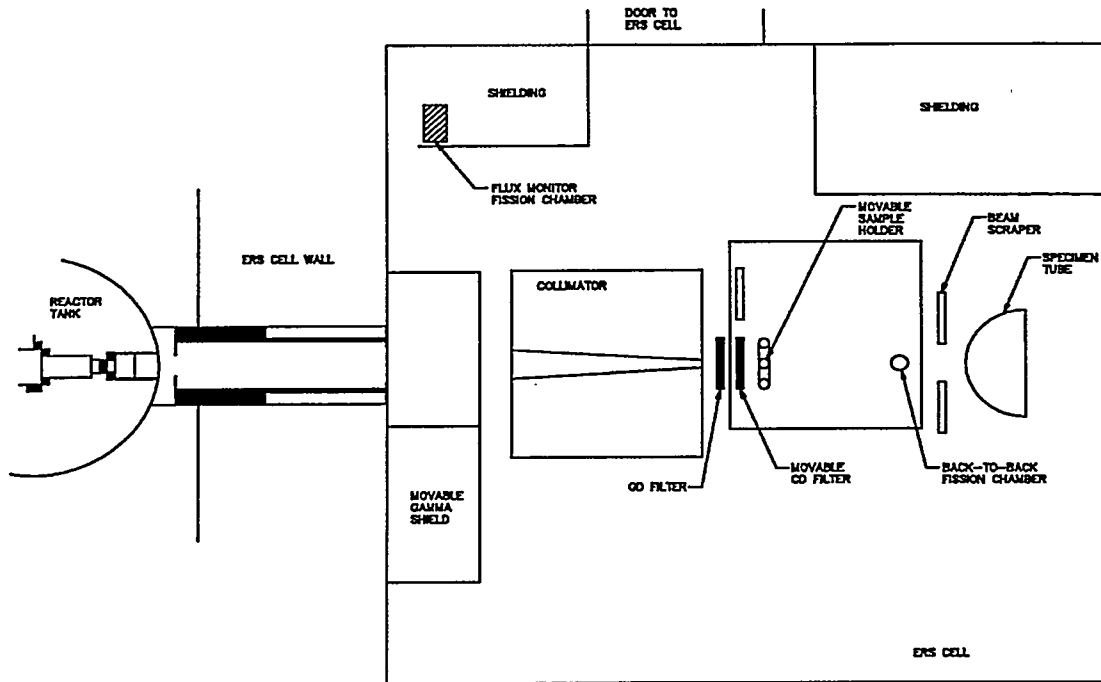
Figure 19: Schematic Layout of Experiment
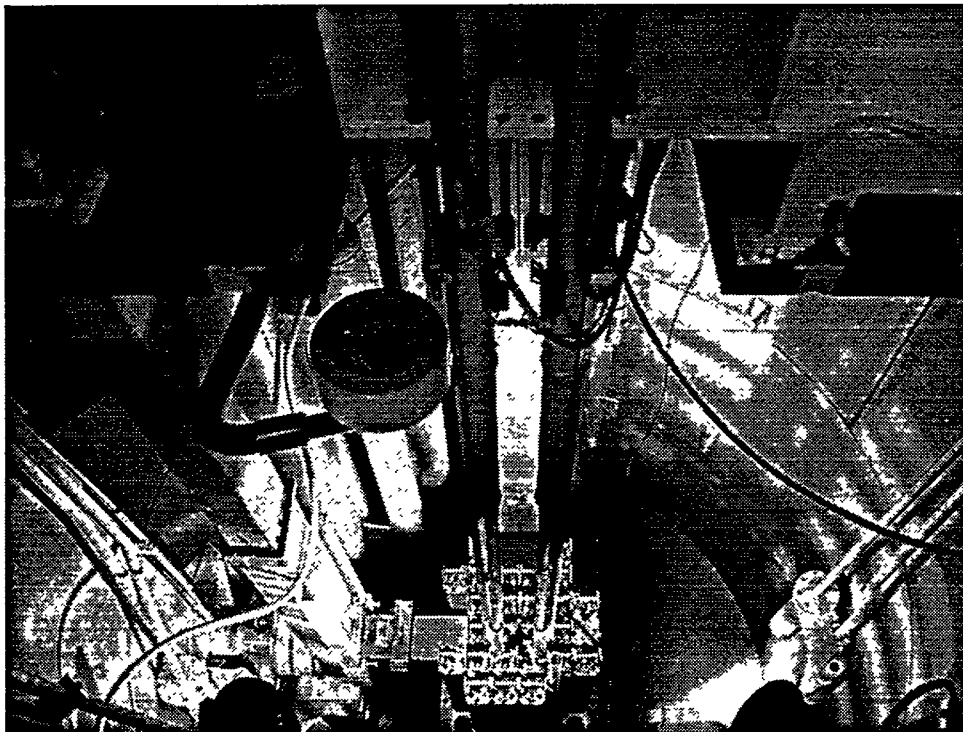
Figure 20: NRAD Core and Reactor Tank

55
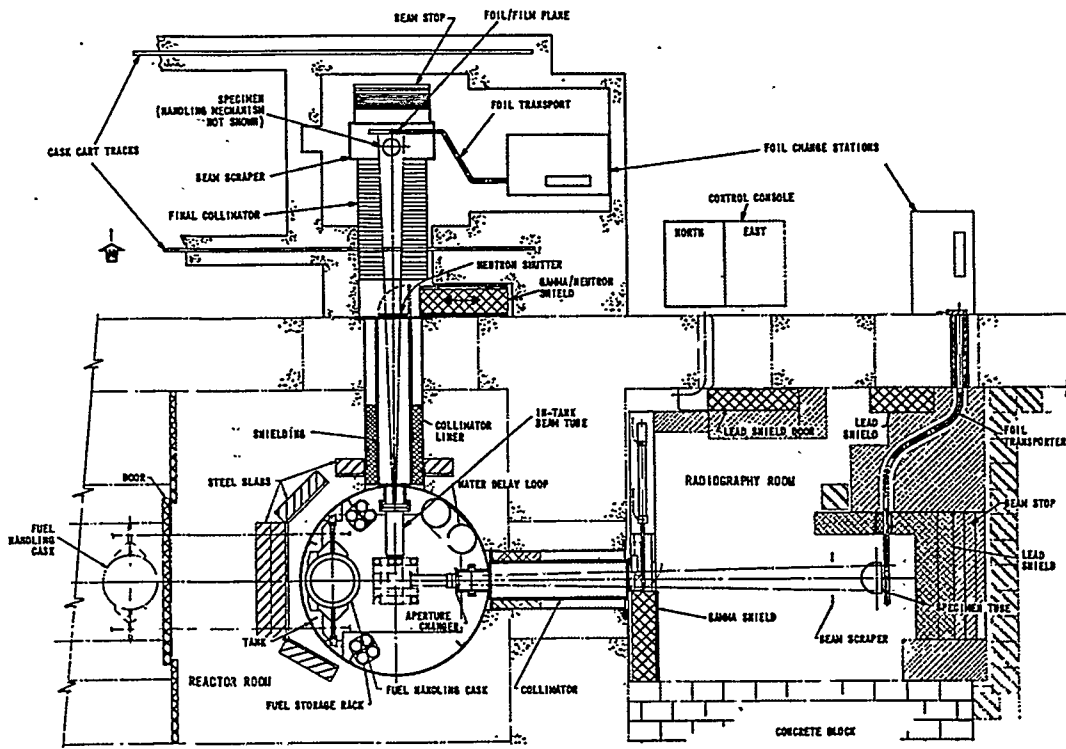
Figure 21: Schematic of NRAD Facility
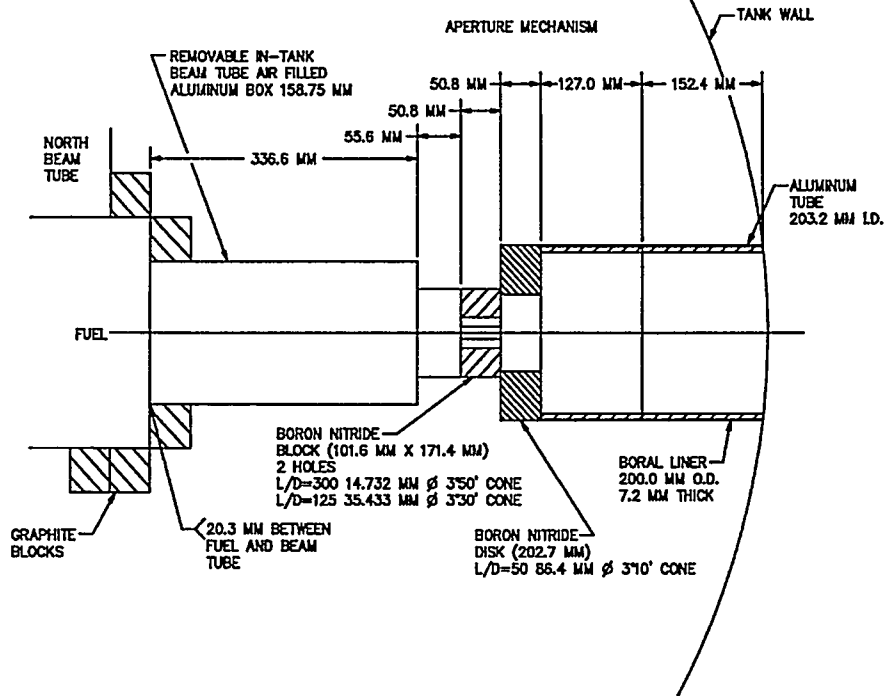
Figure 22: ERS In-Tank Beam Tube

56
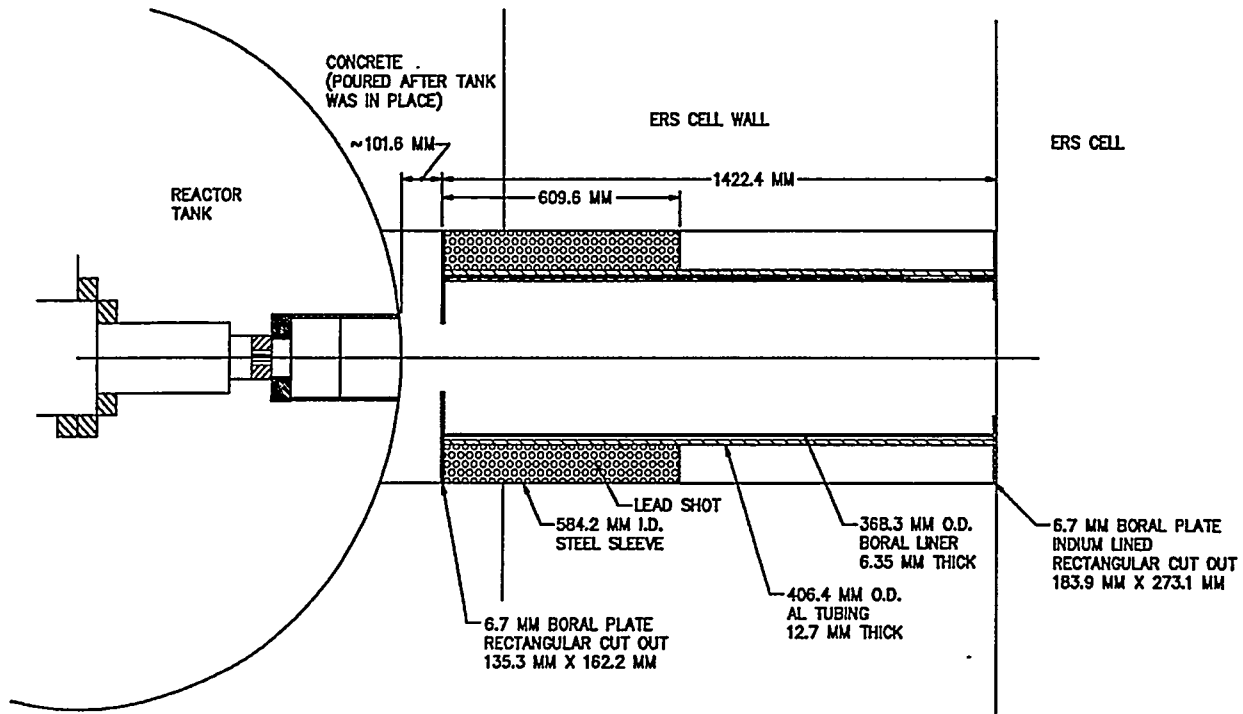
Figure 23: ERS Through-The-Wall Collimator

collimator is located in a steel sleeve. Inside the sleeve are two boral plates which define the shape of the beam. The plate closest to the reactor has a rectangular cutout (13.5 centimeters by 16.2 centimeters). The plate farthest from the reactor is lined with indium and has a cutout measuring 18.4 centimeters by 27.3 centimeters.

The east beam then opens up into the ERS Cell. The ERS Cell is shown in Figure 21. The cell has a floor area of about 3.05 meters by 3.66 meters and a height of 2.44 meters. Personnel can enter this room through a shield door on the north wall. A gamma shield and neutron shutter are located along the west wall of the cell. On the east side of the room, a sealed tube is located which connects to the HFEF main cell. This specimen tube allows samples to be lowered from the main cell for radiography. In front of the tube is a beam scraper consisting of two boral sheets which can be positioned to tailor the beam area for radiography. The collimator and experiment table are located between the gamma shield and beam scraper as shown in Figure 19. To perform measurements on irradiated blanket elements, the experiment will be redesigned to fit around the specimen tube so that elements can be lowered directly into the system from the HFEF main cell.

5.1.2. Collimator

The east beam tube was designed for radiography and, as such, has a very large beam area within the ERS Cell. The beam area is defined by the boron nitride aperture disk and the through-

57

the-wall collimator. The beam area is much larger than the intended samples and had to be reduced and collimated for the experiment. A collimator was built using 34 sheets of borated polyethylene. The sheets are 61 centimeters by 91 centimeters wide and 2.5 centimeters thick. The boron content of the sheets is 15% by weight. Different diameter holes were drilled in each sheet so that when stacked together the hole through all of the sheets would resemble a cone. The hole at the front of the collimator had a diameter of 2.858 centimeters and the hole at the back of the collimator had a diameter of 0.635 centimeters. The conical hole is a convergent collimator and was sized to align with the hole in the boron nitride aperture disk.

The borated polyethylene sheets were placed vertically on an aluminum support table and fastened together with two steel rods through opposite corners of the assembly. The height of the table was chosen so that the conical shaped hole was at beam centerline. In addition, adjustable feet were provided to precisely position the table at the correct height and lock it into place. The collimator was placed as close to the gamma shield as possible without interfering with the operation of the gamma shield during measurements. The gamma shield must be closed for personnel entry into the ERS Cell, but it has to be open to perform measurements.

With the collimator in place, the beam had a divergent angle of 0.85°. This angle with the positioning of the sample created a beam diameter of 1.02 centimeters at the sample. The beam diameter at the detector was 2.87 centimeters. The smallest diameter of the foils was 1.08 centimeters. This meant that the entire beam passed through the sample. The detector area was smaller than the beam area at the detector so every neutron interacting with the detector had to pass through the sample (except background neutrons). This is ideal for a transmission experiment. What should be avoided is beam neutrons that can reach the detector without passing through the sample. If the neutrons causing reactions in the detector did not pass through the sample then the mass signal will not vary as much due to compositional changes in the sample because there will always be a large part of the signal which is unaffected by the sample. This is the same reason that the background rate should be reduced to as low as reasonably achievable. With the geometry of the collimator and placement of the sample and detector shown, the entire beam passed through the sample and a portion of this beam interacted with the detector.

5.1.3. Experiment table

The experiment table is a simple design made of aluminum angle, sheet and bars to support the experimental equipment. The table had a bracket in the front for mounting the fixed gadolinium filter. Mounted underneath the table were two remotely-operated linear actuators which allowed the cadmium filter and sample holders to be positioned within the beam and then removed. The controls for these actuators were located at a table external to the ERS Cell. The linear actuators had limit switches to control the starting and stopping positions of the element sample holders and cadmium filter. The filters and sample holders are described in more detail below.

The table occupies floor space of 57.7 cm by 81.6 cm but the legs are slightly tapered so that the table top surface is only 41.9 cm by 68.3 cm. The table is shown in Figures 24 and 25. Figure
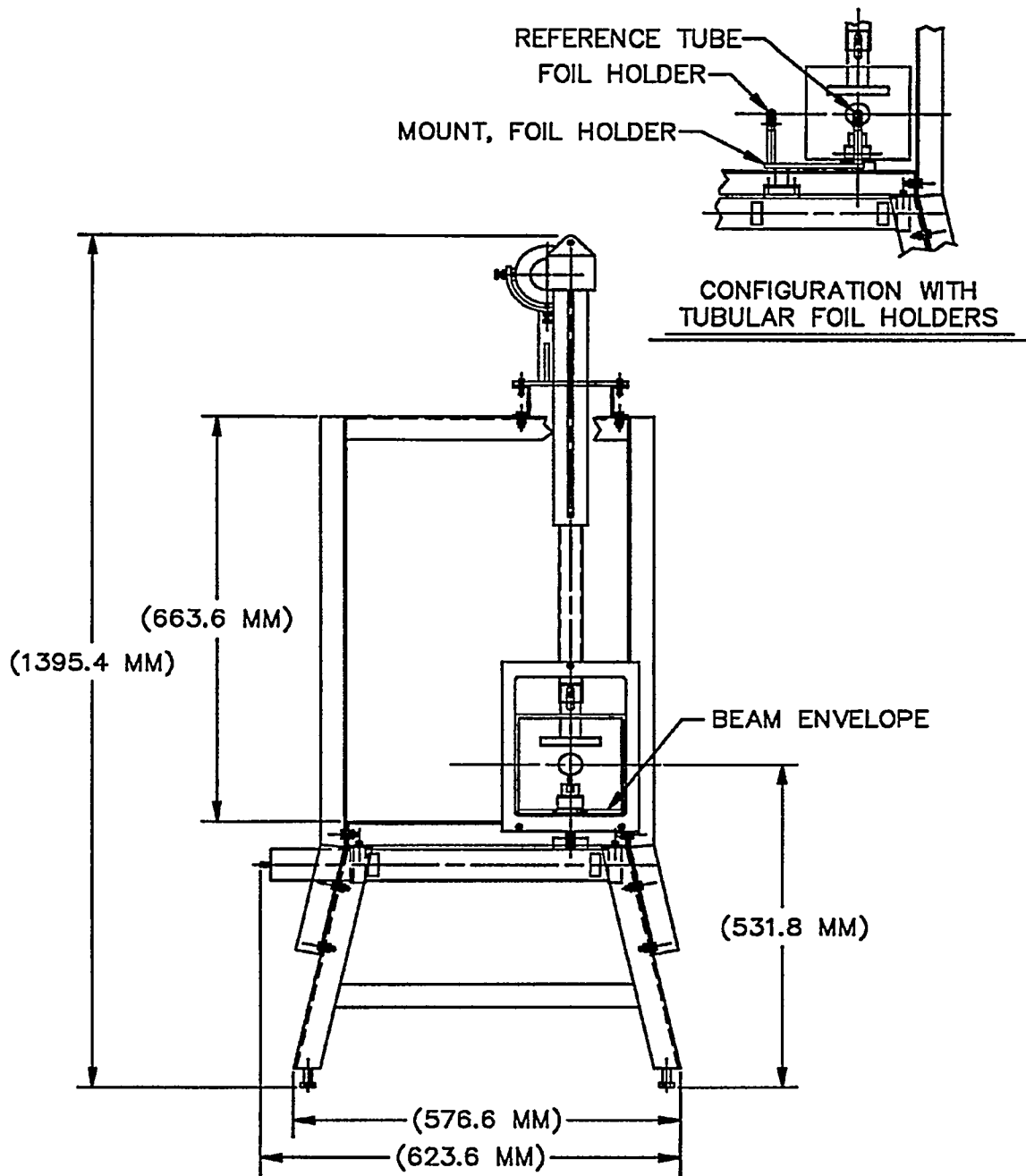
Figure 24: Experiment Table (View Along Beam Axis)
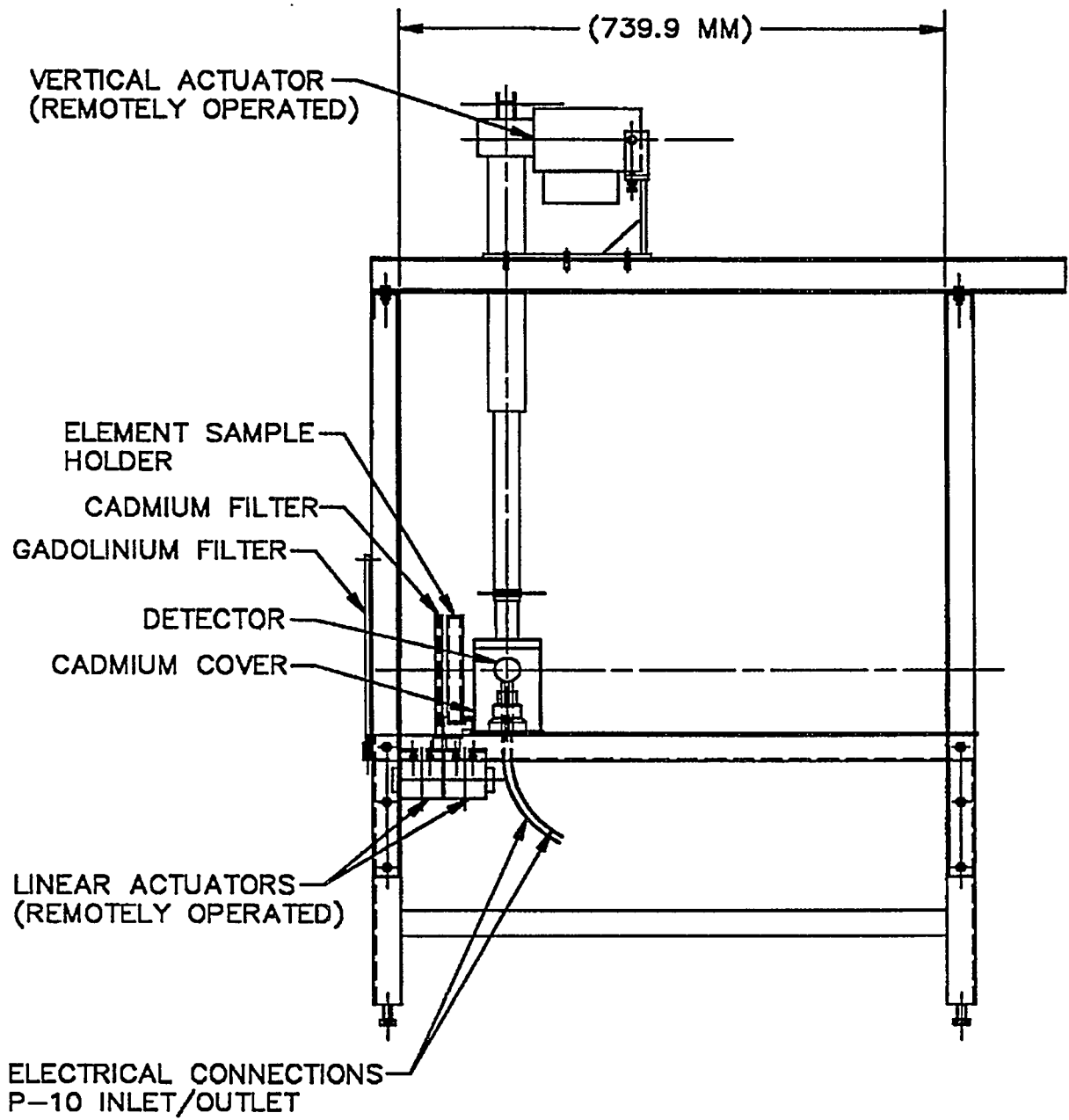
Figure 25: Experiment Table (View Perpendicular to Beam Axis)

60

24 is a view along the beam axis. Figure 25 is a view perpendicular to the beam axis showing the positioning of the filters, sample holder, and detector. Not shown in the figures are the electrical connections for power and control of the actuators. These are all run to an electrical connection strip mounted on the top of the table in the back corner. The table top has a wide slot that securely holds the detector in place. The slot allows the detector to be positioned at distances from the sample of about 1.3 cm up to 61.0 cm and maintain alignment with the neutron beam. Figures 24 and 25 show the detector mounted close to the sample, however, for all measurements performed, the detector was placed in the farthest position - 61.0 cm from the sample. As discussed in Chapter 3, this distance reduces the solid angle of the detector to 0.00067 steradians.

5.1.3.1. Gadolinium filter

The gadolinium filter is mounted in a rectangular aluminum frame. The aluminum frame is held together with four small screws so that the paper-thin gadolinium foils are press fit in place. The foils are exposed on both sides of the frame except on the edges. The holder is positioned on the front of the table by a guide pin with a set screw. The frame is quite large in relation to the beam area (approximately 17.8 cm wide by 22.9 cm high). It is sized to hold gadolinium foils used at NRAD for radiography purposes so that no new foils had to be procured. The frame also allows varying thicknesses of foils and multiple foils to be used as necessary. For the initial experiments, three foils were used to create a total filter thickness of 0.01 cm.

5.1.3.2. Cadmium filter

The cadmium filter holder is more elaborate than the gadolinium filter holder due to the need to position it in and out of the beam remotely during the measurements. The holder is an open aluminum frame (18.4 cm high and 18.1 cm wide) which has a 0.32 cm wide track to allow cadmium foils to be placed in the holder. The opening for the cadmium foils is 15.6 cm wide and 15.8 cm high. The holder is mounted to one of the linear actuators so that the cadmium filter can be positioned in and out of the beam. The cadmium filter holder is designed with an opening at the top so that the filter thickness can be easily changed without having to remove the holder from its mounting. For the initial measurements, three cadmium foils were used to create a total filter thickness of 0.1 cm. The cadmium filter in retracted position (removed from the beam) is shown in Figure 26. Figure 26 also shows the small sample holder, dummy sample holder, and gadolinium filter. The neutron beam runs parallel to the slot in the table.

5.1.3.3. Samples and sample holders

Holders were built for two different types of samples to be examined. A large sample holder was designed to hold plates (5.08 centimeters by 15.24 centimeters) from the Zero Power Physics Reactor (ZPPR) inventory and a small sample holder was designed to hold a stack of ZPPR foils (1.27 centimeter diameter).
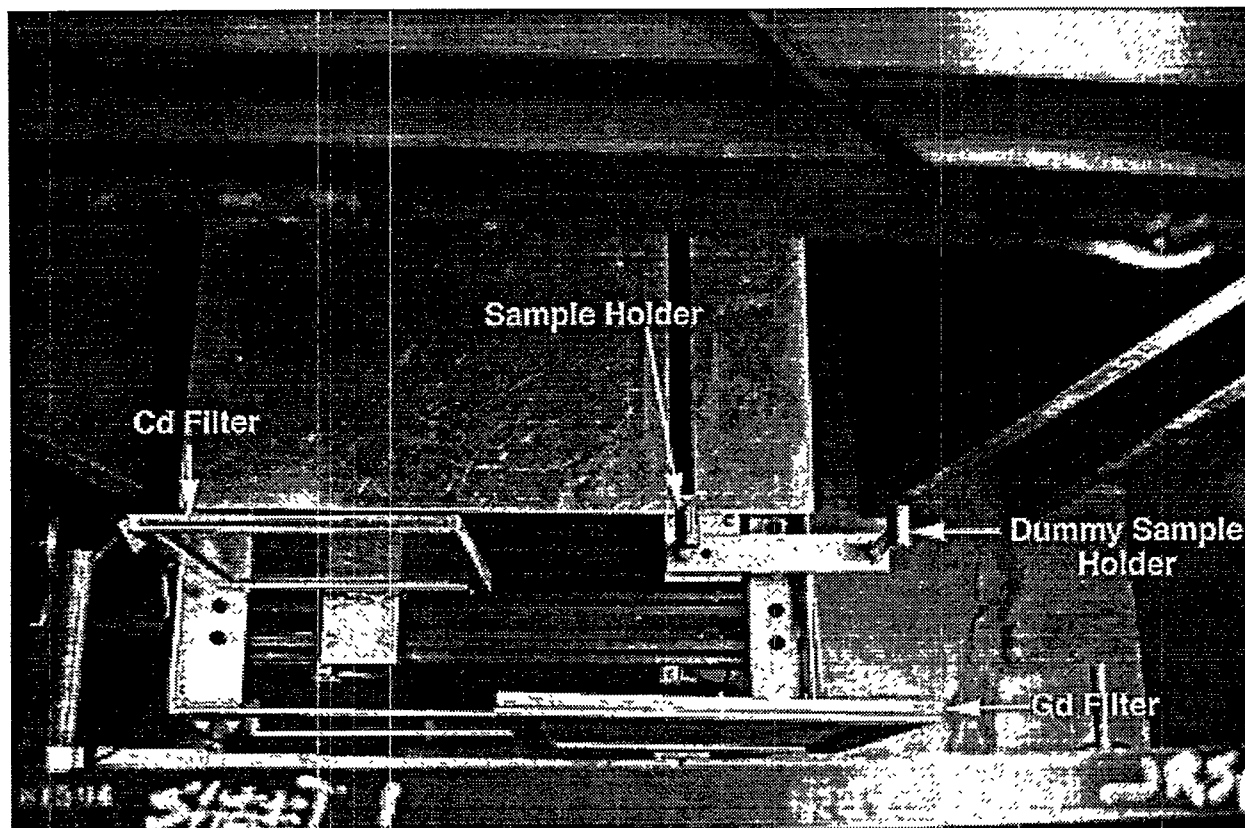
Figure 26: View Looking Down on Experiment Table

The large sample holder is made of aluminum and has a dimension of 16.0 cm by 16.0 cm and a thickness of 2.2 cm. The sample holder was built to hold three ZPPR plates side-by-side with each plate having a dimension of 5.08 cm by 15.24 cm. These 15.24 cm by 15.24 cm layers of ZPPR plates can be stacked up to create thicknesses varying up to about 1.6 cm. The ZPPR plates are depleted uranium plates with a ^{235}U content of 0.22 wt% with each one individually wrapped in aluminum foil to minimize contamination. The large sample holder is shown in Figure 27 with several of the ZPPR plates. The sample holder mounts in an aluminum bracket fixed to one of the linear actuators with four screws. The sample holder mounted to the actuator on the experiment table is shown in Figure 28.

A small sample holder was also fabricated. The small sample holder was designed to hold ZPPR foils. The foils have a diameter of 1.27 cm with the fissile deposit being 1.27 cm in diameter for the uranium foils and 1.08 cm in diameter for the plutonium foils. The small sample holder is made of 0.004 cm thick stainless steel to match the cladding thickness of the blanket elements. The holder is a stainless steel cylindrical shell. The sample holder is loaded by stacking foils in the cylinder, placing a stainless steel disk on top of the foils, and then running lock wire through two holes in the cylinder to hold the foils in place. A close-up of the small sample holder is shown in

62
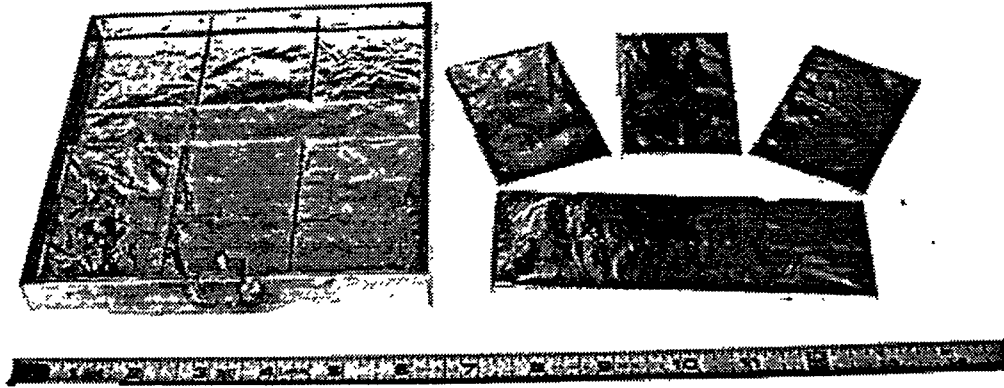
Figure 27: Large Sample Holder and ZPPR Plates

Figure 28: Large Sample Holder on Experiment Table

63
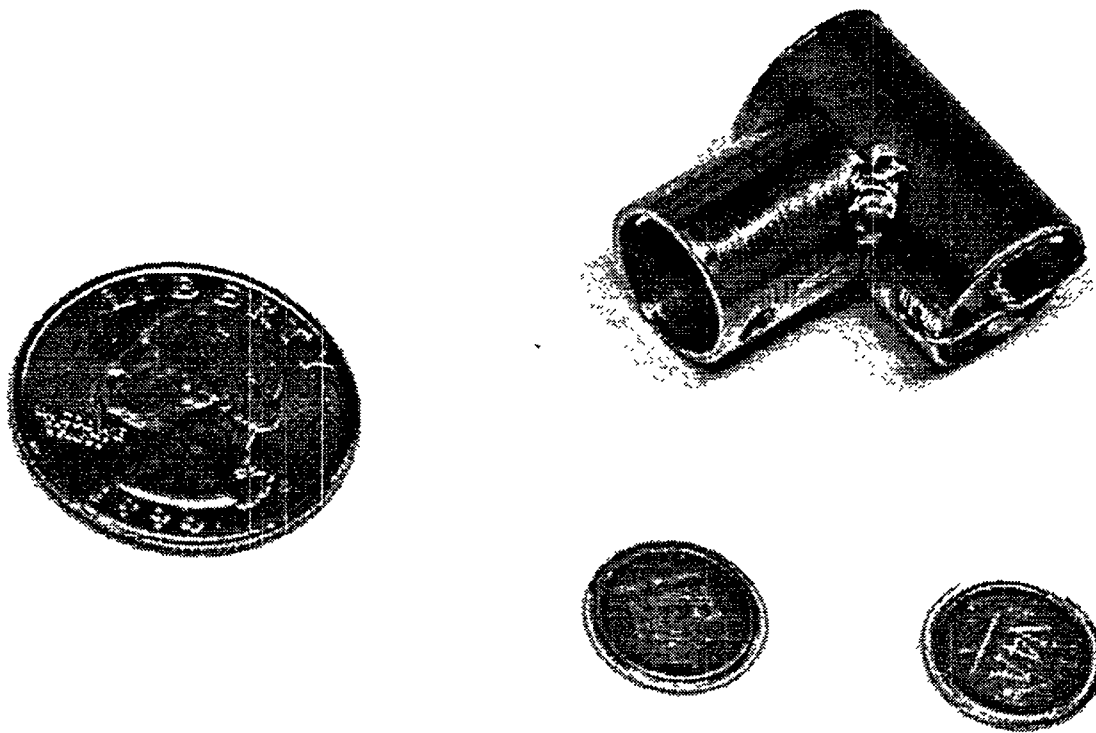
Figure 29: Small Sample Holder and ZPPR Foils

Figure 29. Two ^{239}Pu foils and a quarter are shown in the photo so that the relative size of the sample holder can be assessed. The uranium mass of the small sample holder when loaded to match the thickness of the blanket assembly was approximately 26.33 grams. Since the range of interest for ^{239}Pu content is from 0 weight percent up to about 2 weight percent, the mass of ^{239}Pu in the sample was typically less than 0.52 grams.

The sample holder is positioned along the axis of the beam by a mounting fixture which allows it to be fixed to a bar on one of the actuators for positioning the sample in and out of the beam. The sample holder mounted to the linear actuator was shown in Figure 26. Figure 26 shows the sample holder positioned so that the sample is in the beam. The other sample holder shown in Figure 26 is a dummy sample which is an empty stainless steel sample holder. This allows the effect of the stainless steel holder to be eliminated from the transmission measurements through the subtraction process previously described in Chapters 3 and 4.

5.1.4. Detection system

The detection system was an integral component of the experiment and the choice of a plutonium fission detector impacted the results of the experiment as shown in Chapters 3 and 4. There were two detectors with associated electronics used in this experiment. A back-to-back fission

chamber loaded with two ^{239}Pu foils was the primary detector and a sealed cylindrical fission chamber loaded with ^{235}U was used as a flux monitor. The detectors are described in detail in Section 5.1.4.1 below. Most of the electronics are commercially available units except the pre-amplifiers and pre-amplifier power supplies. The electronic components are discussed in Section 5.1.4.2 below.

5.1.4.1. Detectors

Every detector is unique and settings for the electronics have to be adjusted individually based on the characteristics of the detector. Both of the detectors used in this experiment were fission chambers. For this experiment, the detectors were operated as ionization chambers.

A neutron entering the detector may interact with a fissionable atom and cause a fission event. If a fission event occurs, two heavy fission fragments in addition to other particles are released. Each of the fission fragments has a large amount of kinetic energy and is highly charged. Typically, one of these fission fragments is deposited within the fissile deposit, backing material, or detector housing and does not release its energy to the gas volume of the chamber. However, one of the fragments is typically released to the gas volume of the chamber. This fragment then loses energy and electrical charge by interacting with the gas molecules. These interactions cause molecules to become excited or ionized. After a neutral molecule is ionized, the resulting positive ion and free electron are called an ion pair. These ion pairs serve as the basic electrical charge that is detected by the ionization chamber. By placing a positive charge on one side of the detector, the electrons migrate through the gas to the collection surface (typically a large plate or wire). Once the charge reaches the detection plate or wire it is recorded as an electrical pulse. The pulse is then amplified and recorded as a count by the electronics. This is the basic description of the operation of a fission chamber, refer to Ref. 28 for more information regarding fission chambers.

The flux monitor is a Reuter-Stokes Model RS-P6-0805-134 Fission Counter with an active length of 15.24 cm. The detector is wrapped in cadmium to reduce the count rate. In addition, the monitor is placed within the shielding material along the north wall of the ERS Cell. By doing this the count rate is reduced to approximately 4400 counts per second. This results in a modest loss of counts due to dead time such that a dead time correction is not necessary.

The back-to-back fission chamber used as the main detector for the experiment was built for use in the ZPPR at ANL. The detector is shown in Figure 30. It is a small spherical detector which can be separated to allow two foils to be placed within the center next to each other. Each half of the detector functions as an independent fission chamber and can record a detector signal individually. These chambers are typically loaded with one ^{235}U and one ^{238}U foil and are used to determine a fast and thermal flux rate simultaneously. For this experiment it was loaded with two foils with ^{239}Pu deposits. Side A (the front side) was loaded with foil ID-9-06 which has 100.62 µg of ^{239}Pu and side B (the back side) was loaded with foil ID-9-05 which has 106.84 µg. of ^{239}Pu. The area of each deposit was approximately 2.5 cm^2 (diameter of approximately 1.78 cm). Two ^{239}Pu foils were loaded in the detector to increase the mass of the fissionable material in the detector. By

65
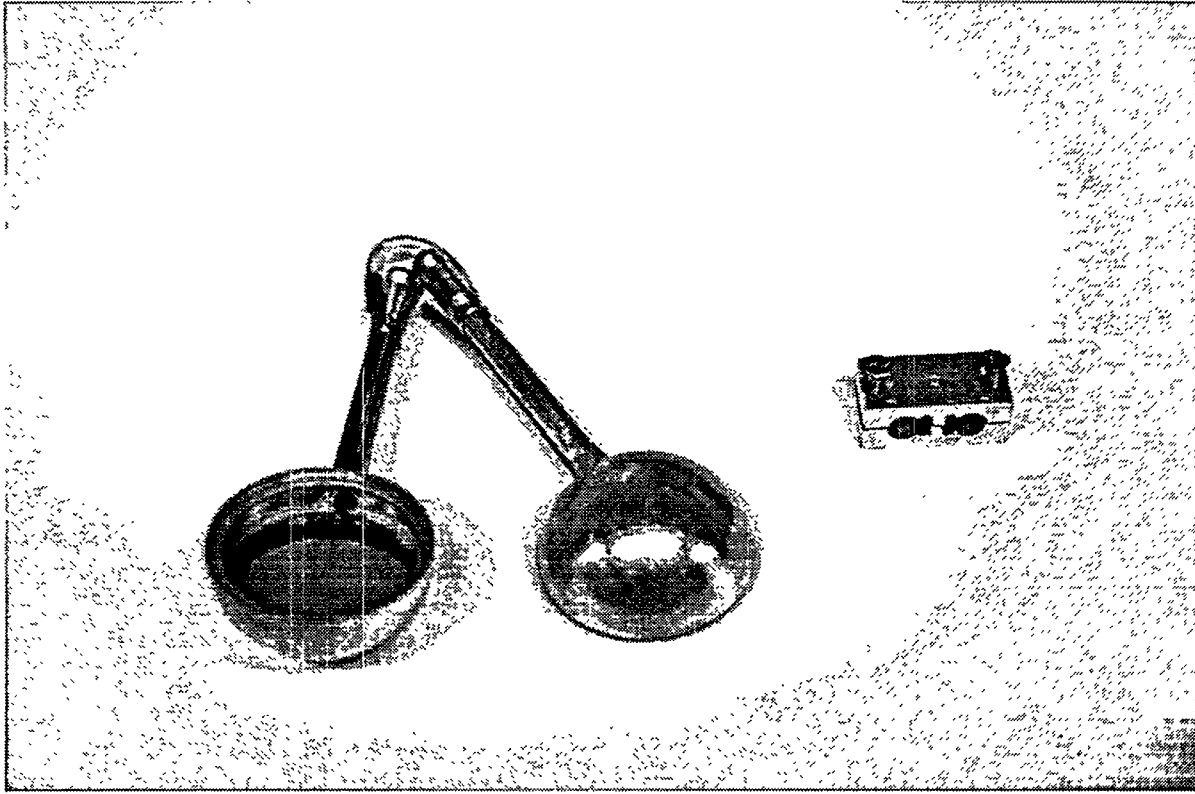
Figure 30: Back-to-Back Fission Chamber

increasing the mass, the probability of interaction is increased, and hence, the efficiency of the detector is increased.

The detector is placed into a simple stand so that it can be mounted to the experiment table. In addition, a 0.1 cm thick cadmium cover with a small opening (diameter of 1.91 cm) was placed around the detector. The cover reduced the background count rate from stray thermalized neutrons within the ERS Cell while the hole allowed the beam to pass without interference. The detector with the cadmium cover mounted on the experiment table is shown in Figure 31. The electrical connection strip shown in Figure 31 contains the connections for control and power of the linear actuators discussed previously.

Fission chambers typically employ ^{235}U or ^{238}U as the active isotope. These have relatively low alpha decay rates and these alpha signals can be easily discriminated by setting a lower threshold on the electrical signal generated from the amplifier. However, the alpha decay rate in plutonium is much higher. Figure 32 shows the multi-channel analyzer spectrum produced from the back-to-back fission chamber. This spectrum is typical of fission chambers with a thin deposit and a small detector gas volume. If the gas volume of the detector were larger, such that the full energy of the fragments could be deposited in the gas, then the spectrum would represent the actual energy of the fission fragments and look similar to the familiar fission fragment energy distribution. This

66
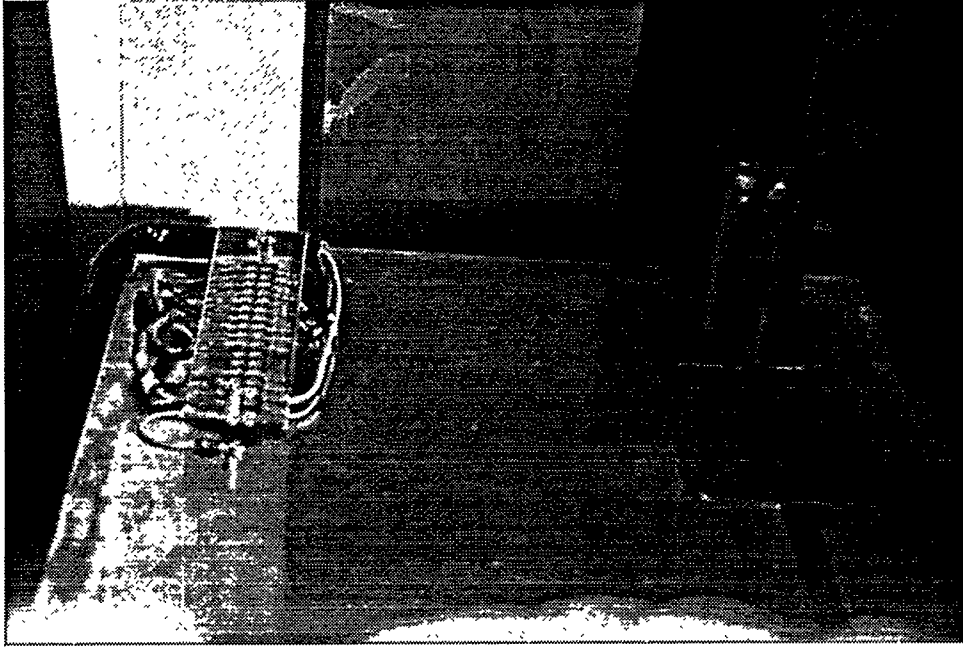
Figure 31: Detector Mounted on Experiment Table
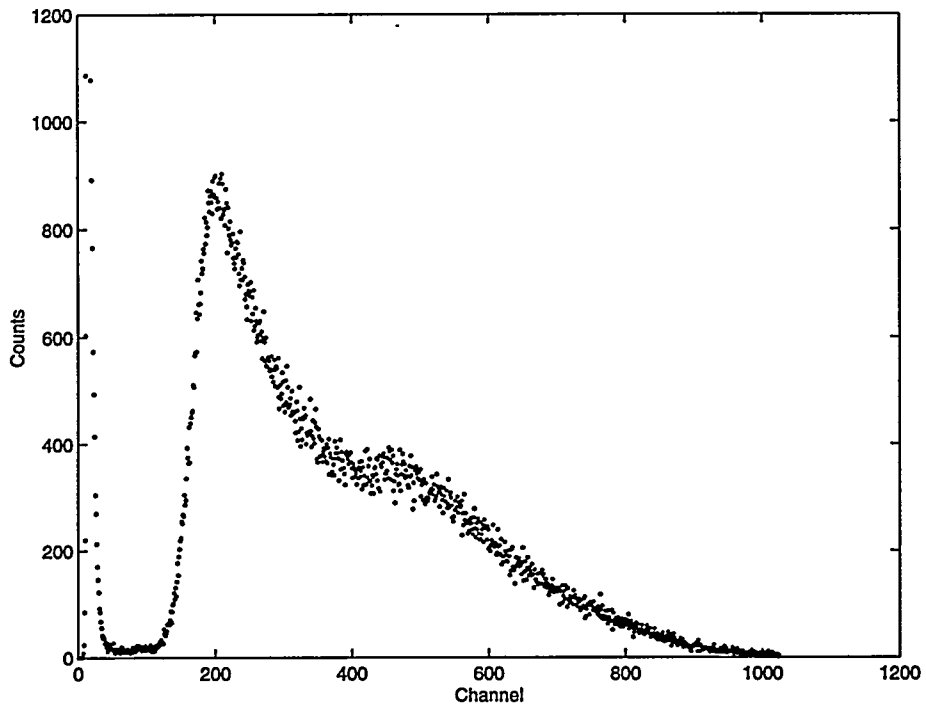
Figure 32: Pulse Height Spectrum from Back-to-Back Fission Chamber

distribution peaks at around 65 MeV and 95 MeV and has a valley around 80 MeV. When the gas volume is small relative to the fission fragment range, the fragments will still have a significant amount of energy when striking the chamber wall which will not be deposited in the gas through ionization. This results in a distortion of the pulse height spectrum and causes a peak much lower than the initial fission fragment energies. This is the case for the back-to-back fission chamber as shown in Figure 32. Also note the very large alpha signal pulse height in the first 50 channels. These are due to alpha decay within the plutonium deposit. By setting the discriminator level to correspond to the valley around channel 80, the alpha signal is essentially eliminated from the detector signal.

5.1.4.2. Electronics

A schematic of the detection system is shown in Figure 33. Note that all of the electronics except the pre-amplifiers for the back-to-back fission chamber are located external to the ERS Cell. The P-10 gas supply (a mixture of 90% argon and 10% methane) for the back-to-back fission chamber was also located external to the ERS Cell.

The components of the system are stored in two NIM bins contained in a cabinet. The instruments are shown in Figure 34. The power supply to the cabinet is ground-isolated and surge protected to eliminate electrical noise from interfering with the counting system. Each system (the flux monitor and the primary detector) has separate components located in the NIM bin, however, an Ortec Model 974 Quad Counter/Timer is used to record the total counts from each detector simultaneously. The flux monitor is powered by a NIM standard high voltage power supply. The detector signal is run through the pre-amplifier to an Ortec Model 572 Amplifier, which in turn is connected to an Ortec Model 550A Single Channel Analyzer. The settings for the various components were shown in Figure 33.

The set-up for the back-to-back fission chamber is similar to that for the flux monitor except that two detector signals are output from the back-to-back chamber. The chamber produces two signals as each half is an individual detector. The signals run through individual pre-amplifiers before being connected in parallel. Once the signals are joined, the combined signal is sent to an Ortec Model 572 Amplifier which in turn is connected to an Ortec Model 550A Single Channel Analyzer. The settings for these components were also shown in Figure 33.

5.2. Experiment Plan

A straight-forward approach was followed for the execution of the experiment. This section is divided into two subsections to describe the operation of the experiments and the procedure followed to perform the measurements. The measurement plan, which includes the types of measurements that were performed, is described in Section 5.2.1. The general procedure that was followed to perform a single measurement is discussed in Section 5.2.2.
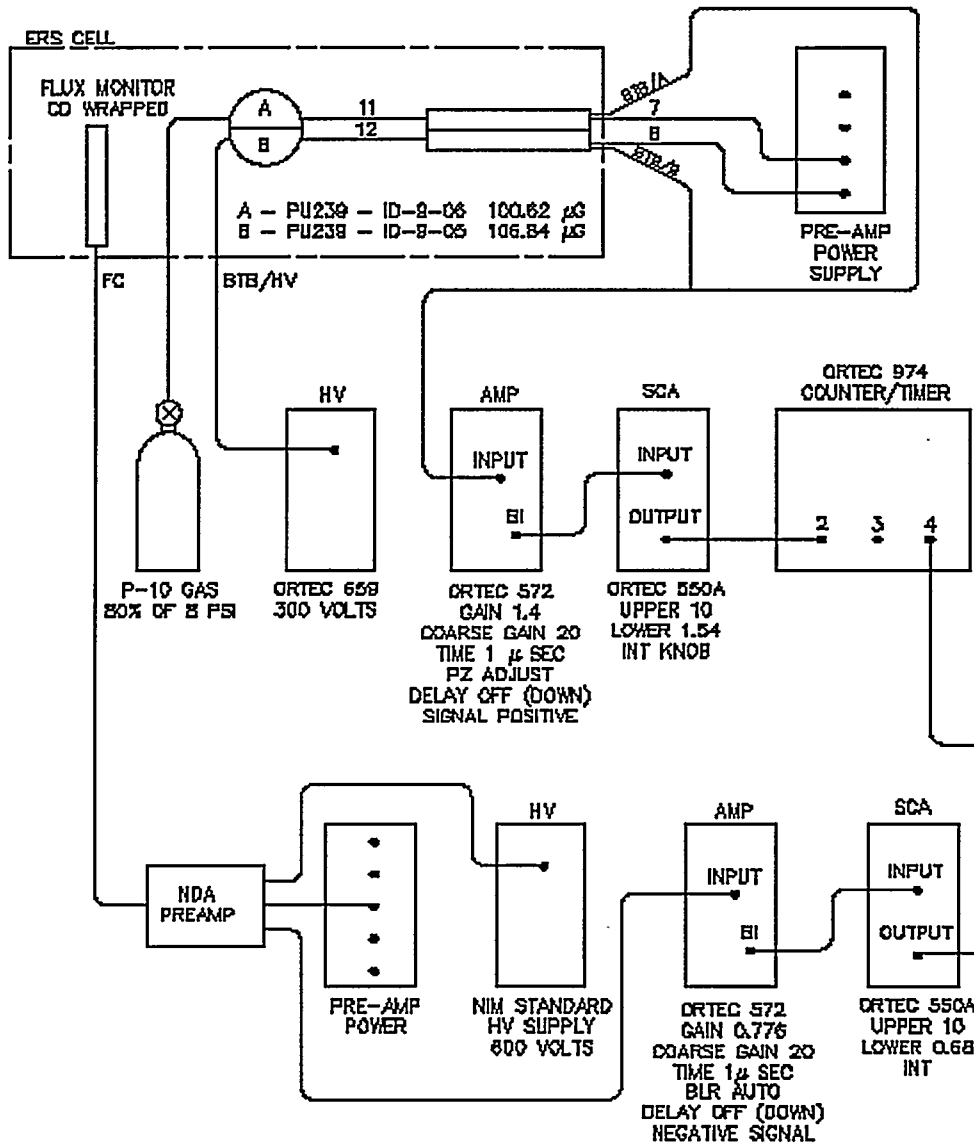
Figure 33: Detection System Schematic
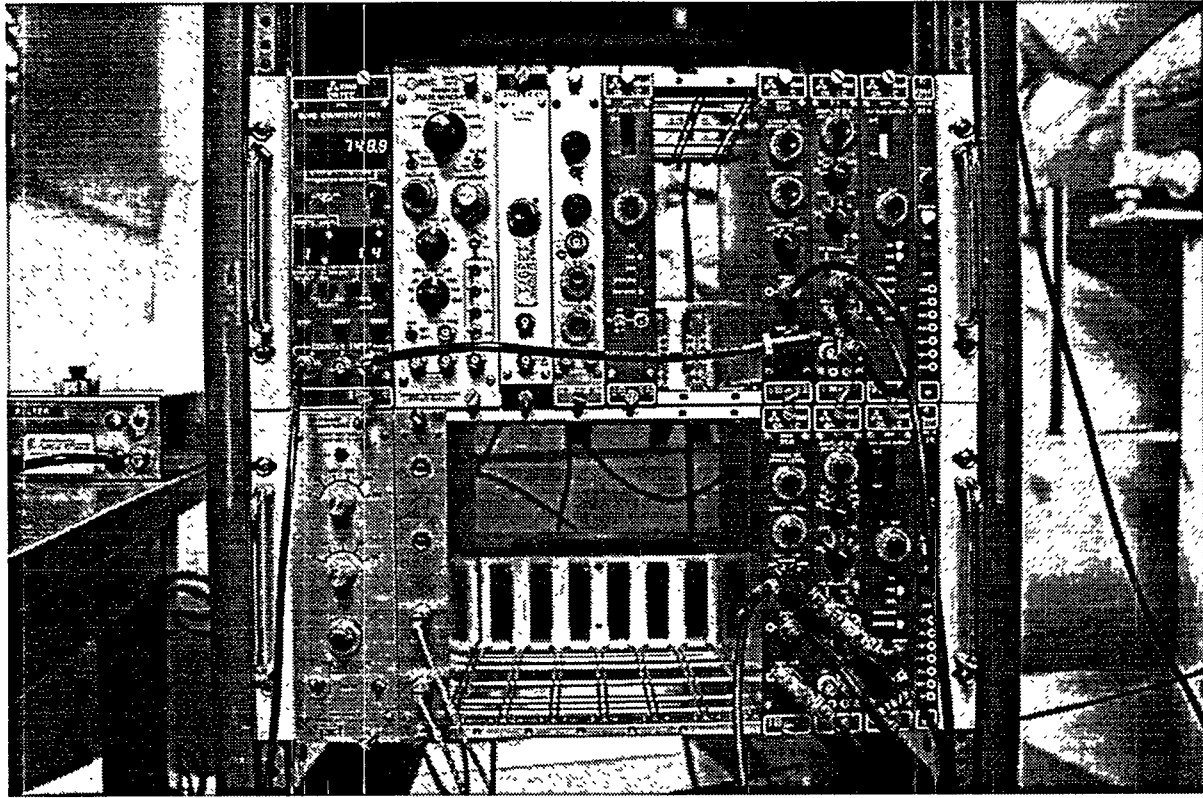
Figure 34: Detector Electronics Cabinet

5.2.1. Measurement plan

The first measurements that were performed were to determine the level of background in the ERS Cell. There were several issues that had to be addressed. The first was to determine the level of noise (background) with respect to the primary signal from the beam. This is known as the signal-to-noise ratio and should be as high as possible. For example, if 50% of the response is the signal of interest and the other 50% of the response is from background, then the signal-to-noise ratio is 2.0. However, if the background is 10% of the total response then the signal-to-noise ratio is 10.0. To limit the error associated with the system, it is desirable to limit the background count rate as much as possible. It was determined that the background levels were too high and shielding had to be added in the ERS Cell to reduce the background to acceptable levels.

Once the background was reduced, proof-of-principle tests were performed. The first tests included two runs - one with no plutonium and one with a reasonably high ^{239}Pu content. This immediately indicated that there was a large change in response based on the plutonium content as indicated in the calculations. After these few initial runs, additional cases were explored to develop a function of the mass signal versus the ^{239}Pu content in the sample. This relation was then directly compared to the relation generated from the calculations.

As a test of the effect of thickness on the mass signal, a series of tests was run with uniform foil thicknesses. As mentioned previously, transmission measurements through actual blanket elements will not be of uniform thickness due to being perpendicular to the axis of the cylinder. The variance in thickness will be determined by the size of the beam in relation to the size of blanket element. The mass signal measured from a blanket element will actually be an integration of the mass signal over the range of thicknesses that the beam traverses the sample. Since the mass signal is a measure of the total macroscopic cross-section times the sample thickness, the response will be weighted in favor of the transmission through the thinner regions of the sample. These measurements indicated the effect of this weighting as it relates to sample thickness.

Composition of the sample was another important issue that was examined. The task was to determine the effect on the mass signal results as the ^{235}U content changes. There is some question as to the nominal content of the ^{235}U in the depleted uranium blankets. These tests verified that small changes in the ^{235}U content are of no consequence and can be neglected as insignificant.

It was shown in Chapter 4 that the thickness of the cadmium filter and gadolinium filter do not significantly affect the measurement results. Therefore, it was not deemed necessary to perform a series of measurements to demonstrate these benign effects.

5.2.2. Measurement procedure

A standard procedure was followed to perform a group of measurements to obtain the mass signal value for a given sample. First, the detector systems were turned on and allowed to warm up for approximately 15 to 30 minutes prior to performing any measurements. This warm-up period allowed the P-10 gas to purge the detector of air. During this warm-up period, the NRAD reactor would go through a start-up procedure and obtain a steady-state power of 250 kW. The reactor operator would place the reactor in automatic mode. In automatic mode, the reactor power is controlled through a flux regulator and operation is independent of operator intervention. After indication from the reactor operator in the control room that the reactor was in automatic mode, a measurement would begin.

While the reactor was being brought to power, a visual check of all instrumentation settings and cabling would be performed. This check guaranteed that all of the system settings were identical to previous measurements and that results for the measurement could be directly compared to previous measurements. After the settings were checked, the cadmium filter and sample were positioned as necessary. The intended position of the filter and sample were verified by viewing a monitor connected to a camera in the ERS Cell. As these filter movements were remotely controlled from outside the ERS Cell and personnel access to the ERS Cell was impossible while the reactor was operating, the camera was a vital necessity. This remote viewing indicated conditions of the experimental equipment.

The count time was then preset on the Counter/Timer. For all measurements the count time was established as 1000 seconds. Typically, the case with the sample and filter removed from the

beam was run first. This value could then be directly compared to previous measurements to get an indication of the reactor output and whether the system was operating properly. After the initial measurement, the cadmium filter was inserted in the beam and another measurement taken. The sample was then placed in the beam and the third measurement performed. Finally, the filter was removed from the beam and the last measurement was performed. This series of four measurements would take about one hour and 15 minutes to complete and then the reactor would be shut down.

For a second sample run on a given day, after the reactor was shut down an entry into the ERS Cell would be performed to change the sample. From operation of the reactor, the radiation level in the ERS Cell would be elevated. Immediately after shutdown the level in the room was as high as 50 mRem/hr. Therefore, the sample was changed as quickly as possible to minimize radiation exposure. The sample could typically be changed in a few minutes. Once the sample was changed, the measurement process was repeated for the new sample.

6. Results

Measurements were performed using the NRAD reactor facility over a period of approximately five months from August, 1997 to December, 1997, with a few additional measurements performed in January and February of 1998. The results of the measurements discussed in Chapter 5 are included here. A key issue and potential hinderance to the success of the experiment was the level of background within the ERS cell with respect to the basic signal from the primary beam. Therefore, extensive background measurements were performed initially to characterize the signal interference from background within the ERS cell.

Once these measurements were completed and background from scattering of the beam reduced to reasonable levels, proof-of-principle measurements were performed to demonstrate that the method is feasible for determining ^{239}Pu content and determine if the measurements behave as predicted by the calculations in Chapters 3 and 4. After the method was demonstrated, sensitivity studies were performed to address the effects from changes in the sample composition and sample thickness.

The data from the measurements is summarized in this chapter, that is, usually only the transmission and the mass signal values are reported here. The raw data is included in Appendix C for all measurements performed.

6.1 Background Measurements

The total response for any measurement is a combination of the direct signal of interest and the background signal. The direct signal of interest for these measurements are neutrons that interact with the detector after being transmitted through the sample and filters. The background signal is comprised of several different components – a contribution from neutrons from the reactor that are scattered but still manage to interact with the detector, alpha decay events in the detector material that are not discriminated from the signal, and general background from neutrons from external sources. External sources of neutrons are any source of neutrons besides those mentioned above. These can include neutrons emanating from spent fuel stored in the HFEF hot cell above the ERS cell, cosmic radiation, and neutrons caused from the interactions of radiation with matter like (γ,n) reactions. The discriminator was set to eliminate a large portion of the alpha decays from the detector deposit as described in Chapter 5. Therefore, this contribution is fairly constant and cannot be further reduced. As the measurement location is fixed, the contribution from external neutron sources also cannot be easily reduced. However, the contribution from neutrons scattering from the beam in the ERS Cell and interacting with the detector can be a significant portion of the total signal. It is postulated that this contribution is indeed a large portion of the total signal because flux monitors within the ERS Cell well away from the neutron beam have recorded significant count rates in the past. In addition, there is a large scattering pathway between the west wall of the ERS Cell and the beam collimator required to allow for the movement of the gamma shield.

73

Table 11: Results of Initial Measurement				
Measurement	BTB Counts	Monitor Counts	Count Time (sec)	BTB Count Rate (cps)
No Sample - No Filter	182912	2257631	500	365.8
No Sample - Filter	53653	2257644	500	107.3
Sample - No Filter	95698	2249741	500	191.4
Sample - Filter	35000	2249939	500	70.0

Because the background should be reduced to as low as reasonably achievable and should be well characterized, background measurements were performed. To do this, a sample holder was loaded with 94 ^{238}U foils to simulate the thickest portion of the depleted uranium in a blanket element. The sample was loaded on the experiment table as described in Chapter 5. The gadolinium filter thickness was 0.01 cm. The cadmium filter thickness was 0.1 cm. For the initial measurement, there was no shielding placed around the experiment table. The results for this series of measurements are shown in Table 11. The measurement configurations are described by the position of the cadmium filter and the sample with respect to the beam. A designation of no sample means that the sample is not in the beam. The notation is shortened throughout for the description of each measurement. For example, the NS-F designation is for a measurement when the sample is removed from the beam (no sample) and the cadmium filter is in the beam (filter). The gadolinium filter is always in the beam. The back-to-back fission chamber located in the beam is noted as BTB. The fission chamber used to monitor the beam flux is referred to as the monitor.

The only measurement of interest for the background study is the measurement when the sample and cadmium filter are in the beam. This is because for every measurement series performed, this case yields the lowest count rate due to the greatest amount of material to attenuate the beam. The other measurements did indicate that the collimator was aligned so that there was a primary signal from the beam, however, accurate alignment of the collimator and proof of alignment will be discussed later.

As shown in Table 11, the count rate was 70.0 counts per second when the sample and filter were in the beam. The detector (with cadmium cover) was then moved six inches to the north of the beam centerline at approximately the same height as the previous measurement and the measurements repeated. As the detector was out of the beam, the measurements for the four filter-sample arrangements were expected to be identical as there was no primary signal from the beam and the signal should be from background only. The results for this case, indicated a count rate of 34.1 cps for the measurement with the sample and cadmium filter in the beam and a range from 33.9 to 34.5 cps for the other three measurements. This count rate was approximately 50 percent of the count rate when the detector was in the beam and indicated an unacceptably high background rate.

Based on these results it was determined to surround the experiment table with borated polyethylene sheets to reduce the background rate as much as possible. Borated polyethylene sheets were added so that there were five sheets on the north side of the table, ten sheets on the south side

74

Table 12: Results of Background Measurements						
Detector Position	BTB Count Rate (cps)	BTB Error (cps)	Monitor Count Rate (cps)	Monitor Error (cps)	C/M	C/M Error
5" North	6.214	0.032	4377.4	0.9	$1.4194 \cdot 10^{-3}$	$7.4 \cdot 10^{-6}$
5" South	6.149	0.039	4368.1	1.0	$1.4077 \cdot 10^{-3}$	$9.0 \cdot 10^{-6}$
5" Above	6.193	0.039	4398.2	1.0	$1.4081 \cdot 10^{-3}$	$9.0 \cdot 10^{-6}$
Beam Centerline	6.181	0.025	4372.8	0.7	$1.4136 \cdot 10^{-3}$	$5.8 \cdot 10^{-6}$

of the table, four sheets above the table, and one sheet on the east side of the table. In addition, gaps above the table were covered with three sheets, four sheets were added on the south side of the collimator, and two sheets were placed on the floor of the ERS cell on the south side of the collimator. Four layers of borated poly sheets were also placed below the collimator and the experiment table to fill a streaming path below the collimator. Measurements were performed, and the results indicated a count rate of 6.2 cps for the measurement with the sample and cadmium filter in the beam. The count rate for the other three measurements were statistically identical. The count rate of 6.2 cps was approximately 8.9 percent of the initial measurement. It should be noted that by reducing the background signal, the total signal was also reduced such that the background contribution to the reduced signal was more than the 8.9% listed above. At this point, the detector was placed back in the beam and a measurement performed. The result indicated a count rate of 40.7 cps for the measurement with the sample and cadmium filter in the beam so the background rate was approximately 15 percent of the new total signal. No more additional shielding could be easily added to the ERS Cell so this was determined to be the final shielding configuration for all of the measurements.

After the shielding configuration was established, additional measurements were performed to determine the background rate for the detector when it was in the beam. The background rate for the detector in the beam could not be determined by direct measurement because there was no mechanism to remove the direct contribution from the beam and still account for the reactor as a significant source of background. The background rate was determined by calculating the spatial gradient from measurements when the detector was located outside of the beam. Measurements were performed with the detector to the north of the beam centerline, to the south of the beam centerline, and above the beam centerline. Results for these cases are shown in Table 12. A linear interpolation was performed between the north and south positions to determine the background level at the beam centerline. The detector count rate (C) over the monitor count rate (M) is also shown in Table 12. The C/M value is the signal count rate normalized by the monitor count rate for each measurement. The data shown in Table 12 indicate a minimal spatial gradient which indicates a high confidence in the computed background rate for the detector position.

As an additional characterization of the background levels, a background count was performed without the reactor running to determine the background rate from alpha decays and external neutron sources. This allowed a determination of the relative contributions to the total sig-

Table 13 : Signal Rate from Different Background Sources		
Source of Signal	Count Rate (cps)	Relative Rate (% of Total Signal)
Total Signal	40.74	100.0
Primary Signal	34.56	84.8
Total Background	6.18	15.2
Reactor Background	4.09	10.1
Alpha Decay and External Sources	2.09	5.1

nal from the different background contributions. The results of these measurements are shown in Table 13. These results indicate that the background rate is approximately 15.2 percent of the total signal for the lowest count rate measurement in a given series of four measurements. The relative background is considerably less for the other measurements. For example, for the case shown in Table 13, the relative background is only 8.0%, 3.9%, and 1.9% for the NS-F, S-NF, and NS-NF measurements, respectively.

With the background rates well characterized, several cases were run to look at the alignment of the collimator. Initially, the collimator was aligned using a laser pointer held at the front of the collimator and sighting the light through a hole in a dummy sample holder and onto the center of the detector. This method was about as precise as possible considering the cramped conditions in the ERS Cell. Because of this alignment approach, it was important to demonstrate that the collimator, sample and detector were aligned properly such that the axis of the sample was positioned along the axis of beam and that the sample area completely covered the detector area. To do this, a sample was prepared with two ^{239}Pu foils and 93 ^{238}U foils (1.3703 wt % ^{239}Pu). Three different measurement series were performed - one with the ^{239}Pu foils in front of the ^{238}U foils in the sample holder, one with the ^{239}Pu foils in the center of the ^{238}U foils, and one with the ^{239}Pu foils behind the ^{238}U foils. The results are listed in Table 14 and shown graphically in Figure 35. It is apparent from the results that all three of the measurements are statistically identical. Another approach is to consider the standard deviation of the average mass signal as shown in Table 14. The three measurement values are within one standard deviation of the mass signal average. This is actually a tighter criterion on the values and further indicates that the three values are statistically identical. If there were a problem with the alignment of the sample, it would have been apparent in these measurements. For example, if the axis of the sample were not parallel to the axis of the beam, a significant difference in mass signal would have been expected between the measurements when the ^{239}Pu foils were at the front and back of the sample holder.

6.2 Proof-of-Principle Measurements

Once background measurements were complete, proof-of-principle measurements were performed to determine the mass signal value as a function of ^{239}Pu content in the sample. As previously described, the small sample holder was used with a stack of ^{238}U foils. The number of foils was determined by setting the theoretical density foil thickness equal to the thickest portion of

Table 14: Results of Beam Alignment Check				
^{239}Pu Foil Position	Transmission	Std. Deviation	Mass Signal	Std. Deviation
Front	0.1043	0.0014	2.260	0.0131
Center	0.1039	0.0014	2.264	0.0132
Back	0.1034	0.0014	2.269	0.0132
Average	0.1039	0.0008	2.265	0.0076
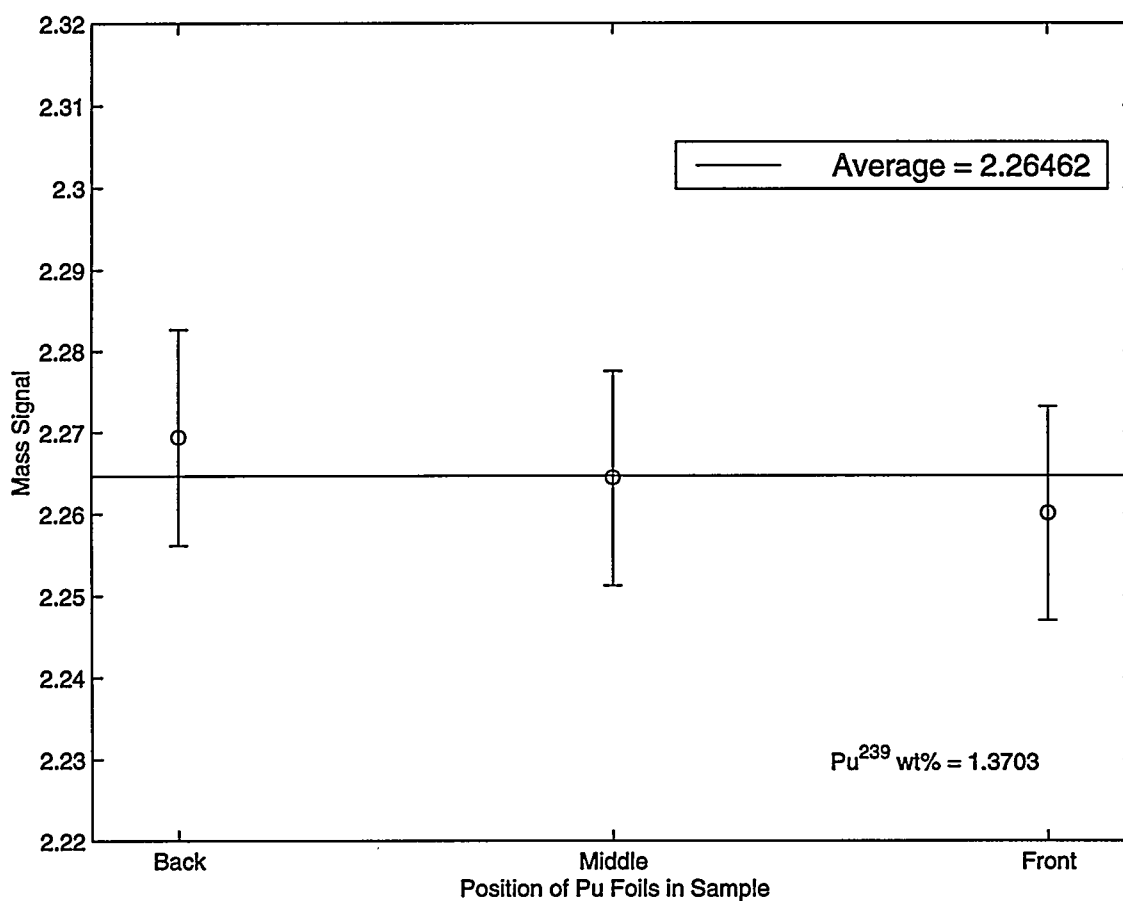
Figure 35: Results of Beam Alignment Check

Table 15: Results of Proof-of-Principle Measurements				
^{239}Pu Content (wt%)	Transmission	Standard Deviation	Mass Signal	Standard Deviation
0.0	0.480	0.0024	0.733	0.0050
0.0	0.479	0.0021	0.736	0.0044
0.073	0.427	0.0020	0.851	0.0047
0.179	0.362	0.0018	1.015	0.0051
0.657	0.192	0.0016	1.648	0.0084
0.657	0.199	0.0014	1.615	0.0071
0.789	0.173	0.0014	1.754	0.0078
0.918	0.150	0.0013	1.895	0.0085
0.990	0.142	0.0010	1.955	0.0071
1.370	0.103	0.0014	2.269	0.0132
1.370	0.100	0.0011	2.306	0.0115
1.606	0.086	0.0011	2.453	0.0128
2.055	0.071	0.0011	2.641	0.0147
2.647	0.050	0.0012	3.001	0.0239
3.177	0.044	0.0012	3.114	0.0260

a blanket element. ^{238}U foils were then removed and ^{239}Pu foils were added to obtain different ^{239}Pu contents in the sample. This replacement simulated the conversion of ^{238}U to ^{239}Pu in a blanket element by maintaining the sample mass as close to the nominal value as possible. The nominal sample mass was approximately 26.33 grams, with most samples within about 50 milligrams of the nominal mass. The largest deviation was about 160 milligrams from nominal.

The results of the measurements are shown in Table 15. Figure 36 shows the data plotted for the range up to 2.0 weight percent ^{239}Pu. Also shown is a curve fit of the calculated values adjusted with a constant bias. As observed from Figure 36, the measured values are in good agreement with the calculated values with a constant bias. The bias is constant for the measurements performed so it is not a function of the ^{239}Pu content, i.e. the bias is not affected by the addition of the plutonium foils in the sample. It was determined that the bias was due to isotopes in the ^{238}U foils not accounted for in the calculations, most notably hydrogen in the glue used to attach the thin aluminum foils on the front and back of each foil. The ^{238}U foils were stamped from a large sheet of depleted ^{238}U in the early 1970's. Each foil was then dipped in a material called Kel-F, which is a non-hydrogenous compound of carbon and fluorine, and covered with a thin aluminum disc (0.00075 inches thick) on each side. The aluminum disks were attached with a small amount of adhesive. In addition, the uranium contains 0.0009 wt% ^{234}U and 0.0056 wt% ^{236}U. For practical purposes the ^{236}U can be treated as ^{238}U. The cross-section for ^{236}U is approximately 10 barns which is identical to the cross-section for ^{238}U. The cross-section for ^{234}U is approximately 50 barns, however, there is such a small amount of ^{234}U that it can also be treated as ^{238}U.
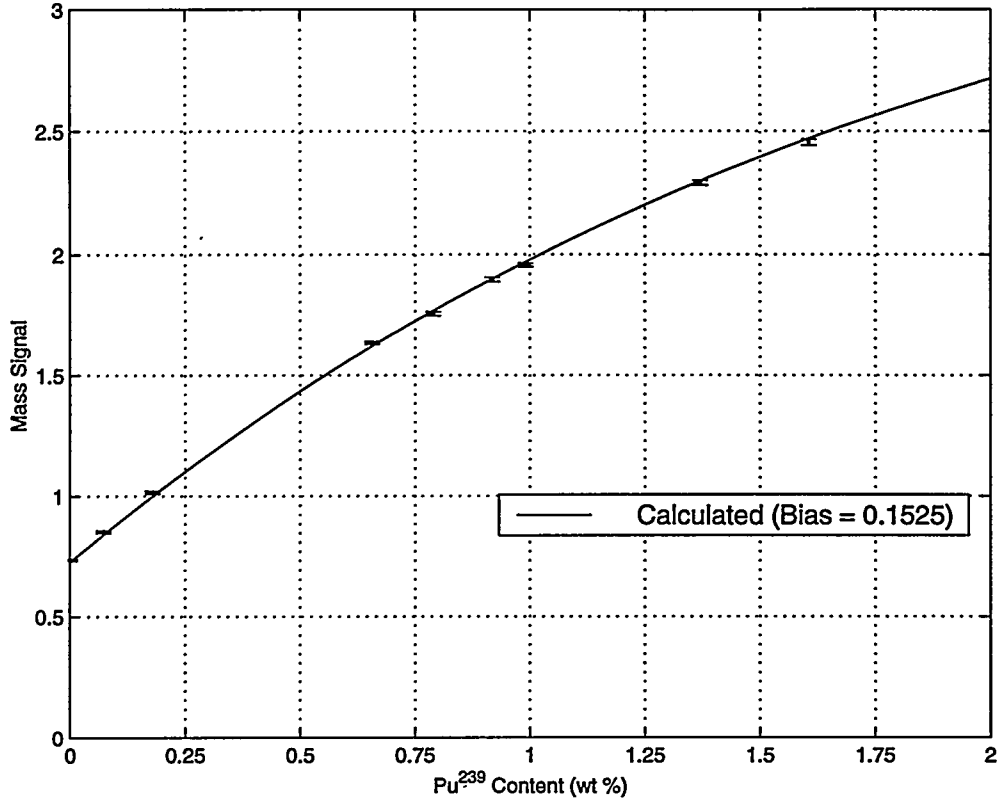
Figure 36: Mass Signal as a Function of ^{239}Pu Content up to 2 wt % ^{239}Pu

Assume that all of the additional material - glue, aluminum foils, etc. - can be lumped into one mass that is described by one total cross-section. This is a reasonable assumption because there is a large number of foils in the sample (greater than 90 for the measurements) and there is no noticeable individual deviation from the calculations. A deviation would have indicated that there was a single foil or a small number of foils that was not identified properly. Considering the effect from the additional material and assuming the entire effect is due to the hydrogen in the sample, the average mass of hydrogen in each foil can be estimated.

The mass signal of the measurements, M_M, differs from the mass signal from the calculations, M_C, by an amount equal to the mass signal of the hydrogen in the sample, M_H, such that $M=M_C+M_H$. The mass signal from the hydrogen is

$$M_H = \Sigma_H x = \sigma_H \frac{\rho N_A}{A} x , \qquad (87)$$

where σ_H is the total microscopic neutron cross-section of hydrogen in cm^2/atom, ρ is the density of the hydrogen in the sample in g/cm^3, N_A is Avogadro's number in atoms/mole, A is the atomic

weight in grams/mole, and x is the sample thickness in cm. The density of the hydrogen in the sample can be written as a function of the mass signal as

$$\rho = \frac{A}{\sigma_H N_A x} M .$$
(88)

Since the calculations deviate from the measurements by a constant bias, it is postulated that the bias is equal to the mass signal from the hydrogen. The density of hydrogen in the sample then becomes

$$\rho = \frac{A}{\sigma_H N_A x} b ,$$
(89)

where b is the bias from the measurements. Using a microscopic total cross-section of approximately 20 barns for hydrogen, the bias from the measurements of 0.1525, and a sample thickness of 1.1 cm results in a density of 0.012 g/cm^3 for the hydrogen in the sample. This is 0.063 weight percent of hydrogen in the sample, which translates into 0.19 mg of hydrogen in a depleted uranium foil that weighs 300 mg.

Because ^{238}U foils were removed when ^{239}Pu foils were added, the contribution to the mass signal from the total amount of hydrogen in the sample changes slightly. The mass signal values have been adjusted to balance the hydrogen content for all of the measurements.

Several additional samples were prepared with ^{239}Pu contents in the range from 2 to 3 weight percent. The results over the entire range of ^{239}Pu content are shown in Figure 37. These values start to deviate from expected as the ^{239}Pu content is increased and may indicate a practical limit to the range of usefulness of such a measurement.

The transmission is an exponential function of the mass signal. Now assume that there is a limit to the mass signal such that the transmission is so small that it can be assumed to be zero. This value of the mass signal is the saturation point. No further attenuation of the beam occurs since the transmission is zero. The mass signal of a sample is a function of the microscopic cross-section multiplied by the atom density and the sample thickness. This means that as the atom density of ^{239}Pu increases, saturation is attained at energies that correspond to the highest cross-sections first. Continually increasing the ^{239}Pu content in the sample then causes saturation to occur at continually lower cross-section values.

As the ^{239}Pu content increases, saturation occurs at the peak of the resonance which causes the sample to become "black" at this energy such that there is no measurable transmission. As the ^{239}Pu content continues to be increased, saturation starts to occur at energies adjacent to the peak of the resonance. Eventually, the entire energy range of interest is saturated and the mass signal becomes constant. In theory, the mass signal would approach an asymptote at this value. In practice,
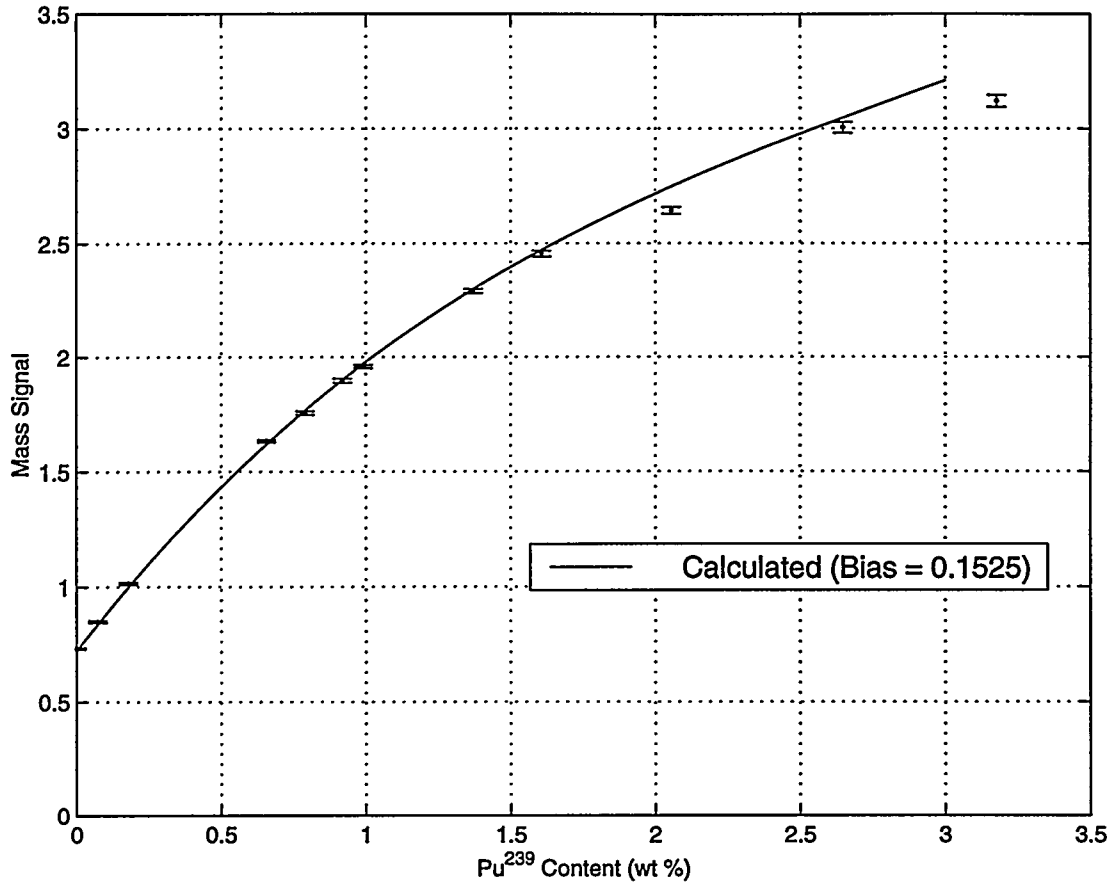
Figure 37: Mass Signal as a Function of ^{239}Pu Content up to 3 wt% ^{239}Pu

a point is reached at which the measured mass signal plus the standard deviation of the mass signal reaches the asymptote. This describes a limit to the amount of ^{239}Pu that can be determined in a sample, however, it does not explain the deviation between the predicted mass signal and the measured mass signal at ^{239}Pu contents above two weight percent.

The difference between the calculated values and measured values could be due to a discrepancy in the cross-sections of ^{239}Pu in the valleys of the resonances. It is known that the evaluated functions used to describe the cross-sections between the resonances tend to over predict the cross-sections in these regions. This can be observed by reviewing the measured cross-section data points compared to the evaluated data in Ref. 9 for ^{239}Pu. If a larger cross-section value is used to compute the mass signal then the mass signal will also be over predicted. This trend becomes apparent at ^{239}Pu contents greater than two weight percent. This is observed in Figure 37 as the discrepancy between measured and predicted mass signals becomes larger. Above two weight percent of ^{239}Pu, saturation has occurred in the energy range of the 0.3 eV resonance. Therefore, the transmission is primarily due to neutrons at energies corresponding to lower cross-section values. Since the actual cross-sections are slightly lower than the evaluated cross-section data used for the
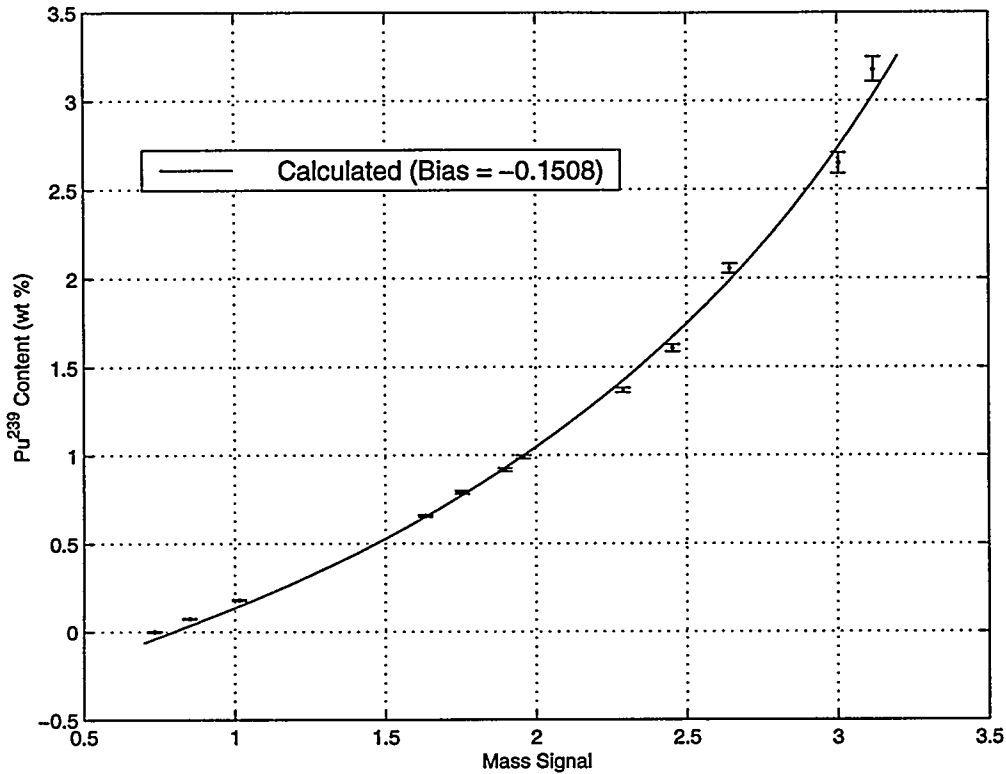
Figure 38: ^{239}Pu Content as a Function of Mass Signal

calculations, the measured mass signal is lower than the calculated mass signal. As the ^{239}Pu content is increased, more neutrons with energies which correspond to lower cross-section values contribute to the transmission. This causes the measured mass signal to further deviate from the calculated mass signal. To use this method above two weight percent ^{239}Pu, a calibration function will be necessary to accurately predict the ^{239}Pu content. This calibration function will have to be generated from measurements on actual samples, since it has been observed that the calculational estimates over predict the ^{239}Pu content in the samples.

After it was demonstrated that there is a significant change in mass signal with ^{239}Pu content and that this filtered method can accurately predict the mass signal, it was desirable to determine the error in such a measurement. Two samples were prepared from ZPPR foils with known quantities of ^{239}Pu. The mass signal was determined from measurement, and this value was used to determine the ^{239}Pu content of the sample based on a calibration curve. The calibration curve was established based on the calculated values and previously measured values, a fifth-order polynomial function was fit to the data relating the ^{239}Pu content to the mass signal. A constant bias was computed from the previously measured data compared to the calculations. The result of this function is shown in Figure 38. The fifth-order polynomial function shown in Figure 38 is described by

82

Table 16: Predicted ^{239}Pu Content for Test Samples		
Actual ^{239}Pu Content (wt%)	1.023	2.205
Mass Signal from Measurement	1.967	2.803
Hydrogen Adjusted Mass Signal	1.969	2.807
Uncertainty in Mass Signal	0.0106	0.0205
Predicted ^{239}Pu Content (wt%)	1.011	2.301
Uncertainty in ^{239}Pu Content (wt%)	0.0242	0.0843
Error in Prediction (%)	1.17	4.35
Predicted Mass	266.9 ±6.4 mg	608.6 ±22.3 mg

$$P = Am^5 + Bm^4 + Cm^3 + Dm^2 + Em + F + b , \qquad (90)$$

where P is the ^{239}Pu content in weight percent, m is the mass signal, A=0.0214, B=-0.1704, C=0.5909, D=-0.8237, E=1.1415, F=-0.47426, and the bias, b=-0.15081. The ^{239}Pu content can now be predicted from a measurement of the mass signal. Also, based on this function the error in the ^{239}Pu content can be determined from the mass signal and the error on the mass signal. The standard deviation on the ^{239}Pu content is

$$\sigma_P^2 = (5Am^4 + 4Bm^3 + 3Cm^2 + 2Dm + E)^2 \sigma_m^2 + m^{10}\sigma_A^2 +$$
$$m^8\sigma_B^2 + m^6\sigma_C^2 + m^4\sigma_D^2 + m^2\sigma_E^2 + \sigma_F^2 + \sigma_b^2 , \qquad (91)$$

where σ is the standard deviation of each parameter and the other terms are as defined previously. The error analysis method was described previously in Section 4.3.

Two measurements were performed on test samples. The results are shown in Table 16. The actual ^{239}Pu content in each sample was determined from the known masses of the foils used to create the samples. The mass signal was then determined from the measurements and adjusted for the hydrogen content in the foils. The ^{239}Pu content in the sample was then predicted based on the measured mass signal. The uncertainties were computed as previously discussed.

The error between the predicted ^{239}Pu content and the actual ^{239}Pu content is 1.17 percent for the first sample shown in Table 16. The uncertainty in the ^{239}Pu content is approximately 2.4 percent, so the prediction is in agreement with the actual quantity of ^{239}Pu in the sample. The error between the predicted ^{239}Pu content and the actual ^{239}Pu content is 4.35 percent for the second sample shown in Table 16. The uncertainty in the ^{239}Pu content is approximately 3.8 percent. The predicted ^{239}Pu content is within two standard deviations of the actual ^{239}Pu content in the sample, which indicates a reasonable agreement between the two values. These two cases demonstrate that this approach can be used to accurately predict the ^{239}Pu content in depleted uranium samples.

Table 17: Results of ^{235}U Content Measurements				
^{235}U Content (wt%)	Transmission	Standard Deviation	Mass Signal	Standard Deviation
0.22	0.475	0.0024	0.744	0.005
0.799	0.444	0.0023	0.811	0.0052
0.99	0.431	0.0023	0.841	0.0053
1.396	0.408	0.0022	0.897	0.0054
1.598	0.409	0.0022	0.895	0.0054
2.167	0.377	0.0021	0.977	0.0056
2.835	0.352	0.0021	1.044	0.0058
3.583	0.32	0.002	1.139	0.0061

6.3 Effect of ^{235}U

Small variations are expected around the nominal value of 0.22 weight percent due to processing differences and due to burnup of the ^{235}U from irradiation. ^{235}U has a small broad resonance at an energy very close to 0.3 eV. Even with this resonance, the effect of these small variations in the ^{235}U content was shown to be negligible based on calculations in Section 4.2.3.

The effect of the ^{235}U content was still explored. These measurements were performed to confirm that the effect on the mass signal from a ^{235}U content in the range around 0.22 is insignificant. Unfortunately, only one sample could be created with ZPPR foils in the range of interest for the ^{235}U content. Because of the limitations of the samples created from ZPPR foils, the effect of the ^{235}U content on the mass signal was studied in the range from 0.22 weight percent up to approximately 3.5 weight percent. By obtaining good agreement between the calculated and measured values for the mass signal over the range of ^{235}U content up to 3.5 weight percent, the results of the calculations are demonstrated to be accurate, i.e. the effect of minor variations around 0.22 weight percent is negligible.

The ^{235}U measurements were performed identically to those with the ^{239}Pu foils. ^{235}U foils were added to the sample and ^{238}U foils were removed to maintain the sample mass as close to nominal as possible. The nominal sample mass was 26.33 grams. Results of the measurements are listed in Table 17 and shown in Figure 39. Figure 39 also shows the calculated values adjusted with a constant bias. As noted previously for the ^{239}Pu measurements, the bias is due to hydrogen in the ^{238}U foils. The ^{235}U foils also have aluminum foils glued on the front and back so these also have a hydrogen contribution. The results are in good agreement with the calculated values with the constant bias applied. Figure 39 may appear to demonstrate a large change in mass signal with ^{235}U content due to the scale of the figure. However, if this change in mass signal from ^{235}U is shown in relation to the change in mass signal from the ^{239}Pu content it is apparent that this is a small effect. Figure 40 demonstrates this relation. In addition, the ^{235}U content is only expected to vary by approximately 0.1 weight percent which is a negligible amount.
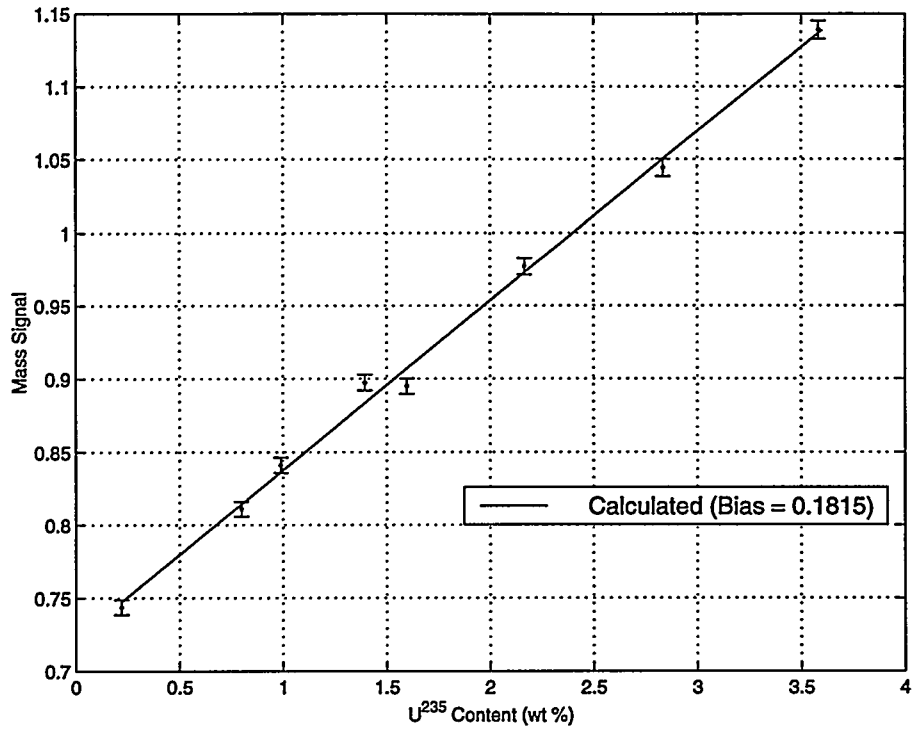
Figure 39: Mass Signal as a Function of ^{235}U Content
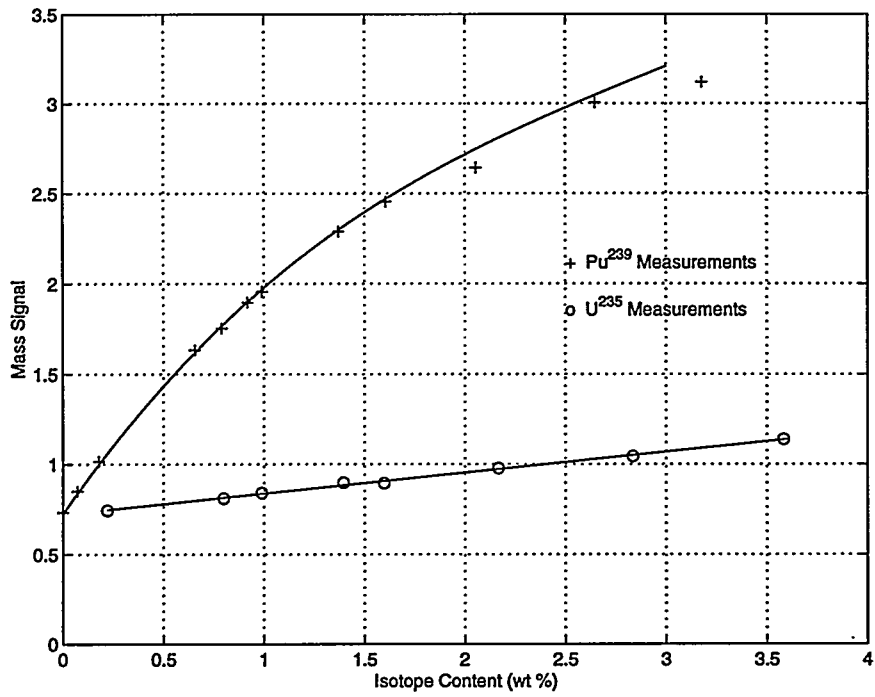
Figure 40: ^{235}U vs. ^{239}Pu Effect on Mass Signal

85

Table 18: Predicted ^{239}Pu Content for Test Sample with Increased ^{235}U		
^{235}U Content (wt%)	0.22	0.793
Actual ^{239}Pu Content (wt%)	2.205	2.213
Mass Signal from Measurement	2.803	2.84
Hydrogen Adjusted Mass Signal	2.807	2.844
Uncertainty in Mass Signal	0.0205	0.0211
Predicted ^{239}Pu Content (wt%)	2.301	2.378
Uncertainty in ^{239}Pu Content (wt%)	0.0843	0.0888
Error in Prediction (%)	4.35	7.46
Predicted Mass	608.6 ±22.3 mg	626.6 ±23.4 mg

A test measurement was performed with a ^{239}Pu content of 2.213 weight percent with an increased amount of ^{235}U (0.793 wt%). This measurement was performed in the same manner as the test measurements discussed in the Section 6.2. The goal was to determine the additional error that was induced in the determination of the ^{239}Pu content by the increased ^{235}U content. The result is shown in Table 18. Also shown in Table 18 is the result for a similar test sample with the nominal ^{235}U content of 0.22 weight percent. Table 18 shows that the predicted ^{239}Pu content is still in good agreement with the actual ^{239}Pu content (approximately 7.46 percent over prediction) even though there is approximately 0.8 weight percent ^{235}U in the sample. The ^{239}Pu content was chosen to match the content of the second case shown in Table 16 so that the results could be compared. This value is also shown in Table 18. Comparing the two results, the difference in the predicted ^{239}Pu contents differs by about 0.077 weight percent (3.35 percent). This difference is due to the ^{235}U content and represents a fairly small change in the predicted values for a large change in ^{235}U content. It demonstrates that reasonable differences in the ^{235}U content on the order of 0.1 to 0.2 weight percent between samples can be neglected without a significant impact on the predicted quantity of ^{239}Pu from the measurement. It also demonstrates that with a priori knowledge of higher ^{235}U contents, the effect on the mass signal can be accounted for in the measurement in a similar fashion to the way in which hydrogen in the foils are treated.

6.4 Sample Thickness Effects

The mass signal as a measure of the exponential in the equation for attenuation is directly related to the thickness, or transmission length, of the sample. For the measurements performed using a stack of foils as the sample, the transmission length is constant for a given measurement. In addition, the transmission length was held as close to nominal as possible for all sensitivity cases such as varying the ^{239}Pu and ^{235}U content of the sample. The thickness is related to the mass since the area of the foils is constant. The ^{239}Pu foils are slightly smaller in diameter, however, the mass was adjusted upward to account for the smaller size. The nominal mass of the sample was 26.33 grams. As mentioned previously, the mass of the samples varied by at most about 130 milligrams, so the samples varied by at most about 0.5% of the nominal mass. The thicknesses were calculated

Table 19: Results of Sample Thickness Measurements				
Sample Thickness (cm)	Transmission	Standard Deviation	Mass Signal	Standard Deviation
0.865	0.562	0.0027	0.576	0.0047
0.924	0.533	0.0026	0.628	0.0048
0.983	0.513	0.0017	0.667	0.0033
1.019	0.503	0.0025	0.687	0.0049
1.043	0.496	0.0014	0.701	0.0028
1.044	0.499	0.0025	0.694	0.0049
1.054	0.493	0.0024	0.707	0.0049
1.067	0.486	0.0024	0.721	0.005
1.092	0.479	0.0024	0.737	0.005
1.102	0.48	0.0016	0.734	0.0033
1.115	0.467	0.0024	0.761	0.005
1.139	0.473	0.0024	0.749	0.005

based on theoretical density so the total thickness of the samples also varied by at most 0.5%. In most cases, the variance was less than 0.2%.

For a measurement on a real blanket element, the beam impinges perpendicular to the axis of the element. Therefore, the transmission length will vary with position, and the mean transmission length of the sample will depend on the shape and size of the collimated neutron beam and the size of the active area of the detector. The smaller the beam diameter and detector area, the closer the mean transmission length through the sample will be to the transmission length at the thickest portion of the element. These effects were studied in Section 4.2.5.

In the mono-energetic case, the mass signal is a direct measure of the term, Σx, which is simply the total macroscopic cross-section of the sample times the thickness of the sample. Therefore, the mass signal should vary linearly with the sample thickness. This same trend is also expected for the present measurements.

A measurement series was performed to measure the effect of the sample thickness on the mass signal. In addition, these measurements were used to confirm that there is another material in the foils that was causing the bias between the calculated and measured values. The results of the measurements are shown in Table 19 and Figure 41. Figure 41 also shows a linear fit of the calculated values discussed in Chapter 4 adjusted with an average bias of 0.1638 but not taking into account the hydrogen content in each foil. A linear fit of the measured data compared to the predicted curve is shown in Figure 42. This figure indicates that the measured data deviate from the expected data. This was as expected since it was assumed in Section 6.1 that the ^{238}U foils contain hydrogen.
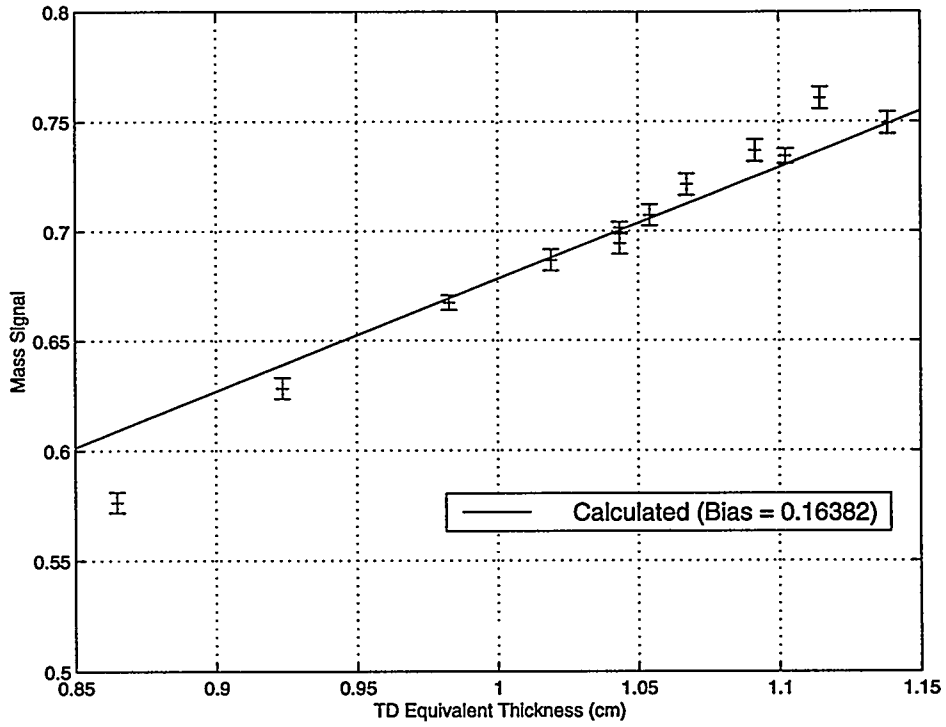
Figure 41: Mass Signal as a Function of Sample Thickness
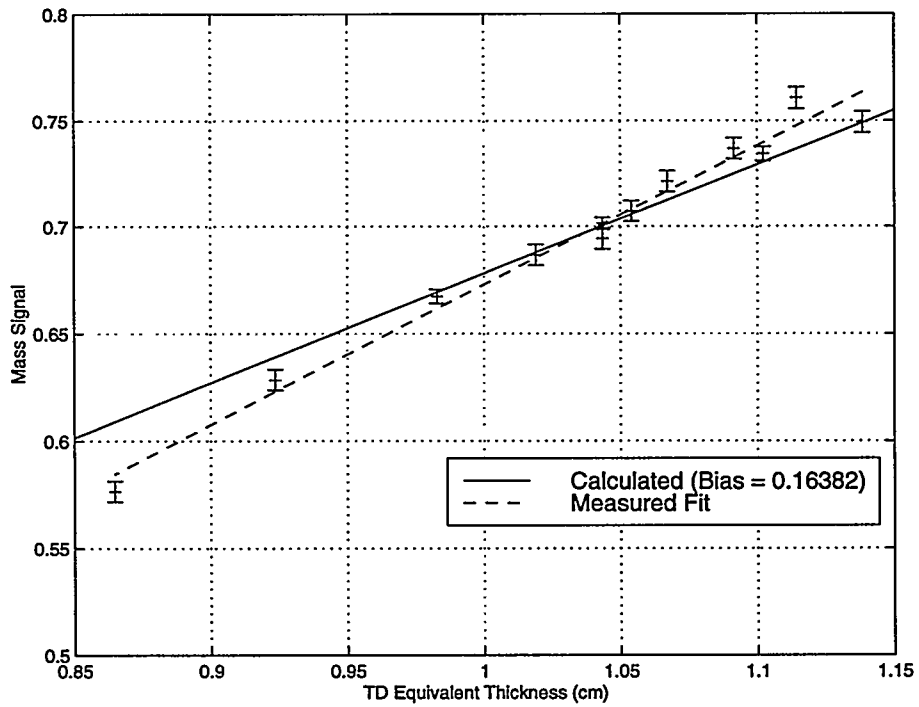
Figure 42: Measured vs. Calculated Data

There are three indicators that the sample contains another material that is causing the deviation from expected. First, for every measurement performed there is a large bias. This in itself does not indicate additional isotopes in the sample, it is only a recognition that the measured values deviate from the calculated values. What is notable is that the bias is different for different series of measurements. If it was an average bias in the system then it would be expected that every measurement would be different from the calculated result by a statistically similar value. This is not the case. For the proof-of-principle measurements the bias was 0.1525; for ^{235}U content measurements the bias was 0.1815; and for the sample thickness measurements the bias was 0.1638. The difference is statistically significant as the standard deviation on the mass signal values was typically around 0.005.

The second indicator was a measurement performed with an empty sample holder. The result of this measurement was a mass signal of 0.00177 +/- 0.00400 - a statistically zero mass signal. This is as expected since there is no depleted uranium mass in the sample holder. If the bias were completely inherent in the system and not due to additional material within the sample holder, the mass signal measured with a sample mass of zero (or zero thickness) should have been equal to the average bias reported for the other measurements.

The third and most conclusive indicator is that the linear fit to the sample thickness measurements varies from the calculated equation. This is significant as it indicates that there is a common material in all of the ^{238}U foils contributing to this discrepancy. For the other measurement series, the total number of foils was fairly constant usually only varying by one or two foils for the entire series. Remember that when ^{235}U and ^{239}Pu foils were added, ^{238}U foils were removed to maintain the total sample mass. However, for the sample thickness measurements, ^{238}U foils were removed from the sample to obtain the various thicknesses. The fact that the bias increases as the sample thickness increases demonstrates that the ^{238}U foils contain an isotope in a significant quantity that was not accounted for in the calculations.

Although, a mass for an additional material in the ^{238}U foils could be calculated (assuming hydrogen) it was not proven definitively. A measurement was then performed using the larger ZPPR plates to try to confirm that there was an additional material in the ^{238}U foils and that it was hydrogen. The ZPPR plates were also dipped in the Kel-F coating and wrapped in aluminum foil but no glue was used. The glue is the known source of hydrogen although there could also be some hydrogen migration into the foils. Since the stack of ZPPR plates contains no glue, the source of hydrogen has been essentially eliminated.

The sample thickness was 1.11 cm using three 0.32 cm thick plates and one 0.16 cm thick plate. The mass signal was determined to be 0.506 with a standard deviation of 0.0042. Comparing this value to Table 19, there is a large difference (approximately 0.25) between the two results indicating that there is hydrogen in the sample causing this discrepancy.

The measured mass signal for the ZPPR plate sample is also approximately 10.5 percent less than the calculated value of 0.565 at a thickness of 1.10 cm. This is partially explained by how the

sample thickness is reported. For all of the previous calculations and measurements, the sample thickness was reported as a theoretical density thickness. The thickness is computed assuming the foil is at theoretical density when in actuality the foil density is somewhat less. For the case of the ZPPR plate sample, the thickness of 1.11 cm was computed based on the reported thicknesses. The thickness of the plate sample at theoretical density is approximately 5 percent less than the nominal thickness. There is still a 5.5% difference between the results for the ZPPR plate sample and the calculated value at an equivalent thickness. It is surmised that this discrepancy is due to uncertainties in the thickness of the sample within the beam and uncertainties in the cross-section data. As noted previously, if the evaluated cross-section data is over predicted, then the mass signal estimate from the calculations will also be over predicted. These two factors can easily account for the 5.5 % difference between the measured and calculated results.

7. Summary and Conclusions

This report describes an experiment performed at ANL using the east beam of the NRAD reactor facility. As discussed in Chapter 2, resonance transmission analysis using the time-of-flight (TOF) technique has been demonstrated by other researchers to yield accurate results of isotopic compositions in small samples and in waste drums. The TOF technique requires a high intensity pulsed neutron source which was not available at ANL. Therefore, the goal of the experiment was to demonstrate that resonance transmission analysis using a filtered neutron beam could be used to determine the ^{239}Pu content in a depleted uranium sample. The depleted uranium samples were identical in thickness to the diameter of EBR-II blanket elements. By using comparative samples, the usefulness of this approach for determining the ^{239}Pu content in EBR-II blanket elements was assessed.

Chapter 3 described the basis of resonance transmission analysis and demonstrated that the mass signal could be obtained from a simple equation relating the flux normalized count rate from four measurements with different sample/filter combinations. Computations in chapter 4 demonstrated that by using a gadolinium filter and cadmium filter in concert with a ^{239}Pu fission chamber the mass signal was representative of the true mass signal in the energy region corresponding to the 0.3 eV resonance in ^{239}Pu. It was demonstrated in Chapter 4 that the 0.3 eV resonance in ^{239}Pu was isolated such that the response of the measurement technique, the mass signal value, was based on the total cross-section of the sample over a small energy region around 0.3 eV. The improvement of using a ^{239}Pu fission chamber over other detection methods was also demonstrated.

By selecting this small energy region, the total cross-section of ^{239}Pu was significantly greater than the cross-sections of ^{238}U and ^{235}U as shown in Figure 4. Since the mass signal is the sum of the total macroscopic cross-sections of the constituent isotopes multiplied by the sample thickness, small changes in the ^{239}Pu content result in large changes in the mass signal. This was demonstrated in Chapter 4 for sample compositions up to three weight percent ^{239}Pu for a sample with a thickness equivalent to a blanket element.

Experiments were performed to demonstrate the validity of the calculations of Chapter 4. The experimental set-up, procedure, and measurement plan were described in Chapter 5. Results of the measurements were presented in Chapter 6.

The measurement results indicated good agreement with the calculational values reported in Chapter 4 corrected by a constant bias. The bias was found to be from additional material in the depleted uranium foils that was not accounted for in the analysis. It was postulated that the effect was due to hydrogen in the glue used to apply aluminum foils to the front and back of the foils. The hydrogen content in each foil was determined to be approximately 0.19 mg, which is approximately 0.06 weight percent.

It was also shown through tests of samples containing up to 3 weight percent [235]U that the [235]U content in the sample only slightly affected the mass signal result. The mass signal effect was negligible for realistic variations in the [235]U content of the sample around the nominal value of 0.22 weight percent. If a larger deviation from nominal is known, then the effect on the mass signal can be accounted for and the result adjusted accordingly. Tests also demonstrated that the mass signal was a linear function of the sample thickness. The effect on the mass signal from changes in the thickness of the sample, determined from the mass of a sample, can be accounted for as the effect is linear.

An apparent slight deviation between the measured and calculated values of [239]Pu in the sample was observed above two weight percent of [239]Pu. It was postulated that this deviation is due to a discrepancy in the cross-sections of [239]Pu in the valley of the resonances highlighted by saturation occurring at the higher cross-sections of the resonances. Above two weight percent, the atom density of [239]Pu becomes large enough that the transmission at energies with large cross-sections becomes essentially zero. At this point, the sample becomes a "black body" or a true absorber at these energies. As the [239]Pu content increases, the sample becomes black at more and more neutron energies. When the sample becomes black at all neutron energies corresponding to the [239]Pu resonances, the measured mass signal is based primarily on the lower cross-sections. It is known that the cross-sections in the valleys of the resonances are over predicted, and therefore, the calculated mass signal is also over predicted. This deviation does not indicate the limit of the measurement system as it can be accounted for by generating a calibration curve from measured data.

There is a practical limit for the technique based on the counting statistics. The transmission is an exponential function. As the [239]Pu content is increased, the transmission becomes smaller and smaller. Based on the statistics, at some [239]Pu content the uncertainty in the transmission is larger than the transmission. This translates into an upper bound on the mass signal and a limit of detectability on the [239]Pu content. At this level of [239]Pu content, the mass signal cannot be distinguished within statistics from the limit on the mass signal, and the [239]Pu content would be greater than the limit of detectability.

Once the calculated predictions of mass signal as a function of [239]Pu content were verified, several test samples were measured to determine the [239]Pu content from the measured mass signal values. These tests were used to demonstrate the method in which the [239]Pu content would be determined and to show that the measured [239]Pu content agreed well with the known quantities. These tests also demonstrated the error expected from such a measurement. The results of the two measurements are summarized in Table 20. The predicted [239]Pu masses shown in Table 23 are in good agreement with the actual [239]Pu masses of the two samples.

Several issues need to be addressed before this method can be used to measure the [239]Pu content in actual EBR-II blanket elements. The first issue is the thickness of the sample. Calculations were performed which showed the effect of the beam diameter on the change in mass signal between a depleted uranium rod sample and a rod sample containing two weight percent [239]Pu. The calculations indicated that a beam diameter between 0.5 and 0.6 cm is best suited for maximi-

Table 20: Summary of Measurements on Unknown Samples		
	Sample 1	Sample 2
Sample Mass (g)	26.416	26.445
^{239}Pu Composition (wt%)	1.023	2.205
^{239}Pu Mass (mg)	270.1	583.1
Measured ^{239}Pu Mass (mg)	266.9 ±6.4	608.6 ±22.3

zing the sensitivity of the system and minimizing the counting time necessary to obtain good statistics. Measurements should be performed on cylindrical samples to verify the results of the calculations.

Another issue is the effect on the response from Doppler-broadening of the resonance. This effect is expected to be small but should be addressed when measuring actual irradiated blanket elements. As the resonance peak is reduced from the elevated temperatures, it is expected that there will be a slight decrease in response. A decrease in response is expected because more area under the resonance will fall outside of the energy range of interest (0.1 eV to 0.5 eV).

The system will also need to be redesigned to accommodate blanket elements. Most notably, the system will need to be relocated around the specimen tube in the NRAD ERS Cell. This tube is connected to the main hot cell of HFEF and allows elements to be lowered into the ERS Cell for radiography. The same process would be used to lower blanket elements into the ERS Cell for measurement. The detector and sample-to-detector spacing would also need to be reconsidered. In addition, the collimator would have to be repositioned.

Resonance transmission analysis using a filtered reactor beam has been shown to be a viable method for determining ^{239}Pu content in depleted uranium samples. This method could be expanded, through the use of different filter materials, to assay other isotopes of interest, most notably ^{235}U or ^{240}Pu. With a movable gadolinium filter, a series of measurements could be performed to obtain a mass signal value for energies less than 0.1 eV, in addition to the energy range from 0.1 eV to 0.5 eV. With two different mass signals, the ^{235}U content could potentially be determined by comparing the mass signal ratio between the two energy regions. By the use of an indium filter, which has a resonance at 1.4 eV, in conjunction with a cadmium filter, the energy region from 0.5 eV to 1.4 eV could be isolated. The 1 eV resonance of ^{240}Pu might then be used to determine the ^{240}Pu content. These are just a few of the possibilities where resonance transmission analysis with filtered neutron beams might be applied.

93

References

1. B.J. Toppel, "A Users Guide for the REBUS-3 Fuel Cycle Analysis Capability," Argonne National Laboratory Report, Report No. ANL-83-2, March 1983.

2. R.T. Klann, "Shielding Analysis for the Leached Hull Monitor," Argonne National Laboratory Internal Memorandum, August 12, 1997.

3. D. Reilly, et aliene, Passive Nondestructive Assay of Nuclear Materials, U.S. Government Printing Office, 1991.

4. R.T. Klann, et aliene, "Neutron Measurements of EBR-II Assemblies," Proceedings of the American Nuclear Society Third Topical Meeting on DOE Spent Nuclear Fuel and Fissile Materials Management, 1998.

5. H.O. Menlove, et aliene, "The Design and Calibration of the Spent-Fuel Neutron Coincidence Counter for Underwater Applications," Los Alamos National Laboratory Report, Report No. LA-12769-MS, May 1994.

6. H.O. Menlove, "Description and Operation Manual for the Active Well Coincidence Counter," Los Alamos National Laboratory Report, Report No. LA-7823-M, May 1979.

7. P.M. Rinard, "Shuffler Instruments for the Nondestructive Assay of Fissile Materials," Los Alamos National Laboratory Report, Report No. LA-12105, May 1991.

8. S.E. Aumeier, et aliene, "The Fuel Conditioning Facility Waste Stream and Blanket Pin Assay," Argonne National Laboratory Report, Report No. ANL-NT-67, May 1998.

9. P.F. Rose, "ENDF-201, ENDF/B-VI Summary Documentation," Brookhaven National Laboratory Report, Report No. BNL-NCS-1741, 4th edition, October 1991.

10. J.J. Duderstadt and L.J. Hamilton, Nuclear Reactor Analysis, John Wiley and Sons, Inc., 1976.

11. W.E. Meyerhof, Elements of Nuclear Physics, McGraw-Hill Book Company, 1967.

12. R.L. Liboff, Introductory Quantum Mechanics, Addison-Wesley Publishing Company, 1988.

13. H.A. Bethe and G. Placzek, Physical Review, vol. 51, 450, 1937.

14. M.G. Strauss, "Resonance Neutron Radiography Using a Pulsed Neutron Source and a 2-Dimensional Scintillation Detector," Proceedings of the First World Conference on Neutron Radiography, D. Reidel Publishing Company, 1983, pages 519-530.

15. R.A. Schrack, et aliene, "Resonance Neutron Radiography," Proceedings of the First World Conference on Neutron Radiography, D. Reidel Publishing Company, 1983, pages 495-502.

16. R.A. Schrack, et aliene, "NBS Work on Neutron Resonance Radiography," Report of a Workshop on Neutron Resonance Radiography held at the Los Alamos National Laboratory, Report No. LA-11393-C, 1988, pages 100-115.

17. M.G. Sowerby, "The Harwell Imaging System for Resonance Radiography and Demonstration Results," Report of a Workshop on Neutron Resonance Radiography held at the Los Alamos National Laboratory, Report No. LA-11393-C, 1988, pages 34-45.

18. P.H. Fowler, "Temperature Imaging Using Epithermal Neutrons," Report of a Workshop on Neutron Resonance Radiography held at the Los Alamos National Laboratory, Report No. LA-11393-C, 1988, pages 46-80.

19. J. Mayers, et aliene, "Temperature Measurement by Neutron Resonance Radiography," Rutherford Appleton Laboratory Report, Report No. RAL-88-017, March 1988.

20. J. Mayers, et aliene, "Temperature Measurement by Neutron Resonance Radiography," Nuclear Instruments and Methods in Physics Research, February 15, 1989, vol. A275, no. 2, pages 453-459.

21. R.A. Schrack, "New Applications of Resonance Neutron Radiography," Radiation Effects, 1986, vol. 95, no. 1-4, pages 1309-1313.

22. R.A. Schrack, "Uranium-235 Measurement in Waste Material by Resonance Neutron Radiography," Nuclear Technology, November 1984, vol. 67, pages 326-332.

23. C.D. Bowman, et aliene, "Neutron Resonance Transmission Analysis of Reactor Spent Fuel Assemblies," Proceedings of the First World Conference on Neutron Radiography, D. Reidel Publishing Company, 1983, pages 503-511.

24. Y.T. Cheng and D.A. Garrett, "Resonance Neutron Radiography," Proceedings of the First World Conference on Neutron Radiography, D. Reidel Publishing Company, 1983, pages 513-517.

25. G.C. McClellan and W.J. Richards, "Neutron Radiography Applications and Techniques at the Hot Fuel Examination Facility," Proceedings of the First World Conference on Neutron Radiography, D. Reidel Publishing Company, 1983, pages 437-443.

26. R.L. Moss and M. Beers, "Use of Epithermal Neutron Radiography to Determine the Extent of Melting in Mixed Oxide LMFBR Fuel Pins Irradiated in the High Flux Reactor, Petten," Proceedings of the Second World Conference on Neutron Radiography, D. Reidel Publishing Company, 1987, pages 349-357.

27. G.R. Imel and T. Urbatsch, "Beam Characterization at the Neutron Radiography Facility (NRAD)," Proceedings of the Fourth World Conference on Neutron Radiography, Gordon and Breach Science Publishers, 1994, pages 673-681.

28. G.F. Knoll, <u>Radiation Detection and Measurement</u>, 2nd edition, John Wiley and Sons, Inc., 1989.

29. HFEF/N Neutron Radiography Facility Reactor Safety Analysis Report, Argonne National Laboratory Document No. W0170-0015-SA-00, August 1977.

30. HFEF/N Neutron Radiography Facility System Design Description, Argonne National Laboratory Document No. W0170-0004-SA-03, June 1978.

31. HFEF/N Neutron Radiography Facility North Radiography Station System Design Description, Argonne National Laboratory Document No. W0170-4002-ES-05, March 1982.

Appendix A: Transmission Code

The code was written to simulate the neutron transmission through the blanket elements and foil samples. The user inputs the thickness of the gadolinium filter, cadmium filter, and the sample. The description of the sample can be entered as a slab thickness or as a normal cylinder. The code uses a random number generator for a Monte Carlo algorithm to determine the attenuation through the sample for each of 11099 groups. The response in each group for each sample/filter combination is written to a data file which can be used for plotting the effect of the various filters and sample composition. The code also calculates the transmission, mass signal, and associated errors for a range of ^{239}Pu contents entered by the user.

```
C-------------------------------------------------------------------
C---SIMULATION OF NRAD NEUTRON TRANSMISSION THROUGH EBR-II BLANKET RODS
C-------------------------------------------------------------------
C
      IMPLICIT INTEGER (I-N)
      IMPLICIT REAL (A-H,O-Z)
      CHARACTER*24 FDATE
      CHARACTER*72 FNAME(3),LINE
      REAL   NA,SUM(5)
      COMMON /BANK/ EL(12000),S(14,12000),CS(3,12000),CNT(5,12000)
      COMMON /PARA/ RAD,FRAC,AMN(5),RAD2,DF1,DF2,RCOL,DDT,NHIST
C
C ---OPENS FILES
C
      CALL GETARG(1,FNAME(1))
      NLEN=0
      DO 10 I=1,72
        IF (FNAME(1)(I:I).NE.' ') THEN
          NLEN=NLEN+1
          ENDIF
   10 CONTINUE
      FNAME(2)=FNAME(1)(1:NLEN)//'.spectrum'
      FNAME(3)=FNAME(1)(1:NLEN)//'.output'
      OPEN(13,FILE=FNAME(1),STATUS='OLD')
      OPEN(14,FILE='xsec',STATUS='OLD')
      OPEN(15,FILE=FNAME(2),STATUS='UNKNOWN')
      OPEN(16,FILE=FNAME(3),STATUS='UNKNOWN')
C
      WRITE(16,*) FDATE()
C
C---READS INPUT FILE
C
C---GADOLINIUM FILTER
      READ (13,1000) LINE
      WRITE (16,1010) LINE
      CALL READFILE(DF1)
      CALL READFILE(RF1)
      CALL READFILE(AF1)
C---CADMIUM FILTER
      READ (13,1000) LINE
      WRITE (16,1010) LINE
      CALL READFILE(DF2)
      CALL READFILE(RF2)
      CALL READFILE(AF2)
C---COLLIMATOR
      READ (13,1000) LINE
```

```
      WRITE (16,1010) LINE
      CALL READFILE(RCOL)
C---SAMPLE
      READ (13,1000) LINE
      WRITE (16,1010) LINE
      READ (13,1000) LINE
      WRITE (16,1020) LINE(1:20),LINE(21:30)
      IF (LINE(21:24).EQ.'ROD') THEN
        NSTY=1
      ELSE
        NSTY=2
      ENDIF
      CALL READFILE(RAD)
      CALL READFILE(RHO)
      CALL READFILE(WT9)
      CALL READFILE(WT5)
C---DETECTOR
      READ (13,1000) LINE
      WRITE (16,1010) LINE
      CALL READFILE(DDT)
C---MISC ENTRIES
      READ (13,1000) LINE
      WRITE (16,1010) LINE
      READ (LINE(38:72),'(I10)') N9
      READ (13,1000) LINE
      WRITE (16,1010) LINE
      READ (LINE(12:72),'(I10)') NHIST
C
C---GENERATE RANDOM NUMBER STARTERS
C
      CALL RANSTA
C
C---DEFINE VARIABLES
C
      NA=0.602252
      AMN(5)=NA*RF1/AF1
      AMN(4)=NA*RF2/AF2
      RAD2=RAD*RAD
      WT9M=WT9
      WT5=WT5/100.0
C
C----REPEAT FOR INCREASING WT% OF PU-239
C
      DO 60 KWT=0,N9
        DO 20 J=1,5
          DO 15 I=1,12000
            CNT(J,I)=0.0
   15     CONTINUE
   20   CONTINUE
      WT9=(WT9M/N9)*KWT/100.0
      write (20,*) 'wt9=',wt9
      WT8=1.0-WT9-WT5
      AMN(2)=RHO*WT9*NA/239.06
      AMN(1)=RHO*WT5*NA/235.04
      AMN(3)=RHO*WT8*NA/238.05
      WRITE(16,*)
      WRITE(16,1030)
      WRITE(16,1030)
      WRITE(16,*)
      WRITE(16,*)      'NUMBER DENSITIES:'
      WRITE(16,1040) 'U-235     =',AMN(1),WT5*100.0,' WT%'
      WRITE(16,1040) 'PU-239    =',AMN(2),WT9*100.0,' WT%'
```

98

```
      WRITE(16,1040) 'U-238    =',AMN(3),WT8*100.0,' WT%'
      WRITE(16,1050) 'GD FILTER =',AMN(4)
      WRITE(16,1050) 'CD FILTER =',AMN(5)
C
C---INITIALIZE DATA
C
      CALL DATA
C
C----OBTAIN THE NRAD SOURCE SPECTRUM FILTERED BY GD, NORM. TO NHIST,
C----THEN OBTAIN THE DETECTOR SPECTRA WITH AND WITHOUT SAMPLE,
C----AS WELL FOR THE CD FILTERED CASE
C
      CALL COUNTS(WT9,NSTY)
C
C----TRANSMISSION EXPERIMENT WITH GD FILTER AND CD DIFFERENCE
C
      DO 30 L=1,4
        SUM(L)=0.0
   30 CONTINUE
      DO 50 L=1,4
        DO 40 K=1,11097
          SUM(L)=SUM(L)+CNT(L+1,K)
   40   CONTINUE
   50 CONTINUE
C
C----WRITE OUTPUT FILE
C
      WRITE (16,1060)
      WRITE (16,1070)
      WRITE(16,1080) (SUM(L),L=1,4)
      RA1=SUM(3)-SUM(4)
      RA2=SUM(1)-SUM(2)
      TRANS=RA1/RA2
      SRA1=SQRT(SUM(3)+SUM(4))
      SRA2=SQRT(SUM(1)+SUM(2))
      STRANS=TRANS*SQRT((SRA1/RA1)**2+(SRA2/RA2)**2)
      AMASS=-LOG(TRANS)
      SAMASS=STRANS/TRANS
      WRITE(16,1090) TRANS,STRANS,STRANS*100.0
      WRITE(16,1100) AMASS,SAMASS,SAMASS*100.0
   60 CONTINUE
C
C----SPECTRA OUT
C
      THRESHOLD=1.0E-10
      DO 80 L=1,5
        DO 70 K=1,11097
          IF (CNT(L,K).LE.THRESHOLD) CNT(L,K)=THRESHOLD
   70   CONTINUE
   80 CONTINUE
      DO 85 K=1,11097
C
C---CSF=CNTS(SAMPLE AND GD FILTER) -
C       CNTS(SAMPLE AND CD AND GD FILTERS)
C
      CSF=CNT(4,K)-CNT(5,K)
      IF (CSF.LT.THRESHOLD) CSF=THRESHOLD
C
C---CF=CNTS(NO SAMPLE AND GD FILTER) -
C       CNTS(NO SAMPLE AND BOTH FILTER)
C
      CF=CNT(2,K)-CNT(3,K)
```

99

```fortran
          IF (CF.LT.THRESHOLD) CF=THRESHOLD
C
          WRITE(15,1110) EL(K),(CNT(L,K),L=1,5),CF,CSF
   85 CONTINUE
C
 1000 FORMAT(A72)
 1010 FORMAT(/,A72)
 1020 FORMAT(A19,2X,A10)
 1030 FORMAT('********************************************',
     &    '*********************')
 1040 FORMAT(A11,1PE11.4,6X,0PF6.2,A4)
 1050 FORMAT(A11,1PE11.4)
 1060 FORMAT(/,'SPECTRAL SUMS',/)
 1070 FORMAT('       GD-FILTER    GD/CD-FILTERS    GD-F/SAMPLE',
     &    '   GD/CD-F/SAMPLE',/)
 1080 FORMAT(4F15.1)
 1090 FORMAT(/,' TRANSMISSION  ',3F15.5)
 1100 FORMAT(' MASS SIGNAL   ',3F15.5)
 1110 FORMAT(8(1PE12.4))
      STOP
      END
C
C-------------------------------------------------
C---SUBROUTINE TO READ A LINE OF INPUT FILE
C-------------------------------------------------
C
      SUBROUTINE READFILE(VAR)
      REAL VAR
      CHARACTER*72 LINE
C
      READ (13,1000) LINE
      READ (LINE(20:72),'(F12.5)') VAR
      WRITE (16,1010) LINE(1:19),VAR
 1000 FORMAT (A72)
 1010 FORMAT (A19,2X,1PE11.4)
      RETURN
      END
C
C-----------------------------------------
C---SUBROUTINE TO CREATE SPECTRA
C-----------------------------------------
C
C---CREATES ORIGINAL, FILTERED, AND TRANSMITTED SPECTRA
C
C---DETECTOR RESPONSE SPECTRA CNT(N,K):
C      WITHOUT FILTER            N = 1
C      WITH GD FILTER              = 2
C      WITH GD + CD FILTER         = 3
C      WITH GD + SAMPLE            = 4
C      WITH GD + CD FILTER + SAMPLE = 5
C
      SUBROUTINE COUNTS(WT9,NSTY)
      IMPLICIT REAL (A-H,O-Z)
      IMPLICIT INTEGER (I-N)
      COMMON /BANK/ EL(12000),S(14,12000),CS(3,12000),CNT(5,12000)
      COMMON /PARA/ RAD,FRAC,AMN(5),RAD2,DF1,DF2,RCOL,DDT,NHIST
C
C----CONSTRUCT NRAD SPECTRUM
C
      CALL FLUX(1,EL(1),F)
      CNT(1,1)=0.001*F
      CALL FLUX(1,EL(2),F)
```

```fortran
      CNT(1,2)=0.009*F
      DO 20 L=3,11097
C---DETERMINES WHICH PART OF SPECTRUM IS RELEVANT
      IF (EL(L).GT.178000.0) THEN
        NX=3
      ELSE IF (EL(L).GT.0.1705) THEN
        NX=2
      ELSE
        NX=1
      ENDIF
C---DETERMINES WIDTH OF ENERGY GROUP
      IF (EL(L).GT.1000000.0) THEN
        DE=100000.0
      ELSE IF (EL(L).GT.10000.0) THEN
        DE=10000.0
      ELSE IF (EL(L).GT.1000.0) THEN
        DE=1000.0
      ELSE IF (EL(L).GT.300.0) THEN
        DE=1.0
      ELSE IF (EL(L).GT.80.0) THEN
        DE=0.1
      ELSE
        DE=0.01
      ENDIF
      CALL FLUX(NX,EL(L),F)
      CNT(1,L)=DE*F
   20 CONTINUE
C
C----NORMALIZE TO NUMBER OF HISTORIES
C
      SUM=0.0
      DO 30 L=1,11097
        SUM=SUM+CNT(1,L)
   30 CONTINUE
      AH=REAL(NHIST)/SUM
      DO 40 L=1,11097
        CNT(1,L)=CNT(1,L)*AH
   40 CONTINUE
C
C----GET GD AND GD/CD TRANSMITTED SPECTRA
C
      S0=0.0
      S1=0.0
      DO 50 L=1,11097
        DG=CNT(1,L)*EXP(-CS(3,L)*DF1)
        S0=S0+DG
        DC=DG*EXP(-CS(2,L)*DF2)
        S1=S1+DC
        CNT(3,L)=DC
        CNT(2,L)=DG
   50 CONTINUE
C
C----REPEAT FOR HISTORIES IN EACH GROUP
C
      DO 110 N=4,5
        DO 100 K=1,11097
          NHI=NINT(CNT(N-2,K))
          IF (NHI.EQ.0) GO TO 100
          DO 80 NH=1,NHI
C
C----START A NEUTRON
C
```

```
            CALL SOURCE(X,Y,Z,NSTY)
C
C----TRANSMISSION
C
    60        CONTINUE
              CALL RANDOM(RR)
              IF (RR.LT.3.0E-38) GO TO 60
              AL=-LOG(RR)/CS(1,K)
              IF (AL.GT.2.0*Y) THEN
                CNT(N,K)=CNT(N,K)+1.0
              ENDIF
    80     CONTINUE
   100   CONTINUE
   110 CONTINUE
C
C----CONVERT TO DETECTOR RESPONSE SPECTRUM
C
       DO 150 J=1,5
         DO 140 L=1,11097
           CNT(J,L)=CNT(J,L)*DDT*S(14,L)
   140     CONTINUE
   150 CONTINUE
       RETURN
       END
C
C--------------------------------------------
C---SUBROUTINE TO CALCULATE NRAD FLUX
C--------------------------------------------
C
C---CALCULATES NRAD FLUX F AT ENERGY E,
C---BASED ON PARAMETERIZATION IN THREE REGIONS:
C       N=1    E < 0.1705 EV              THERMAL MAXWELL
C       N=2    178 KEV > E  > 0.1705 EV  1/E SLOWING DOWN
C       N=3    E > 178 KEV               FISSION SPECTRUM
C
       SUBROUTINE FLUX(N,E,F)
       INTEGER N
       REAL A,B,E,F
C
C---THERMAL REGION
C
       IF (N.EQ.1) THEN
         F=1.132E11*E*EXP(-E/0.03)
C
C---1/E REGION
C
       ELSE IF (N.EQ.2) THEN
         F=1.114E+07/E
C
C---FISSION REGION
C
       ELSE IF (N.EQ.3) THEN
         A=1.036E-06*E
         B=SQRT(2.29E-06*E)
         F=108.02*EXP(-A)*SINH(B)
       ENDIF
       RETURN
       END
C
C----------------------------------------------------------
C---SUBROUTINE TO CREATE A NEUTRON WITHIN COLLIMATOR FROM NRAD
C----------------------------------------------------------
```

```
C
      SUBROUTINE SOURCE(X,Y,Z,NSTY)
      IMPLICIT REAL (A-H,O-Z)
      IMPLICIT INTEGER (I-N)
      COMMON /PARA/ RAD,FRAC,AMN(5),RAD2,DF1,DF2,RCOL,DDT,NHIST
C
      CALL RANDOM(R1)
      CALL RANDOM(R2)
      THETA=R1*2*PI
      R=R2*RCOL
      X=R*COS(THETA)
      Z=R*SIN(THETA)
      IF (NSTY.EQ.1) THEN
         YDIF=RAD2-X*X
         IF (YDIF.LT.0.0) YDIF=0.0
         Y=SQRT(YDIF)
      ELSE IF (NSTY.EQ.2) THEN
         Y=RAD
      ENDIF
      RETURN
      END
C
C------------------------------------------------
C---SUBROUTINE TO READ CROSS-SECTION DATA FILE
C------------------------------------------------
C
      SUBROUTINE DATA
      IMPLICIT REAL (A-H,O-Z)
      IMPLICIT INTEGER (I-N)
      COMMON /BANK/ EL(12000),S(14,12000),CS(3,12000),CNT(5,12000)
      COMMON /PARA/ RAD,FRAC,AMN(5),RAD2,DF1,DF2,RCOL,DDT,NHIST
C
      REWIND 14
      DO 10 L=1,11097
         READ(14,1000) EL(L),(S(I,L),I=1,13)
         S(14,L)=S(6,L)
   10 CONTINUE
C
C----PRECALCULATIONS FOR THE FISSIONABLE ISOTOPES
C
      DO 90 L=1,11097
         DO 60 K=1,3
            DO 50 I=1,3
               J=3*(K-1)+I
               S(J,L)=AMN(K)*S(J,L)
   50       CONTINUE
   60    CONTINUE
C---CADMIUM
         S(10,L)=AMN(4)*S(10,L)
         S(11,L)=AMN(4)*S(11,L)
C---GADOLINIUM
         S(12,L)=AMN(5)*S(12,L)
         S(13,L)=AMN(5)*S(13,L)
C---DETECTOR
         DENS=19.8*0.602252/239.0
         S(14,L)=S(14,L)*DENS
   90 CONTINUE
C
C----GET TOTAL CROSS SECTIONS
C
      DO 150 L=1,11097
```

```
          SUM=0.0
          DO 100 K=1,9
             SUM=SUM+S(K,L)
   100    CONTINUE
          CS(1,L)=SUM
          SUM=0.0
          DO 110 K=10,11
             SUM=SUM+S(K,L)
   110    CONTINUE
          CS(2,L)=SUM
          SUM=0.0
          DO 120 K=12,13
             SUM=SUM+S(K,L)
   120    CONTINUE
          CS(3,L)=SUM
   150 CONTINUE
       RETURN
  1000 FORMAT(14(E11.4,X))
       END
C
C-------------------------------------------------
C----SUBROUTINE TO GENERATE RANDOM NUMBERS
C-------------------------------------------------
C
       SUBROUTINE RANDOM(R)
       INTEGER L,KL,NL,KU,J,II,M,I,N,LL
       REAL RADA(100),R
       COMMON /RAND/  RADA
       DATA L,KL,NL,KU,J,II
      &    /1436379,519,7359357,17,69069,30091/
C
       M=NL*KU
       NL=MOD(M,14247997)
       I=L*KL+NL
       L=MOD(I,3671037)
       N=J*II
       II=MOD(N,31091)
       LL=MOD(N,100)+1
       R=RADA(LL)
       RADA(LL)=REAL(L)/3671037.0
       SAVE
       RETURN
       END
C
C-----------------------------------------------------
C----SUBROUTINE TO GENERATE RANDOM NUMBER STARTERS
C-----------------------------------------------------
C
       SUBROUTINE RANSTA
       INTEGER L,KL,NL,I,M,KU,J
       REAL RADA(100),R
       COMMON /RAND/  RADA
       DATA L,KL,NL,KU /1436379,519,7359357,17/
C
       DO 10 J=1,100
          M=NL*KU
          NL=MOD(M,14247997)
          I=L*KL+NL
          L=MOD(I,3671037)
          R=REAL(L)/3671037.0
          RADA(J)=R
    10 CONTINUE
```

```
SAVE
RETURN
END
```
:

Appendix B: Sample Input Deck for Transmission Code

This appendix contains a sample input file for the calculations performed in Chapter 4.

```sh
#!/bin/sh
set -vx
umask 0022
#
#---------------------------
# SET USER VARIABLES
#---------------------------
#
glg=/usr/local1
rtk=$HOME
current=$rtk/thesis/detector
#
#------------------------------------------------------
# SET RASHELL VARIABLES and START RASHELL
#------------------------------------------------------
#
RAJOBNAME=g10c100cs
RABADGE=klann
RADEST=
RAOUTPUT=output
RATIME=120
RAMEM=50
RALINES=25000
RADATASIZE=100
RAHOST=baldy
RAROUTE=cwd
RAPREPATH=
. $glg/rashell/RASHELL
#
#------------------------------------
# COPY FILES INTO SCRATCH SPACE
#------------------------------------
#
cp $current/xsec xsec
cp $current/res-round2.x res-round2.x
#
#--------------
# INPUT FILE
#--------------
#
input=g10c100cs
cat << 'fileend' >> $input
GADOLINIUM FILTER
    THICKNESS (cm)  = 0.010
    DENSITY (g/cc)  = 7.89
    ATOMIC WEIGHT   = 157.25

CADMIUM FILTER
    THICKNESS (cm)  = 0.100
    DENSITY (g/cc)  = 8.65
    ATOMIC WEIGHT   = 112.41
COLLIMATOR
    RADIUS (cm)     = 0.54991
SAMPLE
    TYPE            = SLAB
    1/2-THICK (cm)  = 0.54991
```

```
    DENSITY (g/cc) = 18.90
    PU-239 WT %    = 3.000
    U-235 WT %     = 0.22
DETECTOR
    THICKNESS (cm) = 0.02
FREQUENCY FOR INCREASING PU-239 WT% = 24
HISTORIES = 10000000
fileend
#
#------------------
# EXECUTE PROGRAM
#------------------
#
res-round2.x $input
#
#------------------------------------------------
# WRITE OUTPUT FILES BACK TO CURRENT DIRECTORY
#------------------------------------------------
#
cp $input.spectrum $current/$input.spectrum
cp $input.output $current/$input.output
```

Appendix C: Experimental Data

Enclosed herein are all of the output files from the measurements. Each file contains the data for one series of four measurements to determine the mass signal for a given configuration. Each file is arranged with the measurement date listed first, followed by a description of the system configuration and sample loading for the measurements, and then by the raw data from the measurements. The column listing the filter and sample arrangement uses a notation where S means the sample is in the beam and NS means there is no sample in the beam. The same is true for the cadmium filter (F for the filter in the beam and NF for no filter in the beam).

The files are grouped according to the arrangement of the results discussed in Chapter 6. The file naming convention is as follows: the first descriptor contains the date of the measurement (first letter of the month and the day number), and the second descriptor distinguishes the case from the others in a given measurement series. For example, the file s30.pu0657 describes a measurement that was performed on September 30 where the sample contained 0.657 weight percent ^{239}Pu. The experimental data files are organized as follows:

Sample Composition Measurements:

Sample Thickness Measurements:

FILE : a26.back

8/26/97
L/D=50
SCRAPER CLOSED
NEUTRON SHUTTER CLOSED
BACKGROUND READINGS ARE ALPHA ONLY (D=1.54)
SAMPLE HOLDER A
 U-238 foils = Group 4
 Total U-238 wt = 26331.83 mg
 Total U-235 wt = 58.06 mg
 Total U mass = 26389.89 mg
 No Pu foils

ARRANGEMENT	BTB COUNTS	MONITOR COUNTS	TIME (SEC)
SNF	95698.0	2249741.0	500.0
SF	35000.0	2249939.0	500.0
NSNF	182912.0	2257631.0	500.0
NSF	53653.0	2257644.0	500.0

FILE: s3.back1

9/3/97
BACKGROUND READINGS
DETECTOR 6 INCHES NORTH OF CENTERLINE
NO ADDITIONAL POLY SHIELDING
L/D=50
SCRAPER OPEN 4 INCHES WIDE
NEUTRON SHUTTER CLOSED
DISCRIMINATOR SET TO 1.7
SAMPLE HOLDER A
 U-238 foils = Group 4
 Total U-238 wt = 26331.83 mg
 Total U-235 wt = 58.06 mg
 No Pu foils

ARRANGEMENT	BTB COUNTS	MONITOR COUNTS	TIME (SEC)
SNF	16948.0	2251960.0	500.0
SF	17044.0	2254583.0	500.0
NSNF	16958.0	2265469.0	500.0
NSF	17227.0	2257287.0	500.0

FILE: s5.back

9/5/97
DETECTOR IN BEAM
B-POLY SHIELDING
L/D=50
SCRAPER OPEN 4 INCHES WIDE
NEUTRON SHUTTER CLOSED
DISCRIMINATOR SET TO 1.7
SAMPLE HOLDER A
 U-238 foils = Group 4
 Total U-238 wt = 26331.83 mg
 Total U-235 wt = 58.06 mg

```
Total U mass = 26389.89 mg
No Pu foils

ARRANGEMENT   BTB COUNTS   MONITOR COUNTS   TIME (SEC)
-----------   ----------   --------------   ----------
    SNF        164523.0      4439309.0        1000.0
    SF          44423.0      4440106.0        1000.0
    NSNF       335393.0      4462901.0        1000.0
    NSF         80783.0      4450326.0        1000.0
```

FILE: s23.above

```
9/4/97
BACKGROUND READINGS
DETECTOR 5 INCHES ABOVE THE BEAM CENTERLINE
B-POLY SHIELDING - FINAL CONFIGURATION
L/D=50
SCRAPER OPEN 4 INCHES WIDE
NEUTRON SHUTTER CLOSED
DISCRIMINATOR SET TO 1.7
SAMPLE HOLDER A
   U-238 foils = Group 4
   total U-238 wt = 26331.83 mg
   total U-235 wt = 58.06 mg
   No Pu foils

ARRANGEMENT   BTB COUNTS   MONITOR COUNTS   TIME (SEC)
-----------   ----------   --------------   ----------
    SNF          6282.0      4402381.0        1000.0
    SF           6230.0      4397859.0        1000.0
    NSNF         6197.0      4396452.0        1000.0
    NSF          6063.0      4396250.0        1000.0
```

FILE: s24.north

```
9/4/97
BACKGROUND READINGS
DETECTOR 5 INCHES NORTH OF CENTERLINE
B-POLY SHIELDING - FINAL CONFIGURATION
L/D=50
SCRAPER OPEN 4 INCHES WIDE
NEUTRON SHUTTER CLOSED
DISCRIMINATOR SET TO 1.7
SAMPLE HOLDER A
   U-238 foils = Group 4
   total U-238 wt = 26331.83 mg
   total U-235 wt = 58.06 mg
   No Pu foils

ARRANGEMENT   BTB COUNTS   MONITOR COUNTS   TIME (SEC)
-----------   ----------   --------------   ----------
    SNF          6223.0      4391666.0        1000.0
    SF          18630.0     13125806.0        3000.0
    NSNF         6232.0      4370641.0        1000.0
    NSF          6196.0      4376406.0        1000.0
```

FILE: s24.south

```
9/4/97
BACKGROUND READINGS
DETECTOR 5 INCHES SOUTH OF THE BEAM CENTERLINE
```

111

```
B-POLY SHIELDING - FINAL CONFIGURATION
L/D=50
SCRAPER OPEN 4 INCHES WIDE
NEUTRON SHUTTER CLOSED
DISCRIMINATOR SET TO 1.7
SAMPLE HOLDER A
   U-238 foils = Group 4
   total U-238 wt = 26331.83 mg
   total U-235 wt = 58.06 mg
   No Pu foils
```

ARRANGEMENT	BTB COUNTS	MONITOR COUNTS	TIME (SEC)
SNF	6193.0	4369473.0	1000.0
SF	6112.0	4368111.0	1000.0
NSNF	6142.0	4368485.0	1000.0
NSF	6149.0	4366245.0	1000.0

FILE: d2.front

```
12/2/97
DETECTOR IN BEAM
B-POLY SHIELDING
L/D=50
SCRAPER OPEN 4 INCHES WIDE
NEUTRON SHUTTER CLOSED
DISCRIMINATOR SET TO 1.7
SAMPLE HOLDER D
   U-238 foils = Group 3 -8AJM
   Pu-239 foils = N4A, P2N
   Total U-238 wt = 26029.74 mg
   Total U-235 wt = 57.39 mg
   Total U mass = 26086.63 mg
   Total Pu-239 wt = 262.05 mg
   Total Other Pu wt = 13.85 mg
   Total Pu mass = 275.90 mg
   Pu-239 wt % = 1.3703
Pu Foils in front of holder
```

ARRANGEMENT	BTB COUNTS	MONITOR COUNTS	TIME (SEC)
SNF	53444.0	4428057.0	1000.0
SF	30526.0	4435431.0	1000.0
NSNF	292768.0	4447647.0	1000.0
NSF	71454.0	4434244.0	1000.0

FILE: d2.middle

```
12/2/97
DETECTOR IN BEAM
B-POLY SHIELDING
L/D=50
SCRAPER OPEN 4 INCHES WIDE
NEUTRON SHUTTER CLOSED
DISCRIMINATOR SET TO 1.7
SAMPLE HOLDER D
   U-238 foils = Group 3 -8AJM
   Pu-239 foils = N4A, P2N
   Total U-238 wt = 26029.74 mg
   Total U-235 wt = 57.39 mg
   Total U mass = 26086.63 mg
   Total Pu-239 wt = 262.05 mg
   Total Other Pu wt = 13.85 mg
   Total Pu mass = 275.90 mg
   Pu-239 wt % = 1.3703
Pu Foils in middle of holder
```

```
ARRANGEMENT   BTB COUNTS   MONITOR COUNTS   TIME (SEC)
-----------   ----------   --------------   ----------
   SNF          53245.0       4432104.0       1000.0
   SF           30437.0       4431345.0       1000.0
   NSNF        292791.0       4445136.0       1000.0
   NSF          72515.0       4436044.0       1000.0
```

FILE: d2.back

```
11/14/97
DETECTOR IN BEAM
B-POLY SHIELDING
L/D=50
SCRAPER OPEN 4 INCHES WIDE
NEUTRON SHUTTER CLOSED
DISCRIMINATOR SET TO 1.7
SAMPLE HOLDER D
   U-238 foils = Group 3 -8AJM
   Pu-239 foils = N4A, P2N
   Total U-238 wt = 26029.74 mg
   Total U-235 wt = 57.39 mg
   Total U mass = 26086.63 mg
   Total Pu-239 wt = 262.05 mg
   Total Other Pu wt = 13.85 mg
   Total Pu mass = 275.90 mg
   Pu-239 wt % = 1.3703
ARRANGEMENT   BTB COUNTS   MONITOR COUNTS   TIME (SEC)
-----------   ----------   --------------   ----------
   SNF          53439.0       4448215.0       1000.0
   SF           30712.0       4447808.0       1000.0
   NSNF        293199.0       4464662.0       1000.0
   NSF          72403.0       4454860.0       1000.0
```

FILE: s30.pu0

```
9/30/97
L/D=50
SCRAPER OPEN 4 INCHES WIDE
NEUTRON SHUTTER CLOSED
SAMPLE HOLDER A
   U-238 foils = Group 4
   Total U-238 wt = 26331.83 mg
   Total U-235 wt = 58.06 mg
   Total U mass = 26389.89 mg
   Pu-239 wt% = 0.0000

ARRANGEMENT   BTB COUNTS   MONITOR COUNTS   TIME (SEC)
-----------   ----------   --------------   ----------
   SNF         158192.0       4349315.0       1000.0
   SF           81485.0       8701075.0       2000.0
   NSNF        324778.0       4388414.0       1000.0
   NSF         154129.0       8733322.0       2000.0
```

FILE: o7.pu0073

```
10/7/97
L/D=50
SCRAPER OPEN 4 INCHES WIDE
NEUTRON SHUTTER CLOSED
SAMPLE HOLDER A
   U-238 foils = Group 4
```

```
Pu-239 foils = A2X
Total U-238 wt = 26331.83 mg
Total U-235 wt = 58.06 mg
Total U mass = 26389.89 mg
Total Pu-239 wt = 13.895 mg
Total Other Pu wt = 0.735 mg
Total Pu mass = 14.63 mg
Pu-239 wt % = 0.0728
```

ARRANGEMENT	BTB COUNTS	MONITOR COUNTS	TIME (SEC)
SNF	145805.0	4429085.0	1000.0
SF	79372.0	8862489.0	2000.0
NSNF	327091.0	4446006.0	1000.0
NSF	77214.0	4426102.0	1000.0

FILE: o3.pu0179

```
10/3/97
L/D=50
SCRAPER OPEN 4 INCHES WIDE
NEUTRON SHUTTER CLOSED
SAMPLE HOLDER A
  U-238 foils = Group 4
  Pu-239 foils = A2X, A2Y
  Total U-238 wt = 26331.83 mg
  Total U-235 wt = 58.06 mg
  Total U mass = 26389.89 mg
  Total Pu-239 wt = 34.24 mg
  Total Other Pu wt = 1.81 mg
  Total Pu mass = 36.05 mg
  Pu-239 wt % = 0.1792
```

ARRANGEMENT	BTB COUNTS	MONITOR COUNTS	TIME (SEC)
SNF	128909.0	4441352.0	1000.0
SF	78268.0	8875239.0	2000.0
NSNF	325929.0	4459833.0	1000.0
NSF	77021.0	4445438.0	1000.0

FILE: s30.pu0657

```
9/30/97
L/D=50
SCRAPER OPEN 4 INCHES WIDE
NEUTRON SHUTTER CLOSED
SAMPLE HOLDER B
  U-238 foils = Group 1 -8ACZ
  Pu-239 foils = P2N
  Total U-238 wt = 26074.67 mg
  Total U-235 wt = 57.49 mg
  Total U mass = 26132.16 mg
  Total Pu-239 wt = 124.84 mg
  Total Other Pu wt = 6.60 mg
  Total Pu mass = 131.44 mg
  Pu-239 wt % = 0.6566
```

ARRANGEMENT	BTB COUNTS	MONITOR COUNTS	TIME (SEC)
SNF	85727.0	4352053.0	1000.0
SF	72793.0	8708915.0	2000.0

```
NSNF       327992.0        4378569.0        1000.0
NSF         78101.0        4361083.0        1000.0
```

FILE: n13.pu0657

```
11/13/97
L/D=50
SCRAPER OPEN 4 INCHES WIDE
NEUTRON SHUTTER CLOSED
SAMPLE HOLDER B
  U-238 foils = Group 1 -8ACZ
  Pu-239 foils = P2N
  Total U-238 wt = 26074.67 mg
  Total U-235 wt = 57.49 mg
  Total U mass = 26132.16 mg
  Total Pu-239 wt = 124.84 mg
  Total Other Pu wt = 6.60 mg
  Total Pu mass = 131.44 mg
  Pu-239 wt % = 0.6566
```

ARRANGEMENT	BTB COUNTS	MONITOR COUNTS	TIME (SEC)
SNF	76237.0	4431503.0	1000.0
SF	33732.0	4429037.0	1000.0
NSNF	294802.0	4468351.0	1000.0
NSF	71787.0	4444666.0	1000.0

FILE: o7.pu0789

```
10/7/97
L/D=50
SCRAPER OPEN 4 INCHES WIDE
NEUTRON SHUTTER CLOSED
SAMPLE HOLDER B
  U-238 foils = Group 1 -8ACZ
  Pu-239 foils = N4Q
  Total U-238 wt = 26074.67 mg
  Total U-235 wt = 57.49 mg
  Total U mass = 26132.16 mg
  Total Pu-239 wt = 150.29 mg
  Total Other Pu wt = 7.94 mg
  Total Pu mass = 158.23 mg
  Pu-239 wt % = 0.7894
```

ARRANGEMENT	BTB COUNTS	MONITOR COUNTS	TIME (SEC)
SNF	77004.0	4431384.0	1000.0
SF	69538.0	8881841.0	2000.0
NSNF	322873.0	4456964.0	1000.0
NSF	76708.0	4433380.0	1000.0

FILE: o2.pu0918

```
10/2/97
L/D=50
SCRAPER OPEN 4 INCHES WIDE
NEUTRON SHUTTER CLOSED
SAMPLE HOLDER C
  U-238 foils = Group 2 -8AMI
  Pu-239 foils = N5L
  Total U-238 wt = 26045.29 mg
```

```
Total U-235 wt = 57.43 mg
Total U mass = 26102.72 mg
Total Pu-239 wt = 174.83 mg
Total Other Pu wt = 9.24 mg
Total Pu mass = 184.07 mg
Pu-239 wt % = 0.9181
```

ARRANGEMENT	BTB COUNTS	MONITOR COUNTS	TIME (SEC)
SNF	72339.0	4460696.0	1000.0
SF	69820.0	8919819.0	2000.0
NSNF	325557.0	4453419.0	1000.0
NSF	76990.0	4452617.0	1000.0

FILE: o1.pu0990

```
10/1/97
L/D=50
SCRAPER OPEN 4 INCHES WIDE
NEUTRON SHUTTER CLOSED
SAMPLE HOLDER C
  U-238 foils = Group 2 -8AMI
  Pu-239 foils = N5L, A2X
  Total U-238 wt = 26045.29 mg
  Total U-235 wt = 57.43 mg
  Total U mass = 26102.72 mg
  Total Pu-239 wt = 188.73 mg
  Total Other Pu wt = 9.97 mg
  Total Pu mass = 198.70 mg
  Pu-239 wt % = 0.9903
```

ARRANGEMENT	BTB COUNTS	MONITOR COUNTS	TIME (SEC)
SNF	139484.0	8919575.0	2000.0
SF	68853.0	8895076.0	2000.0
NSNF	326713.0	4455714.0	1000.0
NSF	78030.0	4453781.0	1000.0

FILE: o6.pu1370

```
10/6/97
L/D=50
SCRAPER OPEN 4 INCHES WIDE
NEUTRON SHUTTER CLOSED
SAMPLE HOLDER D
  U-238 foils = Group 3 -8AJM
  Pu-239 foils = N4A, P2N
  Total U-238 wt = 26029.24 mg
  Total U-235 wt = 57.39 mg
  Total U mass = 26086.63 mg
  Total Pu-239 wt = 262.05 mg
  Total Other Pu wt = 13.85 mg
  Total Pu mass = 275.90 mg
  Pu-239 wt % = 1.3703
```

ARRANGEMENT	BTB COUNTS	MONITOR COUNTS	TIME (SEC)
SNF	56586.0	4440785.0	1000.0
SF	64157.0	8889002.0	2000.0
NSNF	324129.0	4471168.0	1000.0
NSF	76023.0	4456672.0	1000.0

FILE: n14.pu1370

```
11/14/97
L/D=50, SCRAPER OPEN 4 INCHES WIDE
NEUTRON SHUTTER CLOSED
SAMPLE HOLDER D
   U-238 foils = Group 3 -8AJM
   Pu-239 foils = N4A, P2N
   Total U-238 wt = 26029.24 mg
   Total U-235 wt = 57.39 mg
   Total U mass = 26086.63 mg
   Total Pu-239 wt = 262.05 mg
   Total Other Pu wt = 13.85 mg
   Total Pu mass = 275.90 mg
   Pu-239 wt % = 1.3703
```

ARRANGEMENT	BTB COUNTS	MONITOR COUNTS	TIME (SEC)
SNF	53439.0	4448215.0	1000.0
SF	30712.0	4447808.0	1000.0
NSNF	293199.0	4464662.0	1000.0
NSF	72403.0	4454860.0	1000.0

FILE: o2.pu1606

```
10/2/97
L/D=50
SCRAPER OPEN 4 INCHES WIDE
NEUTRON SHUTTER CLOSED
SAMPLE HOLDER D
   U-238 foils = Group 3 -8AJM
   Pu-239 foils = N4A, N4Q, A2Y
   Total U-238 wt = 26029.24 mg
   Total U-235 wt = 57.39 mg
   Total U mass = 26086.63 mg
   Total Pu-239 wt = 307.84 mg
   Total Other Pu wt = 16.27 mg
   Total Pu mass = 324.11 mg
   Pu-239 wt % = 1.6057
```

ARRANGEMENT	BTB COUNTS	MONITOR COUNTS	TIME (SEC)
SNF	53519.0	4438096.0	1000.0
SF	64189.0	8871994.0	2000.0
NSNF	327317.0	4457250.0	1000.0
NSF	77329.0	4448345.0	1000.0

FILE: o7.pu2055

```
10/7/97
L/D=50
SCRAPER OPEN 4 INCHES WIDE
NEUTRON SHUTTER CLOSED
SAMPLE HOLDER D
   U-238 foils = Group 3 -8AJM
   Pu-239 foils = N5L, N5T, A2X, A2Y
   Total U-238 wt = 26029.24 mg
   Total U-235 wt = 57.39 mg
   Total U mass = 26086.63 mg
   Total Pu-239 wt = 395.84 mg
   Total Other Pu wt = 20.91 mg
   Total Pu mass = 416.75 mg
```

117

Pu-239 wt % = 2.0548

ARRANGEMENT	BTB COUNTS	MONITOR COUNTS	TIME (SEC)
SNF	47965.0	4425270.0	1000.0
SF	60731.0	8856987.0	2000.0
NSNF	326408.0	4439211.0	1000.0
NSF	78030.0	4422338.0	1000.0

FILE: n14.pu2647

```
11/14/97
L/D=50
SCRAPER OPEN 4 INCHES WIDE
NEUTRON SHUTTER CLOSED
SAMPLE HOLDER C
  U-238 foils = Group 2 -8AFW, 8AHB
  Pu-239 foils = N5L, N5T, P1R
  Total U-238 wt = 25717.25 mg
  Total U-235 wt = 56.70 mg
  Total U mass = 25773.95 mg
  Total Pu-239 wt = 506.98 mg
  Total Other Pu wt = 26.79 mg
  Total Pu mass = 533.77 mg
  Pu-239 wt % = 2.6467
```

ARRANGEMENT	BTB COUNTS	MONITOR COUNTS	TIME (SEC)
SNF	38044.0	4446450.0	1000.0
SF	27127.0	4445163.0	1000.0
NSNF	292441.0	4464581.0	1000.0
NSF	72010.0	4451655.0	1000.0

FILE: d2.pu3177

```
12/2/97
L/D=50
SCRAPER OPEN 4 INCHES WIDE
NEUTRON SHUTTER CLOSED
SAMPLE HOLDER A
  U-238 foils = Group 4 - 8AHP, 8ADX, 8AHJ
  Pu-239 foils = N4Q, P1R, N5T, P2N
  Total U-238 wt = 25512.32 mg
  Total U-235 wt = 56.25 mg
  Total U mass = 25568.57 mg
  Total Pu-239 wt = 607.28 mg
  Total Other Pu wt = 32.09 mg
  Total Pu mass = 639.37 mg
  Pu-239 wt % = 3.1774
```

ARRANGEMENT	BTB COUNTS	MONITOR COUNTS	TIME (SEC)
SNF	35485.0	4425430.0	1000.0
SF	25794.0	4429738.0	1000.0
NSNF	293194.0	4471264.0	1000.0
NSF	71738.0	4443332.0	1000.0

FILE: j7.pu1023

```
1/7/98
L/D=50, SCRAPER OPEN 4 INCHES WIDE
```

```
NEUTRON SHUTTER CLOSED
SAMPLE HOLDER A
  U-238 foils = Group 4 -8AMR
  Pu-239 foils = N5L, A2Y
  Total U-238 wt = 26074.29 mg
  Total U-235 wt = 57.49 mg
  Total U mass = 26131.78 mg
  Total Pu-239 wt = 195.18 mg
  Total Other Pu wt = 10.31 mg
  Total Pu mass = 205.49 mg
  Pu-239 wt % = 1.0226
```

ARRANGEMENT	BTB COUNTS	MONITOR COUNTS	TIME (SEC)
SNF	61282.0	4448474.0	1000.0
SF	31203.0	4445957.0	1000.0
NSNF	286391.0	4469015.0	1000.0
NSF	70315.0	4458372.0	1000.0

FILE: j7.pu2205

```
1/7/98
L/D=50
SCRAPER OPEN 4 INCHES WIDE
NEUTRON SHUTTER CLOSED
SAMPLE HOLDER A
  U-238 foils = Group 4 -8AMR, 8AQD
  Pu-239 foils = P2N, N4A, P1R
  Total U-238 wt = 25774.47 mg
  Total U-235 wt = 56.38 mg
  Total U mass = 25831.30 mg
  Total Pu-239 wt = 421.32 mg
  Total Other Pu wt = 22.26 mg
  Total Pu mass = 443.58 mg
  Pu-239 wt % = 2.2051
```

ARRANGEMENT	BTB COUNTS	MONITOR COUNTS	TIME (SEC)
SNF	40854.0	4449482.0	1000.0
SF	27860.0	4458652.0	1000.0
NSNF	287939.0	4475465.0	1000.0
NSF	71146.0	4464159.0	1000.0

FILE: d2.u0220

```
12/2/97
L/D=50
SCRAPER OPEN 4 INCHES WIDE
NEUTRON SHUTTER CLOSED
SAMPLE HOLDER A
  U-238 foils = Group 4
  Total U-238 wt = 26331.83 mg
  Total U-235 wt = 58.06 mg
  Total U mass = 26389.89 mg
  U-235 wt% = 0.2200
```

ARRANGEMENT	BTB COUNTS	MONITOR COUNTS	TIME (SEC)
SNF	141735.0	4440486.0	1000.0
SF	37650.0	4448249.0	1000.0
NSNF	292588.0	4464966.0	1000.0
NSF	72092.0	4453333.0	1000.0

FILE: d3.u0799

```
12/3/97
L/D=50, SCRAPER OPEN 4 INCHES WIDE
NEUTRON SHUTTER CLOSED
SAMPLE HOLDER A
  U-238 foils = Group 4 -8AMR
  U-235 foils = 5BWR
  Total U-238 wt = 26085.66 mg
  Total U-235 wt = 210.14 mg
  Total U mass = 26295.80 mg
  U-235 wt % = 0.7991
```

ARRANGEMENT	BTB COUNTS	MONITOR COUNTS	TIME (SEC)
SNF	134877.0	4438676.0	1000.0
SF	37447.0	4442519.0	1000.0
NSNF	292884.0	4465075.0	1000.0
NSF	72027.0	4449845.0	1000.0

FILE: d3.u0990

```
12/3/97
L/D=50
SCRAPER OPEN 4 INCHES WIDE
NEUTRON SHUTTER CLOSED
SAMPLE HOLDER A
  U-238 foils = Group 4 -8AMR
  U-235 foils = 5BQY
  Total U-238 wt = 26089.43 mg
  Total U-235 wt = 260.83 mg
  Total U mass = 26350.26 mg
  U-235 wt % = 0.9899
```

ARRANGEMENT	BTB COUNTS	MONITOR COUNTS	TIME (SEC)
SNF	133297.0	4446909.0	1000.0
SF	38562.0	4449723.0	1000.0
NSNF	292705.0	4460103.0	1000.0
NSF	72259.0	4455129.0	1000.0

FILE: d3.u1396

```
12/3/97
L/D=50
SCRAPER OPEN 4 INCHES WIDE
NEUTRON SHUTTER CLOSED
SAMPLE HOLDER A
  U-238 foils = Group 4 -8AQD
  U-235 foils = 5BSP, 5BWR
  Total U-238 wt = 26055.21 mg
  Total U-235 wt = 368.92 mg
  Total U mass = 26424.13 mg
  U-235 wt % = 1.3961
```

ARRANGEMENT	BTB COUNTS	MONITOR COUNTS	TIME (SEC)
SNF	127237.0	4459164.0	1000.0
SF	37396.0	4461297.0	1000.0
NSNF	294133.0	4481683.0	1000.0
NSF	72327.0	4464750.0	1000.0

FILE: d3.u1598

```
12/3/97
L/D=50
SCRAPER OPEN 4 INCHES WIDE
NEUTRON SHUTTER CLOSED
SAMPLE HOLDER A
   U-238 foils = Group 4 -8AXV, 8AHP
   U-235 foils = 5BSP, 5BQY
   Total U-238 wt = 25803.88 mg
   Total U-235 wt = 419.04 mg
   Total U mass = 26222.92 mg
   U-235 wt % = 1.5980
```

ARRANGEMENT	BTB COUNTS	MONITOR COUNTS	TIME (SEC)
SNF	126916.0	4451424.0	1000.0
SF	37154.0	4456162.0	1000.0
NSNF	293695.0	4471958.0	1000.0
NSF	72841.0	4465532.0	1000.0

FILE: d4.u2167

```
12/4/97
L/D=50
SCRAPER OPEN 4 INCHES WIDE
NEUTRON SHUTTER CLOSED
SAMPLE HOLDER A
   U-238 foils = Group 4 -8AXV, 8AHP
   U-235 foils = 5BSP, 5BQY, 5BWR
   Total U-238 wt = 25815.25 mg
   Total U-235 wt = 571.69 mg
   Total U mass = 26386.94 mg
   U-235 wt % = 2.1666
```

ARRANGEMENT	BTB COUNTS	MONITOR COUNTS	TIME (SEC)
SNF	118246.0	4452941.0	1000.0
SF	36166.0	4450212.0	1000.0
NSNF	290689.0	4476685.0	1000.0
NSF	71337.0	4459825.0	1000.0

FILE: d4.u2835

```
12/4/97
L/D=50
SCRAPER OPEN 4 INCHES WIDE
NEUTRON SHUTTER CLOSED
SAMPLE HOLDER A
   U-238 foils = Group 4 -8AXV, 8AHP, 8AMR
   U-235 foils = 5BSP, 5BQE, 5BQL, 5BWR
   Total U-238 wt = 25570.73 mg
   Total U-235 wt = 746.00 mg
   Total U mass = 26316.73 mg
   U-235 wt % = 2.8347
```

ARRANGEMENT	BTB COUNTS	MONITOR COUNTS	TIME (SEC)
SNF	112407.0	4459223.0	1000.0
SF	35621.0	4461975.0	1000.0
NSNF	291525.0	4474174.0	1000.0
NSF	72440.0	4465361.0	1000.0

FILE: d4.u3583

```
12/4/97
L/D=50
SCRAPER OPEN 4 INCHES WIDE
NEUTRON SHUTTER CLOSED
SAMPLE HOLDER A
   U-238 foils = Group 4 -8AXV, 8AHP, 8AQD
   U-235 foils = 5BSP, 5BQY, 5BWR, 5BQE, 5BQL
   Total U-238 wt = 25543.57 mg
   Total U-235 wt = 949.24 mg
   Total U mass = 26492.81 mg
   U-235 wt % = 3.5830
```

ARRANGEMENT	BTB COUNTS	MONITOR COUNTS	TIME (SEC)
SNF	105342.0	4453538.0	1000.0
SF	35444.0	4458288.0	1000.0
NSNF	292623.0	4480538.0	1000.0
NSF	72595.0	4466435.0	1000.0

FILE: j8.pu2u7

```
1/8/98
L/D=50
SCRAPER OPEN 4 INCHES WIDE
NEUTRON SHUTTER CLOSED
SAMPLE HOLDER A
   U-238 foils = Group 4 -8AMR, 8AXV, 8AHP
   Pu-239 foils = P2N, N4A, P1R
   U-235 foils = 5BWR
   Total U-238 wt = 25530.74 mg
   Total U-235 wt = 208.92 mg
   Total U mass = 25739.66 mg
   Total Pu-239 wt = 421.32 mg
   Total Other Pu wt = 22.26 mg
   Total Pu mass = 443.58 mg
   Pu-239 wt % = 2.2128
   U-235 wt % = 0.7928
```

ARRANGEMENT	BTB COUNTS	MONITOR COUNTS	TIME (SEC)
SNF	39841.0	4461610.0	1000.0
SF	27288.0	4462005.0	1000.0
NSNF	287644.0	4486686.0	1000.0
NSF	71272.0	4472745.0	1000.0

FILE: n12.t000

```
11/12/97
L/D=50
SCRAPER OPEN 4 INCHES WIDE
NEUTRON SHUTTER CLOSED
SAMPLE HOLDER D
   No Pu foils
   No U-238 foils
   Total U-238 wt = 0.0 mg
   Total U-235 wt = 0.0 mg
   Sample only contains 2 Al spacers
   TD Equivalent Thickness = 0.000 cm
```

ARRANGEMENT	BTB COUNTS	MONITOR COUNTS	TIME (SEC)
SNF	290524.0	4433701.0	1000.0
SF	71854.0	4435981.0	1000.0
NSNF	293141.0	4459974.0	1000.0
NSF	72456.0	4442015.0	1000.0

FILE: o31.t086

10/31/97
L/D=50
SCRAPER OPEN 4 INCHES WIDE
NEUTRON SHUTTER CLOSED
SAMPLE HOLDER A
  U-238 foils = Group 4 (74 foils)
  Total U-238 wt = 20659.10 mg
  Total U-235 wt = 45.55 mg
  Total U mass = 20704.65 mg
  TD Equivalent Thickness = 0.86479 cm

ARRANGEMENT	BTB COUNTS	MONITOR COUNTS	TIME (SEC)
SNF	164910.0	4450810.0	1000.0
SF	42540.0	4454107.0	1000.0
NSNF	291652.0	4480504.0	1000.0
NSF	72113.0	4465809.0	1000.0

FILE: o30.t092

10/30/97
L/D=50
SCRAPER OPEN 4 INCHES WIDE
NEUTRON SHUTTER CLOSED
SAMPLE HOLDER A
  U-238 foils = Group 4 (79 foils)
  Total U-238 wt = 22063.03 mg
  Total U-235 wt = 48.65 mg
  Total U mass = 22111.68 mg
  TD Equivalent Thickness = 0.92355 cm

ARRANGEMENT	BTB COUNTS	MONITOR COUNTS	TIME (SEC)
SNF	159782.0	4455494.0	1000.0
SF	41660.0	4451969.0	1000.0
NSNF	293529.0	4462129.0	1000.0
NSF	72042.0	4473652.0	1000.0

FILE: o8.t098

10/8/97
L/D=50
SCRAPER OPEN 4 INCHES WIDE
NEUTRON SHUTTER CLOSED
SAMPLE HOLDER A
  U-238 foils = Group 4 (84 foils)
  Total U-238 wt = 23478.31 mg
  Total U-235 wt = 51.77 mg
  Total U mass = 23530.08 mg
  TD Equivalent Thickness = 0.98280 cm

ARRANGEMENT	BTB COUNTS	MONITOR COUNTS	TIME (SEC)
SNF	169317.0	4449363.0	1000.0
SF	85576.0	8877590.0	2000.0
NSNF	324583.0	4463429.0	1000.0
NSF	77104.0	4441512.0	1000.0

FILE: o16.t098

10/16/97
L/D=50
SCRAPER OPEN 4 INCHES WIDE
NEUTRON SHUTTER CLOSED
SAMPLE HOLDER A
  U-238 foils = Group 4 (84 foils)
  Total U-238 wt = 23478.31 mg
  Total U-235 wt = 51.77 mg
  Total U mass = 23530.08 mg
  TD Equivalent Thickness = 0.98280 cm

ARRANGEMENT	BTB COUNTS	MONITOR COUNTS	TIME (SEC)
SNF	151719.0	4447450.0	1000.0
SF	39521.0	4443384.0	1000.0
NSNF	290007.0	4447244.0	1000.0
NSF	71386.0	4450536.0	1000.0

FILE: o29.t101

10/29/97
L/D=50
SCRAPER OPEN 4 INCHES WIDE
NEUTRON SHUTTER CLOSED
SAMPLE HOLDER B
  U-238 foils = Group 1 (85 foils)
  Total U-238 wt = 24343.38 mg
  Total U-235 wt = 53.67 mg
  Total U mass = 24397.05 mg
  TD Equivalent Thickness = 1.01901 cm

ARRANGEMENT	BTB COUNTS	MONITOR COUNTS	TIME (SEC)
SNF	150165.0	4431052.0	1000.0
SF	39438.0	4434077.0	1000.0
NSNF	293917.0	4456383.0	1000.0
NSF	72361.0	4443469.0	1000.0

FILE: o8.t104

10/8/97
L/D=50
SCRAPER OPEN 4 INCHES WIDE
NEUTRON SHUTTER CLOSED
SAMPLE HOLDER A
  U-238 foils = Group 4 (89 foils)
  Total U-238 wt = 24926.30 mg
  Total U-235 wt = 54.96 mg
  Total U mass = 24981.26 mg
  TD Equivalent Thickness = 1.04341 cm

ARRANGEMENT	BTB COUNTS	MONITOR COUNTS	TIME (SEC)
SNF	163200.0	4461295.0	1000.0
SF	85178.0	8907193.0	2000.0
NSNF	324703.0	4475181.0	1000.0
NSF	76789.0	4449855.0	1000.0

FILE: o15.t104

10/15/97
L/D=50
SCRAPER OPEN 4 INCHES WIDE
NEUTRON SHUTTER CLOSED
SAMPLE HOLDER A
  U-238 foils = Group 4 (89 foils)
  Total U-238 wt = 24926.30 mg
  Total U-235 wt = 54.96 mg
  Total U mass = 24981.26 mg
  TD Equivalent Thickness = 1.04341 cm

ARRANGEMENT	BTB COUNTS	MONITOR COUNTS	TIME (SEC)
SNF	149064.0	4462773.0	1000.0
SF	39913.0	4458199.0	1000.0
NSNF	292813.0	4478874.0	1000.0
NSF	72980.0	4452499.0	1000.0

FILE: o29.t104

10/29/97
L/D=50
SCRAPER OPEN 4 INCHES WIDE
NEUTRON SHUTTER CLOSED
SAMPLE HOLDER A
  U-238 foils = Group 4 (89 foils)
  Total U-238 wt = 24926.30 mg
  Total U-235 wt = 54.96 mg
  Total U mass = 24981.26 mg
  TD Equivalent Thickness = 1.04341 cm

ARRANGEMENT	BTB COUNTS	MONITOR COUNTS	TIME (SEC)
SNF	145521.0	4462328.0	1000.0
SF	38423.0	4472838.0	1000.0
NSNF	288979.0	4514859.0	1000.0
NSF	71601.0	4483701.0	1000.0

FILE: o30.t104

10/30/97
L/D=50
SCRAPER OPEN 4 INCHES WIDE
NEUTRON SHUTTER CLOSED
SAMPLE HOLDER B
  U-238 foils = Group 1 (87 foils)
  Total U-238 wt = 24927.92 mg
  Total U-235 wt = 54.96 mg
  Total U mass = 24982.88 mg
  TD Equivalent Thickness = 1.04348 cm

ARRANGEMENT	BTB COUNTS	MONITOR COUNTS	TIME (SEC)
SNF	148799.0	4467866.0	1000.0
SF	39150.0	4470512.0	1000.0
NSNF	293812.0	4494219.0	1000.0
NSF	72581.0	4474297.0	1000.0

FILE: o31.t105

```
10/31/97
L/D=50
SCRAPER OPEN 4 INCHES WIDE
NEUTRON SHUTTER CLOSED
SAMPLE HOLDER B
  U-238 foils = Group 1 (88 foils)
  Total U-238 wt = 25181.05 mg
  Total U-235 wt = 55.52 mg
  Total U mass = 25236.57 mg
  TD Equivalent Thickness = 1.05407 cm
```

ARRANGEMENT	BTB COUNTS	MONITOR COUNTS	TIME (SEC)
SNF	147227.0	4450879.0	1000.0
SF	38767.0	4454617.0	1000.0
NSNF	293279.0	4468631.0	1000.0
NSF	72123.0	4455848.0	1000.0

FILE: o14.t106

```
10/14/97
L/D=50
SCRAPER OPEN 4 INCHES WIDE
NEUTRON SHUTTER CLOSED

SAMPLE HOLDER A
  U-238 foils = Group 4 (91 foils)
  Total U-238 wt = 25495.42 mg
  Total U-235 wt = 56.21 mg
  Total U mass = 25551.63 mg
  TD Equivalent Thickness = 1.06723 cm
```

ARRANGEMENT	BTB COUNTS	MONITOR COUNTS	TIME (SEC)
SNF	147375.0	4426982.0	1000.0
SF	39791.0	4451353.0	1000.0
NSNF	295399.0	4435511.0	1000.0
NSF	72947.0	4421151.0	1000.0

FILE: o15.t109

```
10/15/97
L/D=50
SCRAPER OPEN 4 INCHES WIDE
NEUTRON SHUTTER CLOSED
SAMPLE HOLDER B
  U-238 foils = Group 1 (91 foils)
  Total U-238 wt = 26074.67 mg
  Total U-235 wt = 57.49 mg
  Total U mass = 26132.16 mg
  TD Equivalent Thickness = 1.09148 cm
```

ARRANGEMENT	BTB COUNTS	MONITOR COUNTS	TIME (SEC)
SNF	144489.0	4448012.0	1000.0
SF	39124.0	4457648.0	1000.0
NSNF	294413.0	4476095.0	1000.0
NSF	72194.0	4444468.0	1000.0

FILE: s30.t110

9/30/97
L/D=50
SCRAPER OPEN 4 INCHES WIDE
NEUTRON SHUTTER CLOSED
SAMPLE HOLDER A
   U-238 foils = Group 4 (94 foils)
   Total U-238 wt = 26331.83 mg
   Total U-235 wt = 58.06 mg
   Total U mass = 26389.89 mg
   TD Equivalent Thickness = 1.10225 cm

ARRANGEMENT	BTB COUNTS	MONITOR COUNTS	TIME (SEC)
SNF	158192.0	4349315.0	1000.0
SF	81485.0	8701075.0	2000.0
NSNF	324778.0	4388414.0	1000.0
NSF	154129.0	8733322.0	2000.0

FILE: o29.t110

10/29/97
L/D=50
SCRAPER OPEN 4 INCHES WIDE
NEUTRON SHUTTER CLOSED
SAMPLE HOLDER A
   U-238 foils = Group 4 (94 foils)
   Total U-238 wt = 26331.83 mg
   Total U-235 wt = 58.06 mg
   Total U mass = 26389.89 mg
   TD Equivalent Thickness = 1.10225 cm

ARRANGEMENT	BTB COUNTS	MONITOR COUNTS	TIME (SEC)
SNF	142759.0	4446514.0	1000.0
SF	37443.0	4446514.0	1000.0
NSNF	292970.0	4461352.0	1000.0
NSF	72835.0	4448339.0	1000.0

FILE: o31.t111

10/31/97
L/D=50
SCRAPER OPEN 4 INCHES WIDE
NEUTRON SHUTTER CLOSED
SAMPLE HOLDER A
   U-238 foils = Group 4 (95 foils)
   Total U-238 wt = 26623.90 mg
   Total U-235 wt = 58.70 mg
   Total U mass = 26682.60 mg
   TD Equivalent Thickness = 1.11447 cm

ARRANGEMENT	BTB COUNTS	MONITOR COUNTS	TIME (SEC)
SNF	140900.0	4460819.0	1000.0
SF	37897.0	4462303.0	1000.0
NSNF	294243.0	4485523.0	1000.0
NSF	72439.0	4475150.0	1000.0

FILE: n12.t113

```
11/12/97
L/D=50
SCRAPER OPEN 4 INCHES WIDE
NEUTRON SHUTTER CLOSED
SAMPLE HOLDER B
  U-238 foils = Group 1 (95 foils)
  Total U-238 wt = 27198.48 mg
  Total U-235 wt = 59.97 mg
  Total U mass = 27258.45 mg
  TD Equivalent Thickness = 1.13852 cm
```

ARRANGEMENT	BTB COUNTS	MONITOR COUNTS	TIME (SEC)
SNF	140283.0	4434079.0	1000.0
SF	37042.0	4439020.0	1000.0
NSNF	292717.0	4471030.0	1000.0
NSF	72043.0	4448617.0	1000.0

FILE: j8.samp1

```
1/8/98
L/D=50
SCRAPER OPEN 4 INCHES WIDE
NEUTRON SHUTTER CLOSED
SAMPLE HOLDER A
  U-238 foils = Group 4 +8ACZ
  Pu-239 foils = None
  Total U-238 wt = 26588.77 mg
  Total U-235 wt = 58.62 mg
  Total U mass = 26647.39 mg
  TD Equivalent Thickness = 1.1130 cm
Same thickness as ZPPR Plate sample
```

ARRANGEMENT	BTB COUNTS	MONITOR COUNTS	TIME (SEC)
SNF	140641.0	4446469.0	1000.0
SF	37505.0	4450063.0	1000.0
NSNF	290849.0	4468531.0	1000.0
NSF	71941.0	4453305.0	1000.0

FILE: j9.samp2

```
1/9/98
L/D=50
SCRAPER OPEN 4 INCHES WIDE
NEUTRON SHUTTER CLOSED
ZPPR PLATE SAMPLE - 7/16 in.
```

ARRANGEMENT	BTB COUNTS	MONITOR COUNTS	TIME (SEC)
SNF	183227.0	4462517.0	1000.0
SF	44606.0	4462376.0	1000.0

```
        NSNF       343002.0        4485667.0        1000.0
        NSF         80170.0        4473831.0        1000.0
```

FILE: f24.plates

```
2/24/98
L/D=50
SCRAPER OPEN 4 INCHES WIDE
NEUTRON SHUTTER CLOSED
ZPPR PLATE SAMPLE - 7/16 in.
No Stainless Steel front and back plate

ARRANGEMENT  BTB COUNTS  MONITOR COUNTS  TIME (SEC)
-----------  ----------  --------------  ----------
    SNF       206079.0      4462550.0      1000.0
    SF         49234.0      4472199.0      1000.0
    NSNF      344821.0      4524329.0      1000.0
    NSF        80371.0      4489882.0      1000.0
```